High-Precision Fidelity Estimation with Common Randomized Measurements

Zhongyi Yang, ¹ Datong Chen, ^{2,3,4} Zihao Li, ^{2,3,4,5} and Huangjun Zhu^{2,3,4,*}

¹ International Center for Quantum Materials,
School of Physics, Peking University, Beijing 100871, China

² State Key Laboratory of Surface Physics, Department of Physics,
and Center for Field Theory and Particle Physics, Fudan University, Shanghai 200433, China

³ Institute for Nanoelectronic Devices and Quantum Computing, Fudan University, Shanghai 200433, China

⁴ Shanghai Research Center for Quantum Sciences, Shanghai 201315, China

⁵ QICI Quantum Information and Computation Initiative, School of Computing and Data Science,
The University of Hong Kong, Pokfulam Road, Hong Kong, China
(Dated: December 1, 2025)

Efficient fidelity estimation of multiqubit quantum states is crucial to many applications in quantum information processing. However, to estimate the infidelity ϵ with multiplicative precision, conventional estimation protocols require (order) $1/\epsilon^2$ different circuits in addition to $1/\epsilon^2$ samples, which is quite resource-intensive for high-precision fidelity estimation. Here we introduce an efficient estimation protocol by virtue of common randomized measurements (CRM) integrated with shadow estimation based on the Clifford group, which only requires $1/\epsilon$ circuits. Moreover, in many scenarios of practical interest, in the presence of depolarizing or Pauli noise for example, our protocol only requires a constant number of circuits, irrespective of the infidelity ϵ and the qubit number. For large and intermediate quantum systems, quite often one circuit is already sufficient. In the course of study, we clarify the performance of CRM shadow estimation based on the Clifford group and 4-designs and highlight its advantages over standard and thrifty shadow estimation.

Introduction—The ability to efficiently learn the properties of unknown quantum states is pivotal for advancing quantum technologies [1-4]. Fidelity estimation, as an archetypal learning task, plays a key role in quantum information processing, with great efforts dedicated to developing efficient estimation protocols based on simple measurements [5–22]. Notably, direct fidelity estimation (DFE) using Pauli measurements is effective for important classes of quantum states like stabilizer states [7, 8]. A major breakthrough came with shadow estimation based on Clifford measurements [23], which can achieve a sample complexity independent of the qubit number n. Similar results can also be generalized to qudit systems with odd prime local dimensions [24]. Subsequent refinements, including thrifty shadow estimation [25–29] and common randomized measurements (CRM) [30–32], have further advanced the field.

Despite the progress mentioned above, to estimate the infidelity ϵ with multiplicative precision, existing protocols, including DFE [7, 8] and shadow estimation [23, 27–29], usually require $\mathcal{O}(1/\epsilon^2)$ distinct measurement settings and samples. This overhead poses a significant challenge for high-precision fidelity estimation (HPFE), as adjusting experimental settings is resource-intensive for platforms like superconducting qubits and trapped ions. Overcoming this bottleneck is critical for practical applications in quantum information processing.

In this paper, we introduce an efficient fidelity estimation protocol that integrates CRM with Clifford-

based shadow estimation. By deriving rigorous upper bounds on the variance in terms of the deviation between the system state and the prior state, we establish a robust performance guarantee for CRM shadow estimation. Our protocol achieves a significant resource reduction, requiring only $\mathcal{O}(1/\epsilon)$ circuits to estimate the infidelity with multiplicative precision when the target state is chosen as the prior. Remarkably, in practical scenarios involving depolarizing, Pauli, or certain coherent noise, our protocol requires only a constant number of circuits, irrespective of the infidelity ϵ and the qubit number. Additionally, the nonstabilizerness of the target state can further enhance the efficiency. For large and intermediate quantum systems, quite often we can even work with only one circuit. Compared with standard and thrifty shadow estimation, our protocol can reduce the circuit sample costs thousands and even millions of times for HPFE with $\epsilon \leq 0.001$, making it particularly appealing for practical applications.

As benchmarks, we elucidate the performance of the alternative protocol based on 4-designs and offer additional insights on Pauli measurements studied before [31]. Like in standard shadow estimation, Clifford and 4-design measurements may exhibit exponential advantages over Pauli measurements with respect to the qubit number. What is surprising is that Clifford measurements are not only simpler but also more efficient than 4-design measurements in HPFE for various practical situations. Our work represents a significant leap toward scalable and resource-efficient quantum state characterization.

CRM Shadow estimation—Consider an n-qubit quantum system whose Hilbert space \mathcal{H} has dimen-

^{*} zhuhuangjun@fudan.edu.cn

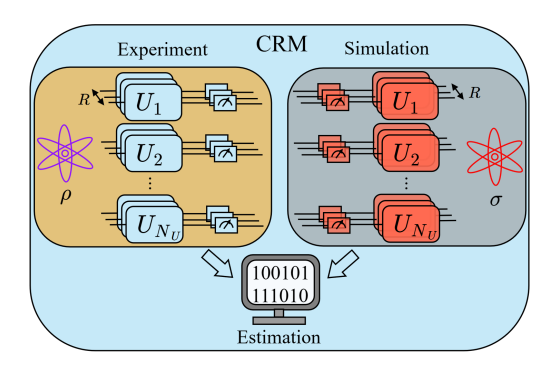


FIG. 1. Schematic of CRM shadow estimation. Here ρ is the unknown system state, σ is the prior state stored in a classical computer, R is the number of circuit reusing, and N_U is the number of circuits sampled. The procedure involving quantum measurements, shown in the orange box, is the same as in thrifty shadow estimation, while the prior state σ is employed to simulate the outcomes of randomized measurements and to construct the CRM estimator, which can usually reduce the variance.

sion $d=2^n$; denote by 1 the identity operator on \mathcal{H} . The basic idea of CRM shadow estimation introduced in Refs. [30–32] is illustrated in Fig. 1. To estimate the expectation value of an observable (Hermitian operator) O with respect to an unknown system state ρ on \mathcal{H} , we first choose a prior state σ and a suitable unitary ensemble \mathcal{U} on \mathcal{H} . In each round, a random unitary U is sampled from \mathcal{U} and applied to the state ρ followed by a measurement in the computational basis. After repeating this procedure (for the same U) R times and obtaining measurement outcomes $\mathbf{s}_1, \mathbf{s}_2, \ldots, \mathbf{s}_R \in \{0,1\}^n$, a CRM estimator for ρ is constructed as $\hat{\rho}_{\sigma} = \hat{\rho} - \hat{\sigma} + \sigma$, where

$$\hat{\rho} = \frac{1}{R} \sum_{k=1}^{R} \mathcal{M}^{-1} (U^{\dagger} | \mathbf{s}_{k} \rangle \langle \mathbf{s}_{k} | U),$$

$$\hat{\sigma} = \sum_{\mathbf{s}} P_{\sigma}(\mathbf{s} \mid U) \mathcal{M}^{-1} (U^{\dagger} | \mathbf{s} \rangle \langle \mathbf{s} | U).$$
(1)

Here $\mathcal{M}^{-1}(\cdot)$ denotes the inverse of the measurement channel determined by \mathcal{U} and is known as the reconstruction map [23], and $P_{\sigma}(\mathbf{s} \mid \mathcal{U}) = \langle \mathbf{s} | \mathcal{U} \sigma \mathcal{U}^{\dagger} | \mathbf{s} \rangle$. Accordingly, $\text{Tr}(O\hat{\rho}_{\sigma})$ is an estimator for $\text{Tr}(O\rho)$, whose variance is denoted by $\mathbb{V}_R(\hat{O})$. Note that $\hat{\rho}$ is the estimator for ρ in thrifty (THR) shadow estimation [27, 28, 31], and may be regarded as a special CRM estimator with $\sigma = 0$. Henceforth the above CRM and THR estimation protocols are referred to as $\text{CRM}(\mathcal{U}, \sigma, R)$ and $\text{THR}(\mathcal{U}, R)$, respectively.

After repeating the above procedure N_U times, N_U estimators for $\text{Tr}(O\rho)$ can be constructed, corresponding to the random unitaries $U_1, U_2, \ldots, U_{N_U}$ sampled in N_U rounds. Then a more precise estimator can be constructed from the empirical mean. In conjunction with the median of means estimation we can further reduce the probability of large devi-

ation. By virtue of a similar reasoning employed in Ref. [23], it is straightforward to derive the following result on the sample cost.

Lemma 1. Suppose O is an observable on \mathcal{H} . Then the circuit sample cost required to estimate the expectation value of O within error ε and with probability at least $1 - \delta$ is upper bounded by

$$N_U \le \left\lceil \frac{68 \mathbb{V}_R(\hat{O})}{\varepsilon^2} \ln\left(\frac{2}{\delta}\right) \right\rceil.$$
 (2)

Here the variance $V_R(\hat{O})$ only depends on the traceless part of O. Lemma 1 applies to both CRM and THR shadow estimation. From now on, we assume that O is a traceless observable (Hermitian operator) on \mathcal{H} , denote by $\Delta = \rho - \sigma$ the deviation of the system state ρ from the prior state σ , and denote by $\epsilon = 1 - \|\sqrt{\rho}\sqrt{\sigma}\|_1^2$ the infidelity between ρ and σ , where $\|\cdot\|_p$ $(p \geq 1)$ denotes the Schatten p-norm. Note that $\epsilon = 1 - \text{Tr}(\rho\sigma)$ when σ is a pure state.

High-precision fidelity estimation—Efficient estimation of the fidelity between the system state ρ and a given target pure state $|\phi\rangle$ is crucial to many applications [7, 15, 33]. Although shadow estimation proves to be useful for this task, the circuit sample cost is usually inversely proportional to the mean square error, which is quite resource-intensive for HPFE. Here we will show that CRM can effectively circumvent this problem, as long as we choose the target pure state as the prior, that is, $\sigma = |\phi\rangle\langle\phi|$. Our solution is based on two simple but crucial observations: 1. the estimation error that can be tolerated in practical applications is usually proportional to the infidelity ϵ ; 2. the estimation error in CRM with the prior state σ tends to decrease monotonically with ϵ . Now, the goal of HPFE is to estimate the fidelity $F = \langle \phi | \rho | \phi \rangle$ or the expectation of the observable $O = \sigma - 1/d$, within error $\varepsilon = r\epsilon$ and significance level δ , where r and δ are precision parameters determined by specific applications.

Variances in CRM shadow estimation—To understand the performance of CRM shadow estimation and its application in HPFE, we need to evaluate the variance $V_R(\hat{O})$. To this end, we first define the 4th cross moment operator introduced in Ref. [29]:

$$\Omega(\mathcal{U}) = \sum_{\mathbf{s}, \mathbf{t}} \mathbb{E}_{U \sim \mathcal{U}} U^{\dagger \otimes 4} \big[(|\mathbf{s}\rangle \langle \mathbf{s}|)^{\otimes 2} \otimes (|\mathbf{t}\rangle \langle \mathbf{t}|)^{\otimes 2} \big] U^{\otimes 4},$$
(3)

where the summation runs over $\mathbf{s}, \mathbf{t} \in \{0,1\}^n$. Then we can lay the groundwork for understanding CRM shadow estimation and its advantages over standard and THR shadow estimation. The following lemma is proved in Sec. S2 in Supplemental Material (SM), which includes Refs. [34–42].

Lemma 2. The variance $\mathbb{V}_R(\hat{O})$ in $CRM(\mathcal{U}, \sigma, R)$ reads

$$\mathbb{V}_{R}(\hat{O}) = \mathbb{V}_{*}(O, \Delta) + \frac{\mathbb{V}(O, \rho) - \mathbb{V}_{*}(O, \rho)}{R}, \quad (4)$$

where $V(O, \rho)$ denotes the variance in standard shadow estimation and

$$\mathbb{V}_*(O,\tau) := \operatorname{Tr} \left\{ \Omega(\mathcal{U}) \left[\mathcal{M}^{-1}(O) \otimes \tau \right]^{\otimes 2} \right\} - \left[\operatorname{Tr}(O\tau) \right]^2$$
(5)

for $\tau = \Delta$ and $\tau = \rho$.

In the large-R limit, we have $\mathbb{V}_R(\hat{O}) = \mathbb{V}_*(O, \Delta)$ and $N_U = \mathcal{O}(\mathbb{V}_*(O, \Delta))$ by Lemma 1, so $\mathbb{V}_*(O, \Delta)$ determines the variance and circuit sample cost. By replacing σ and Δ with 0 and ρ in Eq. (4) we can reproduce the variance in THR shadow estimation [27, 29], which is effective if $\mathbb{V}_*(O, \rho) \ll \mathbb{V}(O, \rho)$, but not so effective if $\mathbb{V}_*(O, \rho) \approx \mathbb{V}(O, \rho)$. In the latter case, CRM is particularly appealing as we will see.

In the rest of this paper, we are mainly interested in estimation protocols based on 3-designs. The following lemma is a simple corollary of Lemmas 1, 2 above and Proposition 1 in Appendix A.

Lemma 3. Suppose \mathcal{U} is a unitary 3-design. Then the variance $\mathbb{V}_R(\hat{O})$ in $CRM(\mathcal{U}, \sigma, R)$ satisfies

$$V_R(\hat{O}) \le V_*(O, \Delta) + \frac{2||O||_2^2}{R}.$$
 (6)

In HPFE with $O = \sigma - 1/d$, the circuit sample cost required to achieve precision $r\epsilon$ satisfies

$$N_U \le \left\lceil \frac{68 \left[V_*(O, \Delta) + \frac{2}{R} \right]}{r^2 \epsilon^2} \ln \left(\frac{2}{\delta} \right) \right\rceil. \tag{7}$$

CRM based on 4-design measurements—From now on we turn to CRM shadow estimation based on more concrete unitary ensembles. First, we clarify the performance of 4-design measurements.

Theorem 1. Suppose \mathcal{U} is a unitary 4-design. Then the variance $\mathbb{V}_*(O,\Delta)$ in $\mathrm{CRM}(\mathcal{U},\sigma,R)$ satisfies

$$\frac{\|\Delta\|_2^2 \|O\|_2^2}{d+2} \le \mathbb{V}_*(O, \Delta) \le \frac{4\|\Delta\|_2^2 \|O\|_2^2}{d} \le \frac{8\epsilon \|O\|_2^2}{d}.$$
(8)

Theorem 1 shows that CRM is very effective for enhancing the performance of shadow estimation based on 4-designs. Notably, the asymptotic variance $\mathbb{V}_*(O,\Delta)$ is mainly determined by $\|\Delta\|_2^2$, which decreases monotonically as the system state ρ and prior state σ gets closer. For HPFE, the prior state σ coincides with the target pure state and we have $O = \sigma - 1/d$ and $\|O\|_2^2 \le 1$, which means $\mathbb{V}_R(\hat{O}) \le 4\|\Delta\|_2^2/d + 2/R \le 8\epsilon/d + 2/R$. In this case, CRM can even improve the scaling behavior of the sample cost with respect to the infidelity. The following theorem is a simple corollary of Lemma 3 and Theorem 1.

Theorem 2. Suppose \mathcal{U} is a unitary 4-design. Then the circuit sample cost required to achieve HPFE in $CRM(\mathcal{U}, \sigma, R)$ satisfies

$$N_U \le \left\lceil \frac{136\left(\frac{2\|\Delta\|_2^2}{d} + \frac{1}{R}\right)}{r^2 \epsilon^2} \ln\left(\frac{2}{\delta}\right) \right\rceil. \tag{9}$$

Since $\|\Delta\|_2^2 \leq 2\epsilon$ thanks to Proposition 2 in Appendix B, CRM based on 4-design measurements can achieve the scaling behavior $N_U = \mathcal{O}(1/\epsilon)$ in the large-R limit, which is much better than the counterpart $\mathcal{O}(1/\epsilon^2)$ for THR. Moreover, CRM can even achieve a constant scaling behavior whenever $\|\Delta\|_2^2 = \mathcal{O}(\epsilon^2)$, which holds for many scenarios of practical interest. Notably, if σ is a Haar-random pure state and $\rho = \mathcal{P}(\sigma)$ with \mathcal{P} being a Pauli channel, then we have $\|\Delta\|_2^2 = \mathcal{O}(\epsilon^2)$ on average thanks to Proposition 3 in Appendix B. For a sufficiently large system with $d \gg 1/(r\epsilon)^2$, the circuit sample cost may even drop to $N_U = 1$.

CRM based on Clifford measurements—In real experiments, it is quite difficult to realize 4-designs. As a simpler alternative, the Clifford group Cl_n forms a 3-design [43–45] and can be regarded as the best approximation to a 4-design among discrete groups [46, 47]. Can we achieve a similar performance in CRM shadow estimation based on Clifford measurements instead of 4-design measurements?

To answer the above question, we first introduce some additional concepts. Let $\overline{\mathcal{P}}_n = \{I, X, Y, Z\}^{\otimes n}$ be the set of n-qubit Pauli operators. The characteristic function Ξ_O of the observable O is defined as $\Xi_O(P) := \operatorname{Tr}(OP)$ for $P \in \overline{\mathcal{P}}_n$, which can be regarded as a vector of d^2 entries. The stabilizer 2-Rényi entropy (2-SRE) of a pure state $\sigma = |\phi\rangle\langle\phi|$ reads $M_2(\phi) = M_2(\sigma) = \log_2(d/\|\Xi_\sigma\|_4^4)$ [48, 49], where $\|\Xi_\sigma\|_p$ for $p \geq 1$ denotes the ℓ_p -norm of Ξ_σ . The cross characteristic function Ξ_{O_1,O_2} and twisted cross characteristic function $\tilde{\Xi}_{O_1,O_2}$ of two observables O_1,O_2 on \mathcal{H} are defined as [29]

$$\Xi_{O_1,O_2}(P) := \operatorname{Tr}(O_1 P) \operatorname{Tr}(O_2 P), \quad P \in \overline{\mathcal{P}}_n,$$

$$\widetilde{\Xi}_{O_1,O_2}(P) := \operatorname{Tr}(O_1 P O_2 P), \quad P \in \overline{\mathcal{P}}_n.$$
(10)

Now, we can introduce an upper bound for $V_*(O, \Delta)$:

$$\mathbb{V}_{\circ}(O,\Delta) := \frac{d+1}{d(d+2)} \left(\|\Xi_{\Delta,O}\|_{2}^{2} + \tilde{\Xi}_{\Delta,O} \cdot \Xi_{\Delta,O} \right), \tag{11}$$

where $\tilde{\Xi}_{\Delta,O} \cdot \Xi_{\Delta,O}$ denotes the inner product between two cross characteristic functions viewed as vectors. Theorems 3 and 5 below are proved in SM Sec. S8.

Theorem 3. The variance $\mathbb{V}_*(O, \Delta)$ associated with $CRM(Cl_n, \sigma, R)$ reads

$$\mathbb{V}_{*}(O,\Delta) = \mathbb{V}_{\circ}(O,\Delta) - \frac{[\text{Tr}(\Delta O)]^{2}}{d+2} \le \frac{2}{d} \|\Xi_{\Delta,O}\|_{2}^{2}$$
$$\le 2\|\Delta\|_{1}^{2} \|O\|_{2}^{2} \le 8\epsilon \|O\|_{2}^{2}. \tag{12}$$

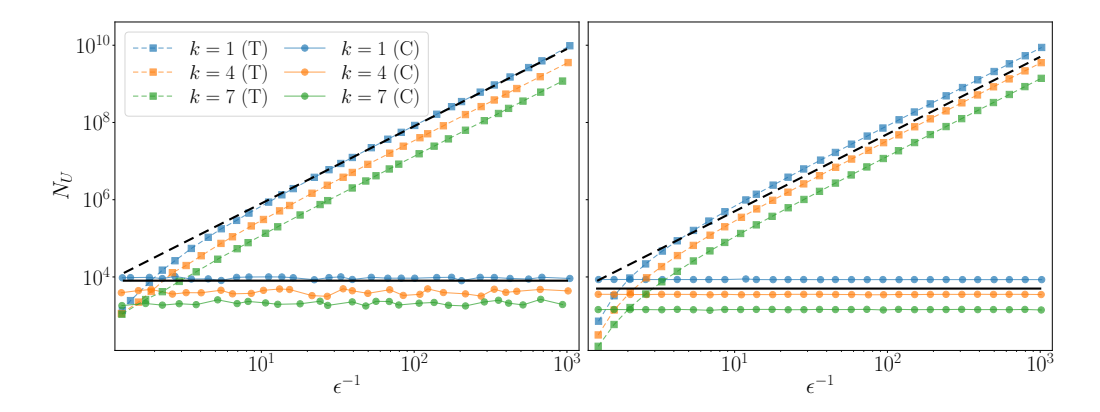


FIG. 2. Circuit sample costs N_U required for HPFE in THR (T) and CRM (C) shadow estimation based on Clifford measurements. Here, r=0.25, $\delta=0.01$, and $R=\lceil 10/\epsilon^2 \rceil$. The target and prior state has the form $\sigma=|S_{7,k}\rangle\langle S_{7,k}|$ with k=1,4,7. Different system states ρ are generated by applying random local rotations described in Sec. S5 3 (left plot) and random Pauli channels described in Sec. S5 2 (right plot) to the target state σ . The black solid and dashed lines represent $N_U=8000$ and $N_U=8000/\epsilon^2$, respectively, in the left plot, while they represent $N_U=5000$ and $N_U=5000/\epsilon^2$ in the right plot.

If σ is a pure state and $O = \sigma - 1/d$, then

$$V_*(O, \Delta) \le 2^{2 - M_2(\sigma)/2} \min\{\sqrt{2}\epsilon, \|\Delta\|_2^2\}.$$
 (13)

Theorem 3 shows that the variance $\mathbb{V}_*(O, \Delta)$ tends to decrease monotonically when the system state ρ and the prior state σ gets closer as in CRM shadow estimation based on 4-designs. This fact is particularly important to HPFE. As a simple corollary of Lemma 3 and Theorem 3, we can deduce the following theorem.

Theorem 4. Suppose σ is a pure state on \mathcal{H} . Then the circuit sample cost N_U required for HPFE in $CRM(Cl_n, \sigma, R)$ satisfies

$$N_U \le \left\lceil \frac{136 \left[2^{1 - M_2(\sigma)/2} \|\Delta\|_2^2 + \frac{1}{R} \right]}{r^2 \epsilon^2} \ln\left(\frac{2}{\delta}\right) \right\rceil. \quad (14)$$

Thanks to Theorems 3 and 4 and Propositions 2-4 in Appendix B, CRM shadow estimation based on Clifford measurements is very effective for fidelity estimation even when the target state is a stabilizer state, for which THR is useless. In the large-R limit, the circuit sample cost N_U tends to decrease exponentially with 2-SRE. In addition, N_U increases at most linearly with $1/\epsilon$ instead of $1/\epsilon^2$, unlike THR. Moreover, constant scaling can be achieved whenever $\|\Delta\|_2^2 = \mathcal{O}(\epsilon^2)$ or $\|\Xi_{\Delta,O}\|_2^2/d = \mathcal{O}(\epsilon^2)$, which holds in many scenarios of practical interest. Notably, this is the case when ρ is related to the target state via a depolarizing or Pauli channel by Proposition 4.

Theorem 5. Suppose σ is a pure state on \mathcal{H} and $\rho = \mathscr{P}(\sigma)$, where \mathscr{P} is a Pauli channel. Then the circuit sample cost N_U required for HPFE in $CRM(Cl_n, \sigma, R)$ satisfies

$$N_U \le \left\lceil 136 \ln\left(\frac{2}{\delta}\right) \left(\frac{2}{r^2} + \frac{1}{Rr^2 \epsilon^2}\right) \right\rceil. \tag{15}$$

If \mathcal{P} is a depolarizing channel, then

$$N_U \le \left\lceil 136 \ln\left(\frac{2}{\delta}\right) \left[\frac{2^{-M_2(\sigma)}}{r^2} + \frac{1}{Rr^2 \epsilon^2} \right] \right\rceil. \tag{16}$$

Numerical illustration—To demonstrate the advantages of CRM over THR in HPFE, we consider an example in which the target state is $|S_{n,k}\rangle :=$ $|0\rangle^{\otimes (n-k)} \otimes |T\rangle^{\otimes k}$, where $|T\rangle := (|0\rangle + e^{\pi i/4} |1\rangle)/\sqrt{2}$ is a magic state and $M_2(|S_{n,k}\rangle) = k \log_2(4/3)$ [29]. Different system states are generated by applying random local rotations (coherent noise) or random Pauli channels (incoherent noise) to σ . Figure 2 shows the circuit sample costs required in THR and CRM as functions of the infidelity ϵ . In both cases, THR requires $\mathcal{O}(1/\epsilon^2)$ circuits, while CRM only requires a constant number of circuits, which is dramatically better. For HPFE with $\epsilon \leq 0.001$, CRM can reduce the circuit sample cost millions of times. As shown in SM Sec. S10, for certain special coherent noise, CRM requires $\mathcal{O}(1/\epsilon)$ circuits, which is suboptimal but still much better than THR. In addition, the 2-SRE of the target state can significantly enhance the performance of Clifford-based CRM in HPFE, which is similar to THR as shown in Ref. [29]. See SM Sec. S10 for more numerical results.

Next, we compare the performance of 4-design, Clifford, and Pauli measurements in HPFE based on CRM shadow estimation. Here we choose the n-qubit magic cluster state $|\mathrm{MC}_n\rangle := \prod_{i=1}^{n-1} \mathrm{CZ}_{i,i+1} | S_{n,n}\rangle$ as the target state, and the system state is affected by depolarizing noise. The circuit sample costs N_U tied to the three measurement ensembles are shown in Fig. 3. For 4-design and Clifford measurements, N_U decrease exponentially with the qubit number n until $N_U=1$, which is expected according to Theorems 2 and 5 given that $M_2(\mathrm{MC}_n)=M_2(S_{n,n})$ increases linearly with n. For Pauli measurements, by contrast,

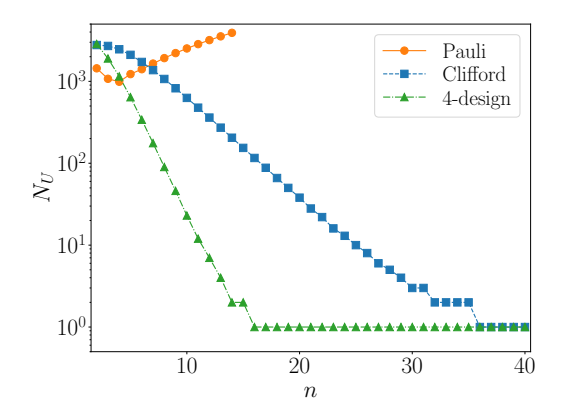


FIG. 3. Circuit sample costs N_U required for HPFE in CRM shadow estimation based on three measurement ensembles, plotted as functions of the qubit number n. Here $r=0.25, \delta=0.01, \epsilon=0.001$, and $R=2\times 10^{10}$. The target state $\sigma=|\mathrm{MC}_n\rangle\langle\mathrm{MC}_n|$ is the n-qubit magic cluster state with $n=2,3,\ldots,40$. Different system states ρ are generated by applying depolarizing noise to the target state: $\rho=(1-p)\sigma+p\mathbb{1}/d$ with $p=\epsilon/(1-d^{-1})$.

 N_U increases exponentially with n for $n \geq 4$. We can expect similar results when $|\mathrm{MC}_n\rangle$ is replaced by generic multiqubit pure states, which have nearly maximal entanglement and nonstabilizerness.

In the above example, 4-design measurements are the most efficient. In certain situations, surprisingly, Clifford measurements can achieve a better scaling behavior with respect to the infidelity, as shown in Appendix C. According to Theorems 1 and 4, intuitively, this peculiar phenomenon would occur when $\|\Delta\|_2^2 = \mathcal{O}(\epsilon)$, but $\|\Xi_{\Delta,O}\|_2^2/d = \mathcal{O}(\epsilon^2)$. This fact is a blessing for practical quantum information processing since it is much easier to realize Clifford measurements than 4-design measurements.

Summary—We introduced a general and highly efficient fidelity estimation protocol by integrating CRM with Clifford-based shadow estimation. To estimate the infidelity ϵ with multiplicative precision, our protocol requires only $\mathcal{O}(1/\epsilon)$ circuits instead of $\mathcal{O}(1/\epsilon^2)$ circuits required in conventional approaches, including standard and THR shadow estimation. Moreover, in practical scenarios affected by depolarizing. Pauli, or certain coherent noise, our protocol demands only a constant number of circuits, irrespective of the infidelity ϵ and the qubit number n. For typical target pure states of large and intermediate quantum systems, only one circuit is required. For HPFE with $\epsilon \leq 0.001$, our protocol can reduce the circuit sample cost by factors of thousands to millions, which is instrumental to practical applications. In the course of study, we derived general analytical formulas for the variances in CRM shadow estimation based on 4-design, Clifford, and Pauli measurements, which are of interest beyond fidelity estimation. Our work marks a substantial step forward in developing scalable learning protocols for high-precision applications, with broad implications for quantum information processing. In the future, it would be desirable to generalize our results to qudits and measurement ensembles based on shallow circuits.

Acknowledgments—This work is supported by the National Natural Science Foundation of China (Grant No. 92365202 and No. 12475011), Shanghai Science and Technology Innovation Action Plan (Grant No. 24LZ1400200), Shanghai Municipal Science and Technology Major Project (Grant No. 2019SHZDZX01), and the National Key Research and Development Program of China (Grant No. 2022YFA1404204).

J. Eisert, D. Hangleiter, N. Walk, I. Roth,
 D. Markham, R. Parekh, U. Chabaud, and
 E. Kashefi, Quantum certification and benchmarking, Nat. Rev. Phys. 2, 382 (2020).

^[2] M. Kliesch and I. Roth, Theory of quantum system certification, PRX Quantum 2, 010201 (2021).

^[3] A. Elben, S. T. Flammia, H.-Y. Huang, R. Kueng, J. Preskill, B. Vermersch, and P. Zoller, The randomized measurement toolbox, Nat. Rev. Phys. 5, 9 (2023)

^[4] V. Gebhart, R. Santagati, A. A. Gentile, E. M. Gauger, D. Craig, N. Ares, L. Banchi, F. Marquardt, L. Pezzè, and C. Bonato, Learning quantum systems, Nat. Rev. Phys. 5, 141 (2023).

^[5] M. Hayashi, K. Matsumoto, and Y. Tsuda, A study of LOCC-detection of a maximally entangled state using hypothesis testing, J. Phys. A: Math. Gen. 39, 14427 (2006).

^[6] O. Gühne, C.-Y. Lu, W.-B. Gao, and J.-W. Pan,

Toolbox for entanglement detection and fidelity estimation, Phys. Rev. A **76**, 030305 (2007).

^[7] S. T. Flammia and Y.-K. Liu, Direct fidelity estimation from few Pauli measurements, Phys. Rev. Lett. 106, 230501 (2011).

^[8] M. P. da Silva, O. Landon-Cardinal, and D. Poulin, Practical characterization of quantum devices without tomography, Phys. Rev. Lett. 107, 210404 (2011).

^[9] S. Pallister, N. Linden, and A. Montanaro, Optimal verification of entangled states with local measurements, Phys. Rev. Lett. 120, 170502 (2018).

^[10] H. Zhu and M. Hayashi, Optimal verification and fidelity estimation of maximally entangled states, Phys. Rev. A 99, 052346 (2019).

^[11] H. Zhu and M. Hayashi, General framework for verifying pure quantum states in the adversarial scenario, Phys. Rev. A 100, 062335 (2019).

^[12] Z. Li, Y.-G. Han, and H. Zhu, Efficient verification

- of bipartite pure states, Phys. Rev. A **100**, 032316 (2019).
- [13] Z. Li, Y.-G. Han, and H. Zhu, Optimal verification of Greenberger-Horne-Zeilinger states, Phys. Rev. Appl. 13, 054002 (2020).
- [14] M. Cerezo, A. Poremba, L. Cincio, and P. J. Coles, Variational Quantum Fidelity Estimation, Quantum 4, 248 (2020).
- [15] X. Zhang, M. Luo, Z. Wen, Q. Feng, S. Pang, W. Luo, and X. Zhou, Direct fidelity estimation of quantum states using machine learning, Phys. Rev. Lett. 127, 130503 (2021).
- [16] X.-D. Yu, J. Shang, and O. Gühne, Statistical methods for quantum state verification and fidelity estimation, Adv. Quantum Technol. 5, 2100126 (2022).
- [17] Q. Wang, Z. Zhang, K. Chen, J. Guan, W. Fang, J. Liu, and M. Ying, Quantum algorithm for fidelity estimation, IEEE Trans. Inf. Theory 69, 273 (2022).
- [18] M. Sun, G. Waite, M. Bremner, and C. Ferrie, Efficient fidelity estimation with few local Pauli measurements (2025), arXiv:2510.08155.
- [19] W. Fang and Q. Wang, Optimal Quantum Algorithm for Estimating Fidelity to a Pure State, in 33rd Annual European Symposium on Algorithms (ESA 2025), Vol. 351 (Schloss Dagstuhl Leibniz-Zentrum für Informatik, 2025) pp. 4:1–4:12.
- [20] W.-H. Zhang, C. Zhang, Z. Chen, X.-X. Peng, X.-Y. Xu, P. Yin, S. Yu, X.-J. Ye, Y.-J. Han, J.-S. Xu, G. Chen, C.-F. Li, and G.-C. Guo, Experimental optimal verification of entangled states using local measurements, Phys. Rev. Lett. 125, 030506 (2020).
- [21] X. Jiang, K. Wang, K. Qian, Z. Chen, Z. Chen, L. Lu, L. Xia, F. Song, S. Zhu, and X. Ma, Towards the standardization of quantum state verification using optimal strategies, npj Quantum Inf. 6, 90 (2020).
- [22] H. Qin, L. Che, C. Wei, F. Xu, Y. Huang, and T. Xin, Experimental direct quantum fidelity learning via a data-driven approach, Phys. Rev. Lett. 132, 190801 (2024).
- [23] H.-Y. Huang, R. Kueng, and J. Preskill, Predicting many properties of a quantum system from very few measurements, Nat. Phys. 16, 1050 (2020).
- [24] C. Mao, C. Yi, and H. Zhu, Qudit shadow estimation based on the Clifford group and the power of a single magic gate, Phys. Rev. Lett. 134, 160801 (2025).
- [25] G. I. Struchalin, Y. A. Zagorovskii, E. V. Kovlakov, S. S. Straupe, and S. P. Kulik, Experimental estimation of quantum state properties from classical shadows, PRX Quantum 2, 010307 (2021).
- [26] W. J. Huggins, B. A. O'Gorman, N. C. Rubin, D. R. Reichman, R. Babbush, and J. Lee, Unbiasing fermionic quantum Monte Carlo with a quantum computer, Nature 603, 416–420 (2022).
- [27] J. Helsen and M. Walter, Thrifty shadow estimation: Reusing quantum circuits and bounding tails, Phys. Rev. Lett. 131, 240602 (2023).
- [28] Y. Zhou and Q. Liu, Performance analysis of multishot shadow estimation, Quantum 7, 1044 (2023).
- [29] D. Chen and H. Zhu, Nonstabilizerness enhances thrifty shadow estimation (2024), arXiv:2410.23977.
- [30] S. J. Garratt and E. Altman, Probing postmeasurement entanglement without postselection, PRX Quantum 5, 030311 (2024).

- [31] B. Vermersch, A. Rath, B. Sundar, C. Branciard, J. Preskill, and A. Elben, Enhanced estimation of quantum properties with common randomized measurements, PRX Quantum 5, 010352 (2024).
- [32] V. Vitale, A. Rath, P. Jurcevic, A. Elben, C. Branciard, and B. Vermersch, Robust estimation of the quantum Fisher information on a quantum processor, PRX Quantum 5, 030338 (2024).
- [33] S.-u. Lee, M. Yuan, S. Chen, K. Tsubouchi, and L. Jiang, Efficient benchmarking of logical magic state (2025), arXiv:2505.09687.
- [34] B. Collins and P. Śniady, Integration with respect to the Haar measure on unitary, orthogonal and symplectic group, Commun. Math. Phys. 264, 773 (2006).
- [35] I. Roth, R. Kueng, S. Kimmel, Y.-K. Liu, D. Gross, J. Eisert, and M. Kliesch, Recovering quantum gates from few average gate fidelities, Phys. Rev. Lett. 121, 170502 (2018).
- [36] M. A. Nielsen and I. L. Chuang, Quantum Computation and Quantum Information: 10th Anniversary Edition (Cambridge University Press, 2010).
- [37] P. Pfeuty, The one-dimensional Ising model with a transverse field, Ann. Phys. 57, 79 (1970).
- [38] S. Sachdev, Quantum phase transitions, Handb. Magn. Adv. Magn. Mater. 2, 1 (2007).
- [39] S. F. E. Oliviero, L. Leone, and A. Hamma, Magicstate resource theory for the ground state of the transverse-field Ising model, Phys. Rev. A 106, 042426 (2022).
- [40] P. S. Tarabunga, E. Tirrito, T. Chanda, and M. Dalmonte, Many-body magic via Pauli-Markov chains from criticality to gauge theories, PRX Quantum 4, 040317 (2023).
- [41] P. S. Tarabunga, E. Tirrito, M. C. Bañuls, and M. Dalmonte, Nonstabilizerness via matrix product states in the Pauli basis, Phys. Rev. Lett. 133, 010601 (2024).
- [42] Y.-M. Ding, Z. Wang, and Z. Yan, Evaluating many-body stabilizer Rényi entropy by sampling reduced Pauli strings: Singularities, volume law, and non-local magic, PRX Quantum 6, 030328 (2025), an open dataset is available at https://github.com/msquare1998/Data-SRE-QMC.
- [43] R. Kueng and D. Gross, Qubit stabilizer states are complex projective 3-designs (2015), arXiv:1510.02767.
- [44] Z. Webb, The Clifford group forms a unitary 3design, Quantum Inf. Comput. 16, 1379 (2016).
- [45] H. Zhu, Multiqubit Clifford groups are unitary 3designs, Phys. Rev. A 96, 062336 (2017).
- [46] H. Zhu, R. Kueng, M. Grassl, and D. Gross, The Clifford group fails gracefully to be a unitary 4-design, arXiv:1609.08172 (2016).
- [47] E. Bannai, G. Navarro, N. Rizo, and P. H. Tiep, Unitary t-groups, J. Math. Soc. Japan 72, 909–921 (2020).
- [48] L. Leone, S. F. E. Oliviero, and A. Hamma, Stabilizer Rényi entropy, Phys. Rev. Lett. 128, 050402 (2022).
- [49] L. Leone and L. Bittel, Stabilizer entropies are monotones for magic-state resource theory, Phys. Rev. A 110, L040403 (2024).

Across this Appendix, \mathcal{H} denotes a d-dimensional Hilbert space on which all operators act, and $\mathbbm{1}$ denotes the identity operator as in the main text. In addition, O denotes a traceless observable, ρ, σ denote two quantum states, $\Delta = \rho - \sigma$, and $\epsilon = 1 - \|\sqrt{\rho}\sqrt{\sigma}\|_1^2$ denotes the infidelity between ρ and σ , which can be simplified as $\epsilon = 1 - \text{Tr}(\rho\sigma)$ when σ is a pure state. In CRM shadow estimation, ρ and σ denote the system state and prior state, respectively; in HPFE, σ also denotes the target pure state.

Appendix A: Variance in shadow estimation based on 3-designs

Here we offer a universal upper bound for the variance in shadow estimation based on 3-designs, which is nearly tight. The following proposition is proved in SM Sec. S1.

Proposition 1. Suppose \mathcal{U} is a unitary 3-design on \mathcal{H} . Then

$$\mathbb{V}(O,\rho) = \frac{d+1}{d+2} \left[\text{Tr}(O^2) + 2 \, \text{Tr}(\rho O^2) \right] - \left[\text{Tr}(\rho O) \right]^2$$

$$\leq 2\|O\|_2^2. \tag{A1}$$

The equality in Eq. (A1) was derived in Ref. [23], which also proved a weaker upper bound, that is, $\mathbb{V}(O,\rho) \leq 3\|O\|_2^2$. When $O = |\phi\rangle\langle\phi| - 1/d$ with $|\phi\rangle$ being a pure state in \mathcal{H} , we have [29]

$$\mathbb{V}(O,\rho) = -F^2 + \frac{d(2F+1)}{d+2} < 2 - \epsilon^2 \le 2, \quad (A2)$$

where $F = \langle \phi | \rho | \phi \rangle$ is the fidelity between ρ and $| \phi \rangle$ and $\epsilon = 1 - F$ is the infidelity. This result shows that the inequality in Eq. (A1) is nearly tight.

Appendix B: Relations between $\|\Delta\|_2^2$, $\|\Delta\|_1^2$, $\|\Xi_{\Delta,O}\|_2^2$, and the infidelity ϵ

To better understand the performance of HPFE based on CRM shadow estimation, here we clarify the relations between $\|\Delta\|_2^2$, $\|\Delta\|_1^2$, $\|\Xi_{\Delta,O}\|_2^2$, and ϵ , assuming that σ is a pure state; see SM Secs. S6 and S7 for additional results.

Proposition 2. The following inequalities hold:

$$2\epsilon^2 \le 2\|\Delta\|_2^2 \le \|\Delta\|_1^2 \le \min\{4\epsilon, 4\|\Delta\|_2^2\};$$
 (B1)

the inequality $\|\Delta\|_2^2 \le 2\epsilon$ is saturated if and only if ρ is a pure state.

Proposition 3. Suppose σ is a Haar-random pure state on \mathcal{H} and $\rho = \mathscr{P}(\sigma)$ with \mathscr{P} being a Pauli channel. Then

$$\overline{\epsilon^2} \le \overline{\|\Delta\|_2^2} \le \frac{2(d+1)}{d} \overline{\epsilon}^2, \ 4\overline{\epsilon^2} \le \overline{\|\Delta\|_1^2} \le 8\overline{\epsilon}^2.$$
 (B2)

Proposition 4. Suppose $O = \sigma - 1/d$; then

$$\|\Xi_{\Delta,O}\|_2^2 = \|\Xi_{\Delta,\sigma}\|_2^2 \le 2^{[3-M_2(\sigma)]/2} d\epsilon.$$
 (B3)

If $\rho = \mathscr{P}(\sigma)$ with \mathscr{P} being a Pauli channel, then

$$\|\Xi_{\Delta,O}\|_2^2 = \|\Xi_{\Delta,\sigma}\|_2^2 \le 2d\epsilon^2.$$
 (B4)

Propositions 2 and 3 follow from Propositions S8 and S9 in SM Sec. S6, respectively. Proposition 4 follows from Lemmas S8 and S10 in SM Sec. S7.

Appendix C: Comparison of Clifford measurements and 4-design measurements

In this appendix, we show that Clifford measurements are not only simpler but also more efficient than 4-design measurements in HPFE in the presence of certain coherent noise of practical interest.

As a complement to Fig. 2, which shows the circuit sample cost of HPFE based on Clifford measurements, here we consider the counterpart based on 4-design measurements. The target and prior state has the form $\sigma = |S_{7,k}\rangle\langle S_{7,k}|$ with k=1,7. Both random local rotations and random Pauli noise are considered as before. The sample costs required in THR and CRM shadow estimation can be determined by virtue of Lemmas 1 and 2 together with the variance formulas for $\mathbb{V}(O,\rho)$, $\mathbb{V}_*(O,\rho)$, and $\mathbb{V}_*(O,\Delta)$ presented in Eq. (A1) and Lemma S5 in SM Sec. S4, and the results are shown in Fig. 4.

For THR shadow estimation based on 4-design measurements, the sample cost scales with $1/\epsilon^2$ for both noise types. For CRM shadow estimation based on 4-design measurements, by contrast, the sample cost scales with $1/\epsilon$ in the first case (random local rotations), but is almost independent of ϵ in the second case (random Pauli noise). Although CRM can significantly improve the scaling behavior, the improvement in the first case is not so dramatic compared with the counterpart for Clifford measurements, which can achieve a constant scaling behavior. Therefore, Clifford measurements are not only simpler but also more efficient for HPFE in the presence of such coherent noise. In addition, 2-SRE (or the parameter k) has little influence on the sample costs for both THR and CRM shadow estimation based on 4-design measurements, unlike the counterparts based on Clifford measurements.

Next, we offer another example to further demonstrate the advantages of Clifford measurements over 4-design measurements. Here the target and prior state σ is a pure state, and the system state has the form $\rho = (\sigma + Z_1 \sigma Z_1)/2$, which means

$$\Delta = \frac{1}{2}(Z_1 \sigma Z_1 - \sigma), \|\Delta\|_2^2 = \epsilon = 1 - \text{Tr}(\rho \sigma).$$
 (C1)

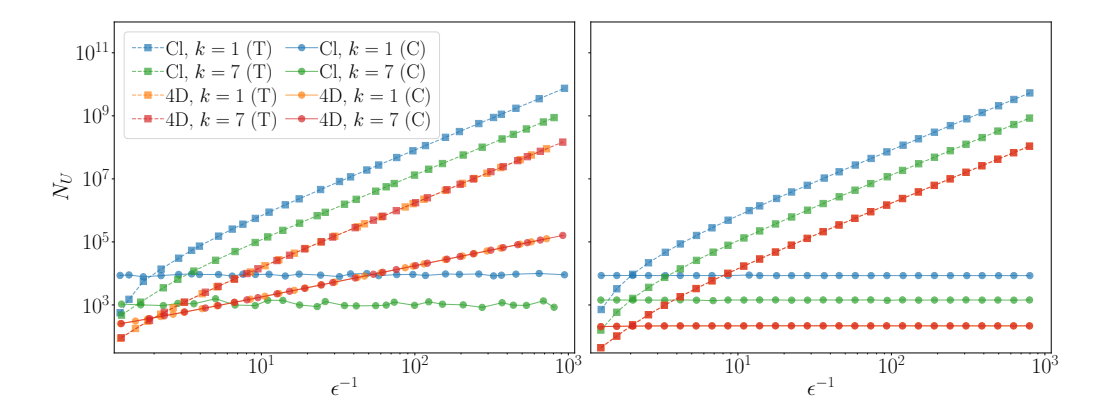


FIG. 4. Circuit sample costs N_U required for HPFE in THR (T) and CRM (C) shadow estimation based on Clifford (Cl) and 4-design (4D) measurements. Here, r = 0.25, $\delta = 0.01$, and $R = \lceil d/\epsilon^2 \rceil$. The target and prior state has the form $\sigma = |S_{7,k}\rangle\langle S_{7,k}|$ with k = 1, 7, and different system states ρ are generated by applying random local rotations described in SM Sec. S5 3 (left plot) and random Pauli channels described in SM Sec. S5 2 (right plot) to the target state σ . The results on 4-design measurements are almost independent of k, especially in the right plot.

According to Theorem 1, the variance $\mathbb{V}_*(O, \Delta)$ in CRM shadow estimation based on 4-design measurements satisfies

$$\frac{(d-1)\epsilon}{d(d+2)} \le \mathbb{V}_*(O,\Delta) \le \frac{4\epsilon}{d}.$$
 (C2)

By contrast, thanks to Theorem 3 and Proposition 4, the variance $\mathbb{V}_*(O,\Delta)$ tied to Clifford measurements satisfies $\mathbb{V}_*(O,\Delta) \leq 4\epsilon^2$, which means a constant scaling behavior of the circuit sample cost N_U with respect to the target precision. So Clifford measurements become more and more advantageous as the target precision rises.

In the numerical simulation, each target state is a seven-qubit pure state of the form $\sigma = |\phi\rangle\langle\phi|$ with

$$|\phi\rangle = \alpha |\phi_0\rangle \otimes |0\rangle + \sqrt{1 - \alpha^2} |\phi_1\rangle \otimes |1\rangle,$$
 (C3)

where $|\phi_0\rangle$ and $|\phi_1\rangle$ are six-qubit Haar-random pure states and α is a random real number such that $\ln \alpha$ is uniformly distributed in the interval [-5,0]. The sample costs required for HPFE are shown in Fig. 5. Notably, 4-design measurements require $\mathcal{O}(1/\epsilon)$ circuits, while Clifford measurements only require a constant number of circuits.

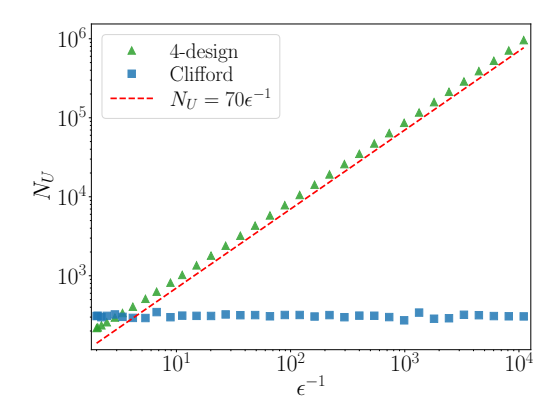


FIG. 5. Circuit sample costs N_U required for HPFE in CRM shadow estimation based on 4-design and Clifford measurements. Here, r=0.25, $\delta=0.01$, and $R=\lceil d/\epsilon^2 \rceil$. The target and prior states σ are random seven-qubit pure states that have the form in Eq. (C3), and the system states have the form $\rho=\frac{1}{2}\sigma+\frac{1}{2}Z_1\sigma Z_1$, where Z_1 denotes the Pauli Z operator acting on the first qubit.

High-Precision Fidelity Estimation with Common Randomized Measurements: Supplemental Material

CONTENTS

S1.	Proof of Proposition 1	2
S2.	Proof of Lemma 2	2
S3.	Average performance of CRM shadow estimation based on 2-designs	4
S4.	Variances in CRM shadow estimation based on 4-design measurements 1. The 4th cross moment operator 2. Exact formula for the variance $\mathbb{V}_*(O,\Delta)$ 3. Proof of Theorem 1	5 5 6 7
S5.	Noise channels 1. Depolarizing and Pauli channels 2. Sampling random Pauli channels 3. Sampling random local rotations	8 8 9 9
S6.	Relations between $\ \Delta\ _2^2$, $\ \Delta\ _1^2$, and the infidelity ϵ 1. Basic relations 2. Technical proofs	10 10 11
S7.	Properties of cross characteristic functions 1. Basic properties 2. Technical proofs	14 14 16
S8.	Variances in CRM shadow estimation based on Clifford measurements 1. Alternative formula for the variance $\mathbb{V}_*(O,\Delta)$ 2. Proof of Theorem 3 3. Variances in HPFE in the presence of depolarizing noise 4. Proof of Theorem 5	18 18 20 21 22
S9.	Variances in CRM shadow estimation based on Pauli measurements	22
S10.	 Additional numerical results CRM shadow estimation based on Clifford measurements a. HPFE in the presence of depolarizing noise b. HPFE in the presence of a special type of coherent noise c. Impact of nonstabilizerness d. Dependence of N_U on the number R of circuit reusing Comparison of different measurement ensembles a. HPFE of the GHZ state and estimation of Pauli operators b. HPFE of the ground state of the transverse-field Ising model 	24 25 25 25 26 26 27 28

In this Supplemental Material (SM), we prove the results presented in Appendix A and the main text, including Proposition 1, Lemma 2, and Theorems 1, 3, and 5. In addition, we clarify the average performance of CRM shadow estimation based on 2-designs and provide additional results on CRM shadow estimation based on 4-design, Clifford, and Pauli measurements. To this end, we explicate the relations between $\|\Delta\|_2^2$, $\|\Delta\|_1^2$, and the infidelity ϵ and elucidate the properties of cross characteristic functions, which are crucial to understanding HPFE based on CRM shadow estimation. Finally, we provide extensive numerical results on the performance of CRM shadow estimation based on Clifford, Pauli, and 4-designs measurements, and explicate the dependence of the circuit sample costs on the nonstabilizerness and the number R of circuit reusing.

Throughout this SM, \mathcal{H} denotes a d-dimensional Hilbert space with $d=2^n$, and \mathbb{I} denotes the identity operator on \mathcal{H} as in the main text. We also denote by $\mathcal{L}(\mathcal{H})$, $\mathcal{L}^{\mathrm{H}}(\mathcal{H})$, and $\mathcal{D}(\mathcal{H})$ the sets of linear operators,

Hermitian operators, and density operators on \mathcal{H} , respectively, and denote by $\mathrm{U}(\mathcal{H})$ the group of unitary operators on \mathcal{H} . In addition, $O, Q \in \mathcal{L}(\mathcal{H})$ and O is traceless; $\rho, \sigma \in \mathcal{D}(\mathcal{H})$, $\Delta = \rho - \sigma$, and $\epsilon = 1 - \|\sqrt{\rho}\sqrt{\sigma}\|_1^2$ denotes the infidelity between ρ and σ , which can be simplified as $\epsilon = 1 - \mathrm{Tr}(\rho\sigma)$ when σ is a pure state. In CRM shadow estimation, ρ and σ denote the system state and prior state, respectively; in HPFE, σ also denotes the target pure state. Furthermore, we denote by $\mathbb{1}^{\otimes 2}$ and SWAP the identity operator and swap operator on $\mathcal{H}^{\otimes 2}$.

Appendix S1: Proof of Proposition 1

The equality in Eq. (A1) of Proposition 1 was derived in Ref. [23], and the inequality follows from Lemma S1 below.

Lemma S1. Suppose $Q \in \mathcal{L}^{H}(\mathcal{H})$ and $\rho \in \mathcal{D}(\mathcal{H})$. Then

$$\operatorname{Tr}(Q^2) + [\operatorname{Tr}(\rho Q)]^2 \ge 2\operatorname{Tr}(\rho Q^2). \tag{S1}$$

Proof of Lemma S1. Note that both sides in Eq. (S1) are invariant under simultaneous unitary transformations of Q and ρ . So we can assume that Q is diagonal in the computational basis without loss of generality. Then $\text{Tr}(\rho Q)$ and $\text{Tr}(\rho Q^2)$ only depend on the diagonal part of ρ , so we can assume that ρ is also diagonal without loss of generality. Now Q and ρ can be expressed as follows:

$$Q = \sum_{i} q_{i} |i\rangle\langle i|, \quad \rho = \sum_{i} \gamma_{i} |i\rangle\langle i|, \tag{S2}$$

where q_i (γ_i) is the eigenvalue of Q (ρ) corresponding to the eigenvector $|i\rangle$. Next, we introduce

$$\varrho = \sum_{i,j} \sqrt{\gamma_i \gamma_j} |i\rangle \langle j|, \qquad |v\rangle = \sum_i q_i |i\rangle \otimes |i\rangle, \tag{S3}$$

where $\varrho \in \mathcal{D}(\mathcal{H})$ is a pure state and $|v\rangle \in \mathcal{H}^{\otimes 2}$ is not necessarily normalized. Then

$$\operatorname{Tr}(Q^{2}) = \sum_{i} q_{i}^{2} = \langle v | v \rangle = \langle v | \mathbb{1} \otimes \mathbb{1} | v \rangle,$$

$$\operatorname{Tr}(\rho Q^{2}) = \sum_{i} \gamma_{i} q_{i}^{2} = \langle v | \varrho \otimes \mathbb{1} | v \rangle = \langle v | \mathbb{1} \otimes \varrho | v \rangle,$$

$$[\operatorname{Tr}(\rho Q)]^{2} = \left(\sum_{i} \gamma_{i} q_{i}\right)^{2} = \langle v | \varrho \otimes \varrho | v \rangle.$$
(S4)

As a simple corollary, we have

$$\operatorname{Tr}(Q^2) + \left[\operatorname{Tr}(\rho Q)\right]^2 - 2\operatorname{Tr}(\rho Q^2) = \langle v | (\mathbb{1} - \varrho) \otimes (\mathbb{1} - \varrho) | v \rangle \ge 0, \tag{S5}$$

where the inequality holds because $1-\varrho$ is positive semidefinite given that ϱ is a density operator. This result implies Eq. (S1) and completes the proof of Lemma S1.

Appendix S2: Proof of Lemma 2

Proof of Lemma 2. To achieve our goal, we first derive a general expression for the variance $\mathbb{V}_R(\hat{O})$ in CRM shadow estimation following Ref. [31]. Note that the estimator $\hat{\rho}$ in Eq. (1) can also be expressed as follows:

$$\hat{\rho} = \sum_{\mathbf{s}} \hat{P}_{\rho}(\mathbf{s} \mid U) \mathcal{M}^{-1} (U^{\dagger} | \mathbf{s} \rangle \langle \mathbf{s} | U), \tag{S6}$$

where $\hat{P}_{\rho}(\mathbf{s} \mid U) = R_{\mathbf{s}}/R$ denotes the experimentally estimated probability of outcome \mathbf{s} after performing computational-basis measurements on the state $U\rho U^{\dagger}$. Here, $(R_{\mathbf{s}})_{\mathbf{s}\in\{0,1\}^n}$ obeys the multinomial distribution Multinomial $(R; (p_{\mathbf{s}})_{\mathbf{s}\in\{0,1\}^n})$, where $p_{\mathbf{s}} = P_{\rho}(\mathbf{s} \mid U) = \langle \mathbf{s} | U\rho U^{\dagger} | \mathbf{s} \rangle$ denotes the theoretical probability of

outcome s when performing a computational-basis measurement on the state $U\rho U^{\dagger}$. Accordingly, the CRM estimator for $\text{Tr}(O\rho)$ reads

$$\hat{O} = \text{Tr}(O\hat{\rho}) = \sum_{\mathbf{s}} \left[\hat{P}_{\rho}(\mathbf{s} \mid U) - P_{\sigma}(\mathbf{s} \mid U) \right] \text{Tr} \left[O \mathcal{M}^{-1} \left(U^{\dagger} | \mathbf{s} \rangle \langle \mathbf{s} | U \right) \right] + \text{Tr}(O\sigma)$$

$$= \sum_{\mathbf{s}} \left[\hat{P}_{\rho}(\mathbf{s} \mid U) - P_{\sigma}(\mathbf{s} \mid U) \right] \left[\mathcal{M}^{-1}(O) \right] (U, \mathbf{s}) + \text{Tr}(O\sigma), \tag{S7}$$

where $[\mathcal{M}^{-1}(O)](U, \mathbf{s}) := \text{Tr}[O\mathcal{M}^{-1}(U^{\dagger}|\mathbf{s}\rangle\langle\mathbf{s}|U)] = \text{Tr}[\mathcal{M}^{-1}(O)U^{\dagger}|\mathbf{s}\rangle\langle\mathbf{s}|U]$. The variance of this estimator reads

$$\mathbb{V}_{R}(\hat{O}) = \mathbb{V} \left\{ \sum_{\mathbf{s}} \left[\hat{P}_{\rho}(\mathbf{s} \mid U) - P_{\sigma}(\mathbf{s} \mid U) \right] \left[\mathcal{M}^{-1}(O) \right] (U, \mathbf{s}) \right\} \\
= \mathbb{E}_{U} \left\{ \sum_{\mathbf{s}, \mathbf{t}} \mathbb{E}_{M} \left\{ \left[\hat{P}_{\rho}(\mathbf{s} \mid U) - P_{\sigma}(\mathbf{s} \mid U) \right] \left[\hat{P}_{\rho}(\mathbf{t} \mid U) - P_{\sigma}(\mathbf{t} \mid U) \right] \right\} \left[\mathcal{M}^{-1}(O) \right] (U, \mathbf{s}) \left[\mathcal{M}^{-1}(O) \right] (U, \mathbf{t}) \right\} \\
- \left\{ \operatorname{Tr}[(\rho - \sigma)O] \right\}^{2}, \tag{S8}$$

where \mathbb{E}_{M} represents the average over the multinomial distribution.

According to well-known results on the multinomial distribution, we have

$$\mathbb{E}_{\mathcal{M}}(R_{\mathbf{s}}R_{\mathbf{t}}) = \begin{cases} R(R-1)P_{\rho}(\mathbf{s} \mid U)P_{\rho}(\mathbf{t} \mid U), & \mathbf{s} \neq \mathbf{t}, \\ R^{2}[P_{\rho}(\mathbf{s} \mid U)]^{2} + RP_{\rho}(\mathbf{s} \mid U)[1 - P_{\rho}(\mathbf{s} \mid U)], & \mathbf{s} = \mathbf{t}, \end{cases}$$
(S9)

$$\mathbb{E}_{\mathcal{M}}\left[\hat{P}_{\rho}(\mathbf{s}\mid U)\hat{P}_{\rho}(\mathbf{t}\mid U)\right] = P_{\rho}(\mathbf{s}\mid U)P_{\rho}(\mathbf{t}\mid U) + \frac{\delta_{\mathbf{s},\mathbf{t}}P_{\rho}(\mathbf{s}\mid U) - P_{\rho}(\mathbf{s}\mid U)P_{\rho}(\mathbf{t}\mid U)}{R}.$$
 (S10)

By virtue of Eq. (S10), the variance $\mathbb{V}_R(\hat{O})$ in Eq. (S8) can be expressed as follows [31]:

$$\mathbb{V}_R(\hat{O}) = \mathbb{V}_U[f_{\rho,\sigma}(U)] + \frac{\mathbb{E}_U[g_{\rho}(U)]}{R},\tag{S11}$$

where

$$f_{\rho,\sigma}(U) := \sum_{\mathbf{s}} [P_{\rho}(\mathbf{s} \mid U) - P_{\sigma}(\mathbf{s} \mid U)] [\mathcal{M}^{-1}(O)](U, \mathbf{s}) = \sum_{\mathbf{s}} P_{\Delta}(\mathbf{s} \mid U) [\mathcal{M}^{-1}(O)](U, \mathbf{s}),$$

$$g_{\rho}(U) := \sum_{\mathbf{s}} P_{\rho}(\mathbf{s} \mid U) \{ [\mathcal{M}^{-1}(O)](U, \mathbf{s}) \}^{2} - \left\{ \sum_{\mathbf{s}} P_{\rho}(\mathbf{s} \mid U) [\mathcal{M}^{-1}(O)](U, \mathbf{s}) \right\}^{2},$$
(S12)

with $\Delta = \rho - \sigma$ and $P_{\Delta}(\mathbf{s} \mid U) = \langle \mathbf{s} | U \Delta U^{\dagger} | \mathbf{s} \rangle$. To complete the proof of Lemma 2, it remains to prove the following equalities:

$$\mathbb{V}_{U}[f_{\rho,\sigma}(U)] = \mathbb{V}_{*}(O,\Delta), \quad \mathbb{E}_{U}[g_{\rho}(U)] = \mathbb{V}(O,\rho) - \mathbb{V}_{*}(O,\rho). \tag{S13}$$

By the definition of $f_{\rho,\sigma}(U)$ we can deduce that

$$\mathbb{E}_{U}[f_{\rho,\sigma}(U)] = \mathbb{E}_{U}\left\{\sum_{\mathbf{s}}[P_{\rho}(\mathbf{s}\mid U) - P_{\sigma}(\mathbf{s}\mid U)][\mathcal{M}^{-1}(O)](U,\mathbf{s})\right\} = \text{Tr}[(\rho - \sigma)O] = \text{Tr}(\Delta O),$$

$$\mathbb{E}_{U}\left\{[f_{\rho,\sigma}(U)]^{2}\right\} = \sum_{\mathbf{s},\mathbf{t}} \mathbb{E}_{U}\left\{[\mathcal{M}^{-1}(O)](U,\mathbf{s})P_{\Delta}(\mathbf{s}\mid U)[\mathcal{M}^{-1}(O)](U,\mathbf{t})P_{\Delta}(\mathbf{t}\mid U)\right\}$$

$$= \sum_{\mathbf{s},\mathbf{t}} \mathbb{E}_{U}\left[\langle \mathbf{s}|U\mathcal{M}^{-1}(O)U^{\dagger}|\mathbf{s}\rangle\langle \mathbf{s}|U\Delta U^{\dagger}|\mathbf{s}\rangle\langle \mathbf{t}|U\mathcal{M}^{-1}(O)U^{\dagger}|\mathbf{t}\rangle\langle \mathbf{t}|U\Delta U^{\dagger}|\mathbf{t}\rangle\right]$$

$$= \text{Tr}\left\{\Omega(U)\left[\mathcal{M}^{-1}(O)\otimes\Delta\right]^{\otimes 2}\right\},$$
(S14)

where the last equality follows from the definition of $\Omega(\mathcal{U})$ in Eq. (3). Therefore,

$$\mathbb{V}_{U}[f_{\rho,\sigma}(U)] = \mathbb{E}_{U}\left\{ [f_{\rho,\sigma}(U)]^{2} \right\} - \left\{ \mathbb{E}_{U}[f_{\rho,\sigma}(U)] \right\}^{2} = \operatorname{Tr}\left\{ \Omega(\mathcal{U}) \left[\mathcal{M}^{-1}(O) \otimes \Delta \right]^{\otimes 2} \right\} - \left[\operatorname{Tr}(\Delta O) \right]^{2} = \mathbb{V}_{*}(O, \Delta), \tag{S15}$$

which confirms the first equality in Eq. (S13). Here the last equality follows directly from the definition of $\mathbb{V}_*(O,\rho)$ in Eq. (5). Similarly, the second equality in Eq. (S13) can be proved as follows:

$$\mathbb{E}_{U}[g_{\rho}(U)] = \mathbb{E}_{U}\left(\sum_{\mathbf{s}} P_{\rho}(\mathbf{s} \mid U) \left\{ \left[\mathcal{M}^{-1}(O) \right](U, \mathbf{s}) \right\}^{2} \right) - \left\{ \mathbb{E}_{U} \sum_{\mathbf{s}} P_{\rho}(\mathbf{s} \mid U) \left[\mathcal{M}^{-1}(O) \right](U, \mathbf{s}) \right\}^{2}$$

$$- \mathbb{E}_{U}\left(\left\{ \sum_{\mathbf{s}} P_{\rho}(\mathbf{s} \mid U) \left[\mathcal{M}^{-1}(O) \right](U, \mathbf{s}) \right\}^{2} \right) + \left\{ \mathbb{E}_{U} \sum_{\mathbf{s}} P_{\rho}(\mathbf{s} \mid U) \left[\mathcal{M}^{-1}(O) \right](U, \mathbf{s}) \right\}^{2}$$

$$= \mathbb{V}(O, \rho) - \text{Tr}\left\{ \Omega(U) \left[\mathcal{M}^{-1}(O) \otimes \rho \right]^{\otimes 2} \right\} + \left[\text{Tr}(\rho O) \right]^{2} = \mathbb{V}(O, \rho) - \mathbb{V}_{*}(O, \rho), \tag{S16}$$

where we have employed the definitions of $\Omega(\mathcal{U})$ and $\mathbb{V}_*(O,\rho)$ in Eqs. (3) and (5), respectively. This observation completes the proof of Lemma 2.

Appendix S3: Average performance of CRM shadow estimation based on 2-designs

In this section, we clarify the average performance of CRM shadow estimation based on 2-designs. For $Q \in \mathcal{L}^{\mathrm{H}}(\mathcal{H})$, define the following ensemble of observables:

$$\mathcal{E}(Q) := \{ UQU^{\dagger} \mid U \in \mathcal{U}(\mathcal{H}) \}, \tag{S17}$$

which inherits the Haar measure on the unitary group $U(\mathcal{H})$. We then define $\mathbb{V}(\mathcal{E}(Q), \rho)$, $\mathbb{V}_*(\mathcal{E}(Q), \rho)$, and $\mathbb{V}_*(\mathcal{E}(Q), \Delta)$ as the average variances over the ensemble $\mathcal{E}(Q)$, where $\Delta = \rho - \sigma$, and ρ and σ denote the system state and prior state, respectively, as in the main text.

Proposition S5. Suppose \mathcal{U} is a unitary 2-design on \mathcal{H} and O is a traceless observable on \mathcal{H} . Then the average variances $\mathbb{V}(\mathcal{E}(O), \rho)$, $\mathbb{V}_*(\mathcal{E}(O), \rho)$, and $\mathbb{V}_*(\mathcal{E}(O), \Delta)$ in $CRM(\mathcal{U}, \sigma, R)$ read

$$\mathbb{V}(\mathcal{E}(O), \rho) = \left[1 + \frac{d - \text{Tr}(\rho^2)}{d^2 - 1}\right] \|O\|_2^2, \tag{S18}$$

$$V_*(\mathcal{E}(O), \rho) = \frac{d \operatorname{Tr}(\rho^2) - 1}{d^2 - 1} ||O||_2^2 < \frac{||O||_2^2}{d},$$
 (S19)

$$V_*(\mathcal{E}(O), \Delta) = \frac{d\|\Delta\|_2^2 \|O\|_2^2}{d^2 - 1}.$$
 (S20)

The results in Eqs. (S18) and (S19) were derived in Ref. [29]. On average, $V_*(\mathcal{E}(O), \rho)$ is already exponentially smaller than $V(\mathcal{E}(O), \rho)$, which means THR shadow estimation is efficient on average. Nevertheless, incorporating an accurate prior state can further reduce the variance and enhance the overall performance significantly. Before proving Proposition S5, we introduce an auxiliary lemma proved in Ref. [29].

Lemma S2. Suppose \mathcal{U} is a unitary 2-design on \mathcal{H} and $A, B \in \mathcal{L}(\mathcal{H})$. Then

$$\mathbb{E}_{U \sim \mathcal{U}} U A U^{\dagger} = \frac{\text{Tr}(A)}{d} \mathbb{1}, \tag{S21}$$

$$\mathbb{E}_{U \sim \mathcal{U}} \left[\left(U A U^{\dagger} \right) \otimes \left(U A U^{\dagger} \right)^{\dagger} \right] = \frac{d |\operatorname{Tr}(A)|^{2} - ||A||_{2}^{2}}{d(d^{2} - 1)} \mathbb{1}^{\otimes 2} + \frac{d ||A||_{2}^{2} - |\operatorname{Tr}(A)|^{2}}{d(d^{2} - 1)} \operatorname{SWAP}, \tag{S22}$$

$$\mathbb{E}_{U \sim \mathcal{U}} \left| \text{Tr} \left(U A U^{\dagger} B \right) \right|^{2} = \frac{d |\text{Tr}(A)|^{2} |\text{Tr}(B)|^{2} + d ||A||_{2}^{2} ||B||_{2}^{2} - |\text{Tr}(A)|^{2} ||B||_{2}^{2} - ||A||_{2}^{2} |\text{Tr}(B)|^{2}}{d(d^{2} - 1)}. \tag{S23}$$

Proof of Proposition S5. Equations (S18) and (S19) were derived in Ref. [29], so it remains to prove Eq. (S20). By assumption \mathcal{U} is a unitary 2-design and O is traceless, so the reconstruction map $\mathcal{M}^{-1}(\cdot)$ has a simple form: $\mathcal{M}^{-1}(O) = (d+1)O$ [23]. In conjunction with the definition of $\mathbb{V}_*(O,\tau)$ in Eq. (5) we can deduce that

$$\mathbb{V}_{*}(\mathcal{E}(O), \Delta) = \mathbb{E}_{W \sim \text{Haar}} \left\{ (d+1)^{2} \operatorname{Tr} \left[\Omega(\mathcal{U}) \left(WOW^{\dagger} \otimes \Delta \otimes WOW^{\dagger} \otimes \Delta \right) \right] - \left[\operatorname{Tr} \left(WOW^{\dagger} \Delta \right) \right]^{2} \right\} \\
= (d+1)^{2} \mathbb{E}_{W \sim \text{Haar}} \mathbb{E}_{U \sim \mathcal{U}} \sum_{\mathbf{s}, \mathbf{t}} \operatorname{Tr} \left[\left(|\mathbf{s}\rangle \langle \mathbf{s}| \otimes |\mathbf{t}\rangle \langle \mathbf{t}| \right) \left(UWOW^{\dagger} U^{\dagger} \right)^{\otimes 2} \right] \operatorname{Tr} \left[\left(|\mathbf{s}\rangle \langle \mathbf{s}| \otimes |\mathbf{t}\rangle \langle \mathbf{t}| \right) \left(U\Delta U^{\dagger} \right)^{\otimes 2} \right] \\
- \frac{\|O\|_{2}^{2} \|\Delta\|_{2}^{2}}{d^{2} - 1}, \tag{S24}$$

where the second equality follows from the definition of $\Omega(\mathcal{U})$ in Eq. (3). Since O and Δ are traceless, according to Lemma S2, we have

$$\mathbb{E}_{W \sim \text{Haar}} \left(UWOW^{\dagger}U^{\dagger} \right)^{\otimes 2} = \frac{\|O\|_{2}^{2}}{d(d^{2} - 1)} U^{\otimes 2} (d\text{SWAP} - 1) U^{\dagger \otimes 2} = \frac{\|O\|_{2}^{2}}{d(d^{2} - 1)} (d\text{SWAP} - 1),$$

$$\mathbb{E}_{U \sim \mathcal{U}} \left(U\Delta U^{\dagger} \right)^{\otimes 2} = \frac{\|\Delta\|_{2}^{2}}{d(d^{2} - 1)} (d\text{SWAP} - 1).$$
(S25)

Based on these results, the above expression of $\mathbb{V}_*(\mathcal{E}(O), \Delta)$ can be simplified as follows:

$$\mathbb{V}_{*}(\mathcal{E}(O), \Delta) = (d+1)^{2} \frac{\|O\|_{2}^{2}}{d(d^{2}-1)} \mathbb{E}_{U \sim \mathcal{U}} \sum_{\mathbf{s}, \mathbf{t}} \left\{ (d\delta_{\mathbf{s}, \mathbf{t}} - 1) \operatorname{Tr} \left[(|\mathbf{s}\rangle \langle \mathbf{s}| \otimes |\mathbf{t}\rangle \langle \mathbf{t}|) \left(U \Delta U^{\dagger} \right)^{\otimes 2} \right] \right\} - \frac{\|O\|_{2}^{2} \|\Delta\|_{2}^{2}}{d^{2}-1} \\
= \frac{\|O\|_{2}^{2} \|\Delta\|_{2}^{2}}{d^{2}(d-1)^{2}} \sum_{\mathbf{s}, \mathbf{t}} (d\delta_{\mathbf{s}, \mathbf{t}} - 1)^{2} - \frac{\|O\|_{2}^{2} \|\Delta\|_{2}^{2}}{d^{2}-1} = \left(\frac{1}{d-1} - \frac{1}{d^{2}-1} \right) \|O\|_{2}^{2} \|\Delta\|_{2}^{2} = \frac{d}{d^{2}-1} \|O\|_{2}^{2} \|\Delta\|_{2}^{2}, \quad (S26)$$

which confirms Eq. (S20) and completes the proof of Proposition S5.

Appendix S4: Variances in CRM shadow estimation based on 4-design measurements

In this section, we derive exact formulas for the 4th cross moment operator and the variances $\mathbb{V}_*(O, \Delta)$ and $\mathbb{V}_*(O, \rho)$ in CRM shadow estimation based on 4-design measurements (see Lemmas S4 and S5 below). On this basis we prove Theorem 1 in the main text.

1. The 4th cross moment operator

Given an ensemble \mathcal{U} of unitary transformations on \mathcal{H} , according to the definition in Eq. (3), the 4th cross moment operator $\Omega(\mathcal{U})$ reads

$$\Omega(\mathcal{U}) = \sum_{\mathbf{s}, \mathbf{t}} \mathbb{E}_{U \sim \mathcal{U}} U^{\dagger \otimes 4} \left[(|\mathbf{s}\rangle \langle \mathbf{s}|)^{\otimes 2} \otimes (|\mathbf{t}\rangle \langle \mathbf{t}|)^{\otimes 2} \right] U^{\otimes 4} = \Omega_{1}(\mathcal{U}) + \Omega_{2}(\mathcal{U}), \tag{S27}$$

where

$$\Omega_{1}(\mathcal{U}) := \sum_{\mathbf{s}} \mathbb{E}_{U \sim \mathcal{U}} U^{\dagger \otimes 4} \big[(|\mathbf{s}\rangle \langle \mathbf{s}|)^{\otimes 4} \big] U^{\otimes 4},
\Omega_{2}(\mathcal{U}) := \sum_{\mathbf{s} \neq \mathbf{t}} \mathbb{E}_{U \sim \mathcal{U}} U^{\dagger \otimes 4} \big[(|\mathbf{s}\rangle \langle \mathbf{s}|)^{\otimes 2} \otimes (|\mathbf{t}\rangle \langle \mathbf{t}|)^{\otimes 2} \big] U^{\otimes 4}.$$
(S28)

Now, suppose \mathcal{U} is a unitary 4-design. To simplify the expressions of $\Omega_1(\mathcal{U})$, $\Omega_2(\mathcal{U})$, and $\Omega(\mathcal{U})$, we need to introduce some auxiliary results. According to Schur-Weyl duality, the tensor power $\mathcal{H}^{\otimes 4}$ can be decomposed as follows:

$$\mathcal{H}^{\otimes 4} = \bigoplus_{\lambda} \mathcal{H}_{\lambda} = \bigoplus_{\lambda} \mathcal{W}_{\lambda} \otimes \mathcal{S}_{\lambda}, \tag{S29}$$

where λ denotes a nonincreasing partition of 4 into no more than d parts, while W_{λ} and S_{λ} denote the corresponding Weyl module and Specht module, which carry irreducible representations of the unitary group $U(\mathcal{H})$ and permutation group S_4 , respectively. Let $D_{\lambda} = \dim(W_{\lambda})$ and $d_{\lambda} = \dim(S_{\lambda})$. The projector onto \mathcal{H}_{λ} can be expressed as follows:

$$P_{\lambda} = \frac{d_{\lambda}}{4!} \sum_{\pi \in S_4} \chi^{\lambda}(\pi) W_{\pi}, \tag{S30}$$

where W_{π} denotes the permutation operator on $\mathcal{H}^{\otimes 4}$ associated with the permutation π , and $\chi^{\lambda}(\pi)$ denotes the character of π corresponding to the representation λ .

Lemma S3. Suppose \mathcal{U} is a unitary 4-design on \mathcal{H} and $Q \in \mathcal{L}^{\mathrm{H}}(\mathcal{H}^{\otimes 4})$. Then

$$\mathbb{E}_{U \sim \mathcal{U}} \operatorname{Tr} \left(U^{\otimes 4} Q U^{\dagger \otimes 4} \right) = \frac{1}{4!} \sum_{\pi \in S_4} \operatorname{Tr}(Q W_{\pi}) W_{\pi^{-1}} \sum_{\lambda} \frac{d_{\lambda}}{D_{\lambda}} P_{\lambda}.$$
 (S31)

We omit the proof of Lemma S3 here; interested readers may refer to Refs. [28, 34, 35] for rigorous proofs and further discussions.

Next, it is convenient to introduce the special subgroup $G = \{e, (12), (34), (12)(34)\}$ of S_4 , where e denotes the identity permutation. Denote by $P_G = \sum_{\pi \in G} W_{\pi}/4$ the projector onto the subspace of $\mathcal{H}^{\otimes 4}$ that carries the trivial representation of G. Note that P_G commutes with each projector P_{λ} in Eq. (S30).

Lemma S4. Suppose \mathcal{U} is a unitary 4-design on \mathcal{H} . Then $\Omega_1(\mathcal{U})$, $\Omega_2(\mathcal{U})$, and the cross moment operator $\Omega(\mathcal{U})$ read

$$\Omega_1(\mathcal{U}) = \frac{24P_{[4]}}{(d+1)(d+2)(d+3)}, \quad \Omega_2(\mathcal{U}) = \frac{1}{6}(d^2 - d)\sum_{\lambda} \frac{d_{\lambda}}{D_{\lambda}} P_G P_{\lambda}, \tag{S32}$$

$$\Omega(\mathcal{U}) = \Omega_1(\mathcal{U}) + \Omega_2(\mathcal{U}) = \frac{24P_{[4]}}{(d+1)(d+2)(d+3)} + \frac{1}{6}(d^2 - d) \sum_{\lambda} \frac{d_{\lambda}}{D_{\lambda}} P_G P_{\lambda}.$$
 (S33)

Proof of Lemma S4. According to Eq. (S28) we have

$$\Omega_1(\mathcal{U}) = \sum_{\mathbf{s}} \mathbb{E}_{U \sim \mathcal{U}} U^{\dagger \otimes 4} \left[(|\mathbf{s}\rangle \langle \mathbf{s}|)^{\otimes 4} \right] U^{\otimes 4} = \frac{24P_{[4]}}{(d+1)(d+2)(d+3)}, \tag{S34}$$

where the second equality follows from Schur-Weyl duality given that \mathcal{U} is a unitary 4-design by assumption. In addition, by virtue of Lemma S3 we can deduce that

$$\Omega_{2}(\mathcal{U}) = \sum_{\mathbf{s} \neq \mathbf{t}} \mathbb{E}_{U \sim \mathcal{U}} U^{\dagger \otimes 4} \left[(|\mathbf{s}\rangle \langle \mathbf{s}|)^{\otimes 2} \otimes (|\mathbf{t}\rangle \langle \mathbf{t}|)^{\otimes 2} \right] U^{\otimes 4}
= \frac{1}{4!} \sum_{\pi \in S_{4}} \sum_{\mathbf{s} \neq \mathbf{t}} \operatorname{Tr} \left[(|\mathbf{s}\rangle \langle \mathbf{s}|)^{\otimes 2} \otimes (|\mathbf{t}\rangle \langle \mathbf{t}|)^{\otimes 2} W_{\pi^{-1}} \right] W_{\pi} \sum_{\lambda} \frac{d_{\lambda}}{D_{\lambda}} P_{\lambda}
= \frac{1}{4!} \left(d^{2} - d \right) \sum_{\pi \in G} W_{\pi} \sum_{\lambda} \frac{d_{\lambda}}{D_{\lambda}} P_{\lambda} = \frac{1}{6} \left(d^{2} - d \right) \sum_{\lambda} \frac{d_{\lambda}}{D_{\lambda}} P_{G} P_{\lambda},$$
(S35)

where the third equality holds because $\text{Tr}[(|\mathbf{s}\rangle\langle\mathbf{s}|)^{\otimes 2}\otimes(|\mathbf{t}\rangle\langle\mathbf{t}|)^{\otimes 2}W_{\pi^{-1}}]$ is equal to 1 (0) when $\pi \in G$ ($\pi \notin G$), while the last equality follows from the definition of P_G . The above two equations together confirm Eq. (S32). Finally, Eq. (S33) follows from Eqs. (S27) and (S32), which completes the proof of Lemma S4.

2. Exact formula for the variance $V_*(O, \Delta)$

Lemma S5. Suppose \mathcal{U} is a unitary 4-design on \mathcal{H} , O is a traceless observable on \mathcal{H} , and $\rho \in \mathcal{D}(\mathcal{H})$ is the system state. Then, the variances $\mathbb{V}_*(O,\Delta)$ and $\mathbb{V}_*(O,\rho)$ in $CRM(\mathcal{U},\sigma,R)$ read

$$\mathbb{V}_{*}(O,\Delta) = \frac{d^{2} + 3d + 4}{d(d+2)(d+3)} [\text{Tr}(\Delta O)]^{2} + \frac{2(d+1)^{2}}{d(d+2)(d+3)} \text{Tr}(\Delta^{2}O^{2})
+ \frac{d+1}{d(d+3)} \text{Tr}(\Delta^{2}) \text{Tr}(O^{2}) - \frac{2(d+1)}{d(d+2)(d+3)} \text{Tr}(\Delta O\Delta O).$$
(S36)
$$\mathbb{V}_{*}(O,\rho) = \frac{d^{2} + 3d + 4}{d(d+2)(d+3)} [\text{Tr}(\rho O)]^{2} + \frac{2(d+1)^{2}}{d(d+2)(d+3)} \text{Tr}(\rho^{2}O^{2})
+ \frac{d+1}{d(d+3)} \text{Tr}(\rho^{2}) \text{Tr}(O^{2}) - \frac{2(d+1)}{d(d+2)(d+3)} \text{Tr}(\rho O\rho O) - \frac{4(d+1)}{d(d+2)(d+3)} \text{Tr}(\rho O^{2}).$$
(S37)

Proof of Lemma S5. By assumption \mathcal{U} is a unitary 4-design and O is traceless, so the reconstruction map $\mathcal{M}^{-1}(\cdot)$ has a simple form: $\mathcal{M}^{-1}(O) = (d+1)O$ [23]. In conjunction with Eq. (5) we can deduce that

$$\mathbb{V}_*(O,\Delta) = \operatorname{Tr}\left\{\Omega(\mathcal{U})\left[\mathcal{M}^{-1}(O)\otimes\Delta\right]^{\otimes 2}\right\} - \left[\operatorname{Tr}(O\Delta)\right]^2 = (d+1)^2 \operatorname{Tr}\left[\Omega(\mathcal{U})(O\otimes\Delta)^{\otimes 2}\right] - \left[\operatorname{Tr}(O\Delta)\right]^2 \\
= (d+1)^2 \operatorname{Tr}\left[\Omega_1(\mathcal{U})(O\otimes\Delta)^{\otimes 2}\right] + (d+1)^2 \operatorname{Tr}\left[\Omega_2(\mathcal{U})(O\otimes\Delta)^{\otimes 2}\right] - \left[\operatorname{Tr}(O\Delta)\right]^2,$$
(S38)

where $\Omega(\mathcal{U})$ is defined in Eq. (3) and the last equality holds because $\Omega(\mathcal{U}) = \Omega_1(\mathcal{U}) + \Omega_2(\mathcal{U})$ according to Eq. (S27). Thanks to Lemma S4, the first term in Eq. (S38) can be evaluated as follows:

$$(d+1)^{2} \operatorname{Tr} \left[\Omega_{1}(\mathcal{U})(O \otimes \Delta)^{\otimes 2} \right] = \frac{24(d+1)}{(d+2)(d+3)} \operatorname{Tr} \left[P_{[4]}(O \otimes \Delta)^{\otimes 2} \right] = \frac{d+1}{(d+2)(d+3)} \sum_{\pi \in S_{4}} \operatorname{Tr} \left[W_{\pi}(O \otimes \Delta)^{\otimes 2} \right]$$

$$= \frac{d+1}{(d+2)(d+3)} \left\{ 2 \left[\operatorname{Tr}(\Delta O) \right]^{2} + \operatorname{Tr}(\Delta^{2}) \operatorname{Tr}(O^{2}) + 2 \operatorname{Tr}(\Delta O \Delta O) + 4 \operatorname{Tr}(\Delta^{2} O^{2}) \right\}.$$
(S39)

Similarly, the second term in Eq. (S38) can be evaluated as follows:

$$(d+1)^{2} \operatorname{Tr} \left[\Omega_{2}(\mathcal{U})(O \otimes \Delta)^{\otimes 2}\right] = \frac{1}{6} \left(d^{2} - d\right) (d+1)^{2} \sum_{\lambda} \frac{d_{\lambda}}{D_{\lambda}} \operatorname{Tr} \left[(O \otimes \Delta \otimes O \otimes \Delta)P_{G}P_{\lambda}\right]$$

$$= \frac{1}{6} \left(d^{2} - d\right) (d+1)^{2} \sum_{\lambda} \frac{d_{\lambda}^{2}}{D_{\lambda}} \frac{1}{4 \times 4!} \sum_{\zeta \in G, \pi \in S_{4}} \chi^{\lambda}(\pi) \operatorname{Tr} \left[(O \otimes \Delta \otimes O \otimes \Delta)W_{\zeta\pi}\right], \tag{S40}$$

where the second equality follows from the definition $P_G = \sum_{\zeta \in G} W_{\zeta}/4$ and the formula for P_{λ} in Eq. (S30). In addition, the dimensions d_{λ}, D_{λ} and characters $\chi^{\lambda}(\pi)$ featured in the above equation can be found in Ref. [46]. After careful calculations of individual terms in Eq. (S40) we can derive the following result:

$$(d+1)^{2} \operatorname{Tr} \left[\Omega_{2}(\mathcal{U})(O \otimes \Delta)^{\otimes 2}\right] = \frac{(d+1)(d^{2}+3d+4)}{d(d+2)(d+3)} \left[\operatorname{Tr}(\Delta O)\right]^{2} - \frac{2(d+1)(d-1)}{d(d+2)(d+3)} \operatorname{Tr}\left(\Delta^{2} O^{2}\right) + \frac{2(d+1)}{d(d+2)(d+3)} \operatorname{Tr}\left(\Delta^{2}\right) \operatorname{Tr}\left(O^{2}\right) - \frac{2(d+1)^{2}}{d(d+2)(d+3)} \operatorname{Tr}(\Delta O \Delta O).$$
 (S41)

Combining Eqs. (S38), (S39), and (S41), we get

$$\mathbb{V}_{*}(O,\Delta) = \frac{d^{2} + 3d + 4}{d(d+2)(d+3)} \left[\text{Tr}(\Delta O) \right]^{2} + \frac{2(d+1)^{2}}{d(d+2)(d+3)} \operatorname{Tr}(\Delta^{2} O^{2})
+ \frac{d+1}{d(d+3)} \operatorname{Tr}(\Delta^{2}) \operatorname{Tr}(O^{2}) - \frac{2(d+1)}{d(d+2)(d+3)} \operatorname{Tr}(\Delta O \Delta O),$$
(S42)

which confirms Eq. (S36).

Finally, Eq. (S37) can be proved in a similar way, and the additional term compared with Eq. (S36) is tied to the fact that $\text{Tr}(\rho) \neq 0$. This observation completes the proof of Lemma S5.

3. Proof of Theorem 1

Before proving Theorem 1, we need to introduce another auxiliary lemma.

Lemma S6. Suppose $A, B \in \mathcal{L}^H(\mathcal{H})$ are traceless Hermitian operators on \mathcal{H} , and W_{π} is the permutation operator on $\mathcal{H}^{\otimes 4}$ associated with some permutation π in S_4 . Then

$$[\operatorname{Tr}(AB)]^{2} \leq \|A\|_{2}^{2} \|B\|_{2}^{2}, \quad |\operatorname{Tr}(ABAB)| \leq \operatorname{Tr}(A^{2}B^{2}) \leq \|A\|_{2}^{2} \|B\|^{2} \leq \|A\|_{2}^{2} \|B\|_{2}^{2}, \tag{S43}$$
$$\left|\operatorname{Tr}[W_{\pi}(A \otimes B)^{\otimes 2}]\right| \leq \|A\|_{2}^{2} \|B\|_{2}^{2}. \tag{S44}$$

Proof of Lemma S6. The first two inequalities in Eq. (S43) follow from the operator Cauchy-Schwarz inequality, the third inequality follows from the operator Hölder inequality, and the last inequality holds because $||B|| \le ||B||_2$.

Next, we turn to Eq. (S44). Recall that any permutation can be expressed as a product of disjoint cycles. Since A, B are traceless by assumption, $\text{Tr}[W_{\pi}(A \otimes B)^{\otimes 2}]$ vanishes whenever π contains a trivial cycle (or has a fixed point). If π does not contain any trivial cycle, then π is composed of either one cycle of length 4 or two cycles of length 2. In the former case, $\text{Tr}[W_{\pi}(A \otimes B)^{\otimes 2}]$ is equal to either Tr(ABAB) or $\text{Tr}(A^2B^2)$. In the latter case, $\text{Tr}[W_{\pi}(A \otimes B)^{\otimes 2}]$ is equal to either $[\text{Tr}(AB)]^2$ or $\text{Tr}(A^2)$ $\text{Tr}(B^2) = ||A||_2^2 ||B||_2^2$. So Eq. (S44) is a simple corollary of Eq. (S43).

Proof of Theorem 1. By virtue of Lemmas S5 and S6 we can deduce that

$$\mathbb{V}_{*}(O,\Delta) = \frac{d^{2} + 3d + 4}{d(d+2)(d+3)} [\text{Tr}(\Delta O)]^{2} + \frac{2(d+1)^{2}}{d(d+2)(d+3)} \text{Tr}(\Delta^{2} O^{2})
+ \frac{d+1}{d(d+3)} \text{Tr}(\Delta^{2}) \text{Tr}(O^{2}) - \frac{2(d+1)}{d(d+2)(d+3)} \text{Tr}(\Delta O \Delta O)
\geq \frac{2(d+1)^{2}}{d(d+2)(d+3)} \text{Tr}(\Delta^{2} O^{2}) + \frac{d+1}{d(d+3)} \text{Tr}(\Delta^{2}) \text{Tr}(O^{2}) - \frac{2(d+1)}{d(d+2)(d+3)} \text{Tr}(\Delta^{2} O^{2})
\geq \frac{d+1}{d(d+3)} \text{Tr}(\Delta^{2}) \text{Tr}(O^{2}) \geq \frac{\|\Delta\|_{2}^{2} \|O\|_{2}^{2}}{d+2},$$
(S45)

which confirms the first inequality in Eq. (8). On the other hand, we have

$$\mathbb{V}_{*}(O,\Delta) \leq \left[\frac{d^{2}+3d+4}{d(d+2)(d+3)} + \frac{2(d+1)^{2}}{d(d+2)(d+3)} + \frac{d+1}{d(d+3)} + \frac{2(d+1)}{d(d+2)(d+3)} \right] ||O||_{2}^{2} ||\Delta||_{2}^{2} \\
= \frac{2(2d^{2}+6d+5)}{d(d+2)(d+3)} ||O||_{2}^{2} ||\Delta||_{2}^{2} \leq \frac{4}{d} ||O||_{2}^{2} ||\Delta||_{2}^{2},$$
(S46)

which confirms the second inequality in Eq. (8). The last inequality in Eq. (8) follows from Proposition 2, which completes the proof of Theorem 1.

Appendix S5: Noise channels

1. Depolarizing and Pauli channels

In this section, we review some noise channels that are relevant to the current study. A depolarizing channel \mathcal{N} is defined via the following action:

$$\mathcal{N}(\sigma) = (1 - p)\sigma + p\frac{1}{d}, \quad \sigma \in \mathcal{D}(\mathcal{H}),$$
 (S47)

where $0 \le p \le 1$ quantifies the strength of noise. Note that $\mathcal{N}(\sigma)$ always commutes with σ .

Recall that $\overline{\mathcal{P}}_n = \{I, X, Y, Z\}^{\otimes n}$ denotes the set of *n*-qubit Pauli operators. We can label the elements in $\overline{\mathcal{P}}_n$ using integers $0, 1, \ldots, d^2 - 1$, which leads to the expression $\overline{\mathcal{P}}_n = \{P_i\}_{i=0}^{d^2 - 1}$. By convention $P_0 = \mathbb{1} = I^{\otimes n}$, but the specific labeling of other elements is not essential to us. An *n*-qubit Pauli channel \mathscr{P} has the form:

$$\mathscr{P}(\sigma) = \sum_{P \in \overline{\mathcal{P}}_n} p(P) P \sigma P = \left(1 - \sum_{i=1}^{d^2 - 1} p_i\right) \sigma + \sum_{i=1}^{d^2 - 1} p_i P_i \sigma P_i, \quad \sigma \in \mathcal{D}(\mathcal{H}),$$
 (S48)

where $p_i \ge 0$ for $i = 0, 1, \dots, d^2 - 1$ and $\sum_{i=0}^{d^2 - 1} p_i = 1$. Note that \mathscr{P} is completely characterized by the vector $\mathbf{p} = (p_1, p_2, \dots, p_{d^2 - 1})$. Let

$$\|\mathbf{p}\|_a = \left(\sum_{i=1}^{d^2 - 1} p_i^a\right)^{1/a}, \quad a \ge 1.$$
 (S49)

Then the above Pauli channel can also be expressed as follows:

$$\mathscr{P}(\sigma) = (1 - \|\mathbf{p}\|_1)\sigma + \sum_{i=1}^{d^2 - 1} p_i P_i \sigma P_i. \tag{S50}$$

If there is only one nonzero element p_k in \mathbf{p} , then the channel reduces to a single-error Pauli channel:

$$\mathscr{P}(\sigma) = (1 - p_k)\sigma + p_k P_k \sigma P_k. \tag{S51}$$

In general, $\mathscr{P}(\sigma)$ does not necessarily commute with σ . Nevertheless, if σ is a stabilizer state, then $P_i \sigma P_i$ is also a stabilizer state for each $i = 0, 1, \ldots, d^2 - 1$; moreover, each $P_i \sigma P_i$ is either identical to σ or orthogonal to σ , so $\mathscr{P}(\sigma)$ commutes with σ .

2. Sampling random Pauli channels

In this section, we explain the numerical simulation procedure for sampling a random Pauli channel as employed in the main text. We begin by generating a random real vector $\mathbf{p} = (p_1, p_2, \dots, p_{d^2-1})$ of dimension $d^2 - 1$, where each entry p_i is independently sampled from the uniform distribution over [0, 1]. Next, we choose a parameter β with $0 \le \beta \le 1$ and renormalize the vector such that $\|\mathbf{p}\|_1 = \beta$. Then the resulting vector \mathbf{p} can be used to define a Pauli channel according to Eq. (S50). On average we have $\bar{\epsilon} \sim \|\mathbf{p}\|_1 = \beta$ by Eq. (S65) in Sec. S6. By adjusting the parameter β we can control the average infidelity $\bar{\epsilon}$ or generate a desired distribution.

3. Sampling random local rotations

A rotation operator for a single qubit is a unitary operator of the form

$$\exp\left(-\mathrm{i}\frac{\theta}{2}\boldsymbol{v}\cdot\boldsymbol{\sigma}\right),\tag{S52}$$

where σ denotes the vector composed of the three Pauli operators, v is a normalized real unit vector in dimension 3 that denotes the rotation axis, and $\theta \in [0, 2\pi)$ denotes the rotation angle. A local rotation operator on \mathcal{H} is a unitary operator that can be expressed as a tensor product of n rotation operators for a single qubit:

$$U = \bigotimes_{k} U_{k}, \quad U_{k} = \exp\left(-i\frac{\theta_{k}}{2}\boldsymbol{v}_{k}\cdot\boldsymbol{\sigma}\right) = \cos\left(\frac{\theta_{k}}{2}\right)I - i\sin\left(\frac{\theta_{k}}{2}\right)(\boldsymbol{v}_{k}\cdot\boldsymbol{\sigma}), \tag{S53}$$

where v_k denotes the rotation axis of qubit k and $\theta_k \in [0, 2\pi)$ denotes the corresponding rotation angle. Here we are interested in local rotation operators because they can model local coherent noise.

The following proposition clarifies the average gate infidelity of the above rotation operator, which is instructive for sampling random unitary operators in numerical simulations.

Proposition S6. Suppose U is the rotation operator presented in Eq. (S53), and $|\phi\rangle$ is a Haar-random pure state in \mathcal{H} . Then the average gate infidelity $\bar{\epsilon}$ of U reads

$$\bar{\epsilon} = 1 - \mathbb{E}_{|\phi\rangle \sim \text{Haar}} \operatorname{Tr} \left[|\phi\rangle \langle \phi| U |\phi\rangle \langle \phi| U^{\dagger} \right] = \frac{d(1-\xi)}{d+1},$$
 (S54)

where $\xi = \prod_{k} [\cos(\theta_k/2)]^2$.

By virtue of Eq. (S53) and Proposition S6 we can introduce a method for sampling a random rotation operator with a given average gate infidelity $\bar{\epsilon}$. First, we randomly choose n rotation axes v_1, v_2, \ldots, v_n uniformly and independently on the Bloch sphere. Then, we generate a random real vector $\mathbf{h} = (h_1, h_2, \ldots, h_n) \in \mathbb{R}^n$, where each entry is sampled from the uniform distribution over (0,1] and renormalize the vector such that

$$\prod_{k} h_k = \xi = 1 - \frac{(d+1)\bar{\epsilon}}{d}.$$
(S55)

Finally, the rotation angle for each qubit can be chosen as follows:

$$\theta_k = \arccos(2h_k - 1), \quad k = 1, 2, \dots, n. \tag{S56}$$

By virtue of the axes v_k and angles θ_k for k = 1, 2, ..., n we can construct a local rotation operator as in Eq. (S53). Based on this method, it is also straightforward to sample a random rotation operator such that $1/\bar{\epsilon}$ is uniformly distributed in a certain interval.

Proof of Proposition S6. According to Schur-Weyl duality, we have

$$\mathbb{E}_{|\phi\rangle \sim \text{Haar}}(|\phi\rangle\langle\phi| \otimes |\phi\rangle\langle\phi|) = \frac{\mathbb{1} + \text{SWAP}}{d(d+1)}.$$
 (S57)

Therefore,

$$\mathbb{E}_{|\phi\rangle\sim\text{Haar}}\operatorname{Tr}\left[|\phi\rangle\langle\phi|U|\phi\rangle\langle\phi|U^{\dagger}\right] = \mathbb{E}_{|\phi\rangle\sim\text{Haar}}\operatorname{Tr}\left[(|\phi\rangle\langle\phi|\otimes|\phi\rangle\langle\phi|)\left(U\otimes U^{\dagger}\right)\right] = \frac{d+|\operatorname{Tr}(U)|^{2}}{d(d+1)} = \frac{1+d\xi}{d+1}, \quad (S58)$$

which implies Eq. (S54). Here the last equality holds because $Tr(U) = d \prod_k \cos(\theta_k/2) = d\sqrt{\xi}$.

1. Basic relations

According to the discussions in the main text, the deviation $\Delta = \rho - \sigma$ of the system state ρ from the prior state σ plays a crucial role in CRM shadow estimation. In this section, we focus on the case in which σ is a pure state and clarify the relations between $\|\Delta\|_2^2$, $\|\Delta\|_1^2$, and the infidelity ϵ , which are crucial to understanding the performance of HPFE. The following three propositions are proved in Sec. S6 2, in which Propositions S8 and S9 strengthen Propositions 2 and 3 in the main text.

Proposition S7. Suppose $\sigma, \rho \in \mathcal{D}(\mathcal{H}), \ \Delta = \rho - \sigma, \ and \ \epsilon \ is the infidelity between <math>\rho$ and σ . Then

$$2\|\Delta\|_{2}^{2} \le \|\Delta\|_{1}^{2} \le 4\epsilon,\tag{S59}$$

where the first inequality is saturated if and only if (iff) rank(Δ) ≤ 2 , and the second inequality is saturated iff both ρ and σ are pure states.

Proposition S8. Suppose $\sigma, \rho \in \mathcal{D}(\mathcal{H})$, where σ is a pure state, $\Delta = \rho - \sigma$, and ϵ is the infidelity between ρ and σ . Then

$$2\|\Delta\|_{2}^{2} \le \|\Delta\|_{1}^{2} \le \frac{4(d-1)}{d}\|\Delta\|_{2}^{2},\tag{S60}$$

$$\frac{d}{d-1}\epsilon^2 \le \|\Delta\|_2^2 \le 2\epsilon,\tag{S61}$$

$$4\epsilon^2 \le \|\Delta\|_1^2 \le 4\epsilon. \tag{S62}$$

Here the first inequality in Eq. (S60) is saturated iff $\operatorname{rank}(\Delta) \leq 2$, and the second inequality is saturated iff all eigenvalues of Δ , except for the smallest one, are equal. The first inequality in Eq. (S61) is saturated iff $\rho = (1 - \epsilon)\sigma + \epsilon(1 - \sigma)/(d - 1)$, and the second inequality is saturated iff ρ is a pure state. The first inequality in Eq. (S62) is saturated iff ρ and σ commute, and the second inequality is saturated iff ρ is a pure state or is orthogonal to σ .

Now, suppose \mathscr{N} is a noise channel and $\rho = \mathscr{N}(\sigma)$. If \mathscr{N} is induced by coherent noise, then ρ is a pure state and $\|\Delta\|_2^2 = 2\epsilon$, which saturates the upper bound in Eq. (S61). If \mathscr{N} is the depolarizing channel defined in Eq. (S47), then $\|\Delta\|_2^2 = d\epsilon^2/(d-1)$, which saturates the lower bound in Eq. (S61).

Next, suppose $\mathcal{N} = \mathcal{P}$ is the Pauli channel characterized by the vector $\mathbf{p} = (p_1, p_2, \dots, p_{d^2-1})$ as in Eq. (S50). Then

$$\Delta = \mathcal{P}(\sigma) - \sigma = \sum_{i=1}^{d^2 - 1} p_i (P_i \sigma P_i - \sigma), \quad \|\Delta\|_1 \le \sum_{i=1}^{d^2 - 1} p_i \|P_i \sigma P_i - \sigma\|_1 \le 2\|\mathbf{p}\|_1.$$
 (S63)

If in addition σ is a pure state, then the infidelity ϵ between ρ and σ reads

$$\epsilon = 1 - \text{Tr}[\mathscr{P}(\sigma)\sigma] = \sum_{i=1}^{d^2 - 1} p_i [1 - \text{Tr}(P_i \sigma P_i \sigma)] \le ||\mathbf{p}||_1.$$
 (S64)

If in addition σ is a stabilizer state, then ρ commutes with σ , which means $2\|\Delta\|_2^2 \leq \|\Delta\|_1^2 = 4\epsilon^2$. To be concrete, we have $\|\Delta\|_1 = 2\epsilon = 2\sum_i' p_i$, where the summation runs over all i such that $\text{Tr}(P_i\sigma P_i\sigma) = 0$, that is, P_i does not commute with all stabilizer operators of σ . If instead σ is a Haar-random pure state, then $\|\Delta\|_2$, $\|\Delta\|_1$, and ϵ usually have the same order of magnitude as $\|\mathbf{p}\|_1$ according to the following proposition.

Proposition S9. Suppose $\sigma = |\phi\rangle\langle\phi|$ is a Haar-random pure state on \mathcal{H} , \mathscr{P} is the Pauli channel characterized by the vector $\mathbf{p} = (p_1, p_2, \dots, p_{d^2-1})$, $\rho = \mathscr{P}(\sigma)$, $\Delta = \rho - \sigma$, and ϵ is the infidelity between ρ and σ . Then

$$\bar{\epsilon} = 1 - \mathbb{E}_{|\phi\rangle \sim \text{Haar}} \operatorname{Tr}[\sigma \mathscr{P}(\sigma)] = \frac{d}{d+1} \|\mathbf{p}\|_1,$$
 (S65)

$$\mathbb{E}_{|\phi\rangle \sim \text{Haar}} \|\Delta\|_{2}^{2} = \frac{d}{d+1} \|\mathbf{p}\|_{1}^{2} + \frac{d}{d+1} \|\mathbf{p}\|_{2}^{2}, \tag{S66}$$

$$\overline{\epsilon}^2 \le \overline{\epsilon^2} \le \frac{d}{d-1} \overline{\epsilon^2} \le \mathbb{E}_{|\phi\rangle \sim \text{Haar}} \|\Delta\|_2^2 \le \frac{2(d+1)}{d} \overline{\epsilon}^2, \tag{S67}$$

$$4\bar{\epsilon}^2 \le 4\bar{\epsilon}^2 \le \mathbb{E}_{|\phi\rangle \sim \text{Haar}} \|\Delta\|_1^2 \le \frac{8(d^2 - 1)}{d^2} \bar{\epsilon}^2 \le 8\bar{\epsilon}^2.$$
 (S68)

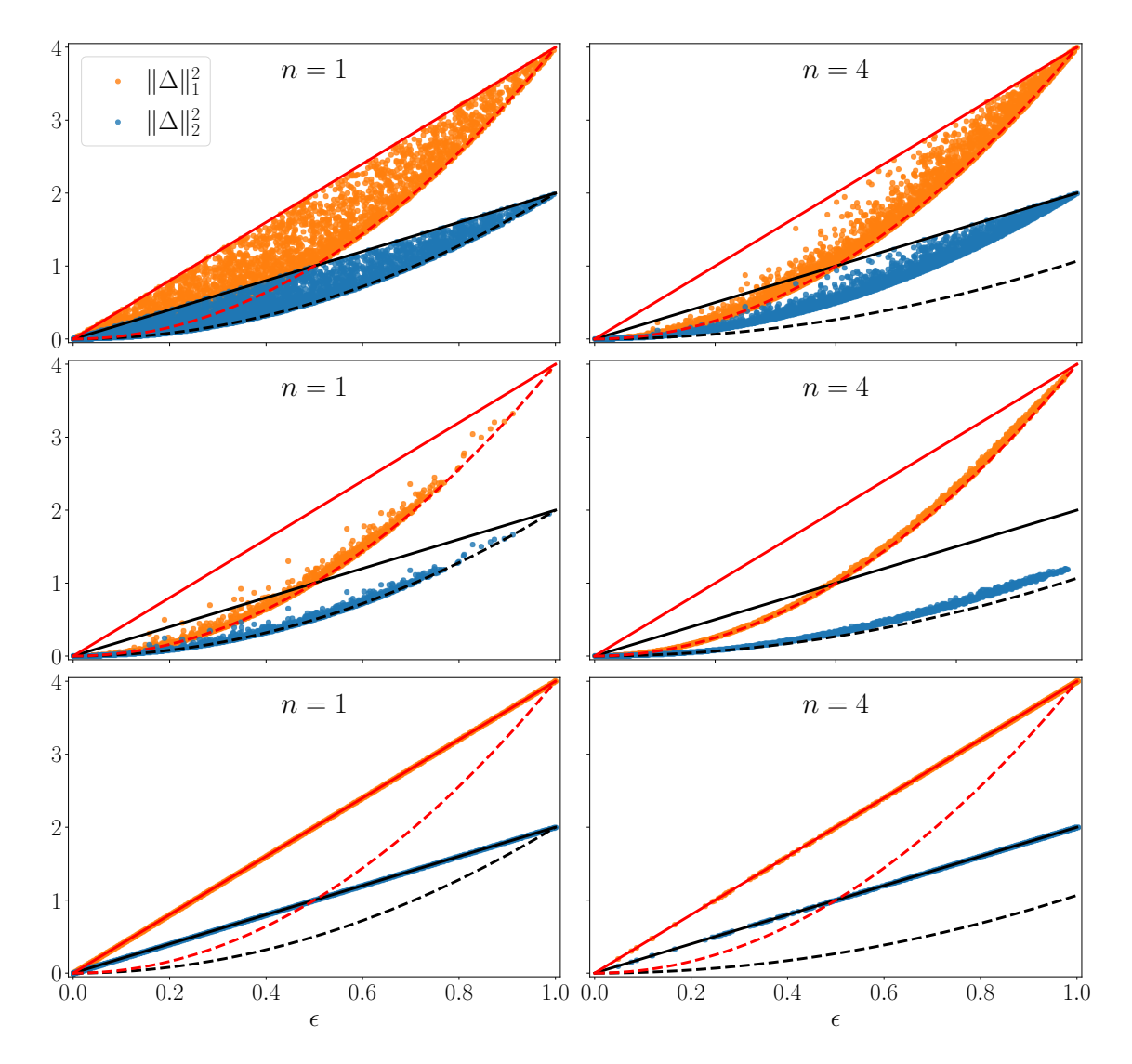


FIG. S1. Scatter plots on the relations between $\|\Delta\|_1^2$, $\|\Delta\|_2^2$, and the infidelity ϵ , where $\Delta = \rho - \sigma$. Here each σ is an n-qubit Haar-random pure state with n=1,4 and $\rho=\mathcal{N}(\sigma)$, where \mathcal{N} denotes a random single-error Pauli channel for the first row, a random Pauli channel (described in Sec. S52) for the second row, and a random coherent channel [random local rotations with rotation axes randomly oriented on the Bloch sphere and rotation angles uniformly distributed in the interval $[0,2\pi)$] for the third row. For each plot, 2000 Haar-random pure states together with 2000 random channels are generated. The red solid and dashed lines represent the upper and lower bounds for $\|\Delta\|_2^2$ presented in Eq. (S62), while the black solid and dashed lines represent the upper and lower bounds for $\|\Delta\|_2^2$ presented in Eq. (S61).

Figure S1 illustrates the relations between $\|\Delta\|_2^2$, $\|\Delta\|_1^2$, and the infidelity ϵ under three different noise models, namely, single-error Pauli noise, general Pauli noise, and coherent noise. In the first two cases, $\|\Delta\|_2^2$ and $\|\Delta\|_1^2$ are usually close to their lower bounds in Eqs. (S61) and (S62) (see also Proposition S9). Especially for the second case, the scaling behaviors of $\|\Delta\|_2^2$ and $\|\Delta\|_1^2$ are similar to the counterparts under depolarizing noise. In the third case, by contrast, both $\|\Delta\|_2^2$ and $\|\Delta\|_1^2$ coincide with their respective upper bounds in Eqs. (S61) and (S62) because $\mathcal{N}(\sigma)$ remains a pure state under coherent noise.

2. Technical proofs

Proof of Proposition S7. By definition Δ is traceless and can be expressed as $\Delta = \Delta_+ - \Delta_-$, where Δ_+ and Δ_- are positive semidefinite operators that have orthogonal supports and satisfy $\text{Tr}(\Delta_+) = \text{Tr}(\Delta_-)$.

Therefore,

$$\|\Delta\|_{1}^{2} = (\|\Delta_{+}\|_{1} + \|\Delta_{-}\|_{1})^{2} = 2\|\Delta_{+}\|_{1}^{2} + 2\|\Delta_{-}\|_{1}^{2} \ge 2\|\Delta_{+}\|_{2}^{2} + 2\|\Delta_{-}\|_{2}^{2} = 2\|\Delta\|_{2}^{2}, \tag{S69}$$

where the inequality is saturated iff $\operatorname{rank}(\Delta_+) = \operatorname{rank}(\Delta_-) \le 1$. This result confirms the first inequality in Eq. (S59) and shows that this inequality is saturated iff $\operatorname{rank}(\Delta) \le 2$.

The second inequality in Eq. (S59) follows from the well-known relation between the trace distance and fidelity, and is known to be saturated when ρ and σ are pure states [36].

Proof of Proposition S8. By assumption ρ is a density operator and σ is a rank-1 projector, so Δ is traceless and has at most one negative eigenvalue. Let $\mu_1, \mu_2, \ldots, \mu_d$ be the eigenvalues of Δ arranged in nonincreasing order, that is, $\mu_1 \geq \mu_2 \geq \cdots \geq \mu_d$. Then $\mu_1, \mu_2, \ldots, \mu_{d-1} \geq 0$, $\mu_d \leq 0$, and $\mu_1 + \mu_2 + \cdots + \mu_{d-1} = -\mu_d$. Therefore,

$$\|\Delta\|_{1} = \sum_{j=1}^{d} |\mu_{j}| = 2|\mu_{d}|, \quad \|\Delta\|_{1}^{2} = 4\mu_{d}^{2},$$

$$\|\Delta\|_{2}^{2} = \sum_{j=1}^{d} \mu_{j}^{2} \le 2\mu_{d}^{2} = \frac{1}{2} \|\Delta\|_{1}^{2}, \quad \|\Delta\|_{2}^{2} \ge \mu_{d}^{2} + \frac{\left(\sum_{j=1}^{d-1} \mu_{j}\right)^{2}}{d-1} = \frac{d}{d-1} \mu_{d}^{2} = \frac{d}{4(d-1)} \|\Delta\|_{1}^{2},$$
(S70)

which imply Eq. (S60). Here the first inequality is saturated iff $\mu_1 = -\mu_d$ and $\mu_j = 0$ for j = 2, 3, ..., d-1, while the second inequality is saturated iff $\mu_j = -\mu_d/(d-1)$ for j = 1, 2, ..., d-1. These observations further confirm the saturation conditions of the inequalities in Eq. (S60). The first inequality in Eq. (S60) and its saturation condition also follow from Proposition S7.

The inequalities in Eq. (S61) and their saturation conditions are simple corollaries of Lemma S7 below and the following relation:

$$\|\Delta\|_2^2 = \operatorname{Tr}\left[\left(\rho - \sigma\right)^2\right] = 1 + \operatorname{Tr}\left(\rho^2\right) - 2\operatorname{Tr}(\rho\sigma) = 2\epsilon - 1 + \operatorname{Tr}\left(\rho^2\right). \tag{S71}$$

The first inequality in Eq. (S62) can be proved as follows:

$$\|\Delta\|_1^2 = 4\mu_d^2 = 4\left[\min_{|\psi\rangle\in\mathcal{H}} \text{Tr}(\Delta|\psi\rangle\langle\psi|)\right]^2 \ge 4\left[\text{Tr}(\Delta\sigma)\right]^2 = 4\epsilon^2. \tag{S72}$$

The inequality in Eq. (S72) holds because $\min_{|\psi\rangle\in\mathcal{H}}[\operatorname{Tr}(\Delta|\psi\rangle\langle\psi|)] \leq \operatorname{Tr}(\Delta\sigma) = -\epsilon \leq 0$; it is saturated iff σ is an eigenstate of Δ with eigenvalue μ_d , that is, ρ and σ commute. So the first inequality in Eq. (S62) is saturated iff ρ and σ commute.

Finally, we turn to the second inequality in Eq. (S62). Let $\rho = \sum_{l} q_{l} |\psi_{l}\rangle \langle \psi_{l}|$ be a convex decomposition of ρ into pure states, where $q_{l} > 0$ for all l, and let $\epsilon_{l} = 1 - \langle \psi_{l} | \sigma | \psi_{l} \rangle$. Then $\epsilon = 1 - \text{Tr}(\rho \sigma) = \sum_{l} q_{l} \epsilon_{l}$ and

$$\|\Delta\|_{1} = \left\| \sum_{l} q_{l} |\psi_{l}\rangle\langle\psi_{l}| - \sigma \right\|_{1} \le \sum_{l} q_{l} \||\psi_{l}\rangle\langle\psi_{l}| - \sigma\|_{1} = 2 \sum_{l} q_{l} \sqrt{\epsilon_{l}}. \tag{S73}$$

In conjunction with the Cauchy-Schwarz inequality we can deduce that

$$\|\Delta\|_1^2 \le 4\left(\sum_l q_l\sqrt{\epsilon_l}\right)^2 \le 4\left(\sum_l q_l\right)\left(\sum_l q_l\epsilon_l\right) = 4\sum_l q_l\epsilon_l = 4\epsilon, \tag{S74}$$

which confirms the second inequality in Eq. (S62). Alternatively, this inequality follows from Proposition S7. If ρ is a pure state, then $\|\Delta\|_1^2 = 2\|\Delta\|_2^2 = 4\epsilon$, so the second inequality in Eq. (S62) is saturated. If ρ is orthogonal to σ , then $\epsilon = 1$ and $\|\Delta\|_1 = 2$, so the second inequality in Eq. (S62) is also saturated.

Conversely, if the second inequality in Eq. (S62) is saturated, then the inequality in Eq. (S74) is saturated, which means all ϵ_i are equal to each other, and a similar conclusion holds for all convex decompositions of ρ into pure states. It follows that all pure states in the support of ρ have the same fidelity with σ . This condition can hold iff ρ is a pure state or is orthogonal to σ . Therefore, the second inequality in Eq. (S62) is saturated iff ρ is a pure state or is orthogonal to σ , which completes the proof of Proposition S8.

Next, we prove an auxiliary lemma employed in the proof of Proposition S8.

Lemma S7. Suppose $\sigma, \rho \in \mathcal{D}(\mathcal{H})$, where σ is a pure state, and let $\epsilon = 1 - \text{Tr}(\rho \sigma)$ be the infidelity between ρ and σ . Then

$$(1 - \epsilon)^2 + \frac{\epsilon^2}{d - 1} \le \operatorname{Tr}(\rho^2) \le 1, \tag{S75}$$

where the first inequality is saturated iff $\rho = (1 - \epsilon)\sigma + \epsilon(1 - \sigma)/(d - 1)$ and the second inequality is saturated iff ρ is a pure state. If in addition ρ commutes with σ , then

$$Tr(\rho^2) \le 1 - 2\epsilon + 2\epsilon^2, \tag{S76}$$

and the upper bound is saturated iff rank[$(1 - \sigma)\rho(1 - \sigma)$] ≤ 1 .

Proof of Lemma S7. The second inequality in Eq. (S75) and the saturation condition are trivial. To prove the first inequality in Eq. (S75), let

$$\varrho = \sigma \rho \sigma + (1 - \sigma)\rho(1 - \sigma) = (1 - \epsilon)\sigma + B, \tag{S77}$$

where $B = (1 - \sigma)\rho(1 - \sigma)$ is a positive operator supported in a (d-1)-dimension subspace of \mathcal{H} . In addition, B satisfies

$$\operatorname{Tr}(B) = \epsilon, \quad \frac{\epsilon^2}{d-1} \le \operatorname{Tr}(B^2) \le \epsilon^2,$$
 (S78)

where the first inequality is saturated iff B is proportional to $\mathbb{1} - \sigma$, and the second inequality is saturated iff B is proportional to a rank-1 projector, that is, rank(B) ≤ 1 . Therefore,

$$\operatorname{Tr}(\rho^2) \ge \operatorname{Tr}(\varrho^2) = (1 - \epsilon)^2 + \operatorname{Tr}(B^2) \ge (1 - \epsilon)^2 + \frac{\epsilon^2}{d - 1},\tag{S79}$$

which confirms the first inequality in Eq. (S75). If $\rho = (1 - \epsilon)\sigma + \epsilon(1 - \sigma)/(d - 1)$, then it is straightforward to verify that the first inequality in Eq. (S75) is saturated. Conversely, if this inequality is saturated, then the two inequalities in Eq. (S79) are saturated, which means $\rho = \varrho$ and B is proportional to $1 - \sigma$, so $\rho = (1 - \epsilon)\sigma + \epsilon(1 - \sigma)/(d - 1)$.

Next, suppose ρ commutes with σ . Then $\rho = \varrho$ and

$$\operatorname{Tr}(\rho^2) = \operatorname{Tr}(\varrho^2) = (1 - \epsilon)^2 + \operatorname{Tr}(B^2) \le (1 - \epsilon)^2 + \epsilon^2 = 1 - 2\epsilon + 2\epsilon^2,$$
 (S80)

which confirms Eq. (S76). Here the inequality follows from Eq. (S78) and is saturated iff $\operatorname{rank}(B) \leq 1$. This observation completes the proof of Lemma S7.

Proof of Proposition S9. According to Schur-Weyl duality, we have

$$\mathbb{E}_{|\phi\rangle \sim \text{Haar}}(\sigma \otimes \sigma) = \frac{\mathbb{1} + \text{SWAP}}{d(d+1)}.$$
 (S81)

Therefore, for any two Pauli operators P_i and P_j in \mathcal{P}_n , we have

$$\mathbb{E}_{|\phi\rangle \sim \text{Haar}} \operatorname{Tr}(P_i \sigma P_j \sigma) = \mathbb{E}_{|\phi\rangle \sim \text{Haar}} [\operatorname{Tr}(P_i \sigma) \operatorname{Tr}(P_j \sigma)] = \operatorname{Tr} \left[(P_i \otimes P_j) \mathbb{E}_{|\phi\rangle \sim \text{Haar}} (\sigma \otimes \sigma) \right] = \frac{d\delta_{i0} \delta_{j0} + \delta_{ij}}{d+1}, \text{ (S82)}$$

which implies that

$$\mathbb{E}_{|\phi\rangle \sim \text{Haar}} \operatorname{Tr}(P_i P_j \sigma P_j P_i \sigma) = \frac{d\delta_{ij} + 1}{d+1}.$$
 (S83)

Next, by definition we have

$$\operatorname{Tr}[\sigma \mathscr{P}(\sigma)] = \operatorname{Tr}\left[(1 - \|\mathbf{p}\|_1)\sigma^2 + \sum_{i=1}^{d^2 - 1} p_i P_i \sigma P_i \sigma \right] = (1 - \|\mathbf{p}\|_1) + \sum_{i=1}^{d^2 - 1} p_i \operatorname{Tr}(P_i \sigma P_i \sigma). \tag{S84}$$

Together with Eq. (S82), this equation implies that

$$\mathbb{E}_{|\phi\rangle \sim \text{Haar}} \operatorname{Tr}[\sigma \mathscr{P}(\sigma)] = (1 - \|\mathbf{p}\|_1) + \frac{1}{d+1} \sum_{i=1}^{d^2 - 1} p_i = 1 - \frac{d}{d+1} \|\mathbf{p}\|_1,$$

$$\bar{\epsilon} = 1 - \mathbb{E}_{|\phi\rangle \sim \text{Haar}} \operatorname{Tr}[\sigma \mathscr{P}(\sigma)] = \frac{d}{d+1} \|\mathbf{p}\|_1,$$
(S85)

which confirm Eq. (S65).

In addition, Δ and $\|\Delta\|_2^2$ can be expressed as follows:

$$\Delta = \mathscr{P}(\sigma) - \sigma = \sum_{i=1}^{d^2 - 1} p_i (P_i \sigma P_i - \sigma),$$

$$\|\Delta\|_2^2 = \|\mathscr{P}(\sigma) - \sigma\|_2^2 = \sum_{i,j=1}^{d^2 - 1} p_i p_j [\operatorname{Tr}(P_i P_j \sigma P_j P_i \sigma) - \operatorname{Tr}(P_i \sigma P_i \sigma) - \operatorname{Tr}(P_j \sigma P_j \sigma) + 1]$$

$$= \|\mathbf{p}\|_1^2 + \sum_{i,j=1}^{d^2 - 1} p_i p_j \operatorname{Tr}(P_i P_j \sigma P_j P_i \sigma) - 2\|\mathbf{p}\|_1 \sum_{i=1}^{d^2 - 1} p_i \operatorname{Tr}(P_i \sigma P_i \sigma).$$
(S86)

In conjunction with Eqs. (S82) and (S83) we can derive that

$$\mathbb{E}_{|\phi\rangle \sim \text{Haar}} \|\Delta\|_{2}^{2} = \|\mathbf{p}\|_{1}^{2} + \sum_{i,j=1}^{d^{2}-1} \frac{p_{i} p_{j} (d\delta_{ij} + 1)}{d+1} - \frac{2\|\mathbf{p}\|_{1}^{2}}{d+1} = \frac{d}{d+1} \|\mathbf{p}\|_{1}^{2} + \frac{d}{d+1} \|\mathbf{p}\|_{2}^{2}, \tag{S87}$$

which confirms Eq. (S66).

Finally, we turn to Eqs. (S67) and (S68). The first two inequalities in Eq. (S67) are trivial; the third inequality follows from Proposition S8; the last inequality is a simple corollary of Eqs. (S65) and (S66) together with the following inequalities:

$$\frac{\|\mathbf{p}\|_{1}^{2}}{d^{2}-1} \leq \|\mathbf{p}\|_{2}^{2} \leq \|\mathbf{p}\|_{1}^{2},\tag{S88}$$

which also imply that $\mathbb{E}_{|\phi\rangle\sim \text{Haar}} \|\Delta\|_2^2 \geq d\bar{\epsilon}^2/(d-1)$.

Equation (S68) follows from Proposition S8 and Eq. (S67), which completes the proof of Proposition S9. \Box

Appendix S7: Properties of cross characteristic functions

In this section, we clarify the key properties of cross characteristic functions defined in Eq. (10), which are crucial to understanding the variance in CRM shadow estimation based on the Clifford group.

1. Basic properties

Lemma S8. Suppose $\sigma, \rho \in \mathcal{D}(\mathcal{H}), \ \Delta = \rho - \sigma, \ \epsilon$ is the infidelity between ρ and σ , and $Q \in \mathcal{L}^{\mathrm{H}}(\mathcal{H})$. Then

$$\tilde{\Xi}_{\Delta,Q} \cdot \Xi_{\Delta,Q} \le \|\tilde{\Xi}_{\Delta,Q}\|_2^2 = \|\Xi_{\Delta,Q}\|_2^2 \le \min\left\{d\|\Delta\|_1^2\|Q\|_2^2, \sqrt{d}\|\Delta\|_1\|\Delta\|_2\|\Xi_Q\|_4^2\right\} \le 4d\epsilon\|Q\|_2^2. \tag{S89}$$

If σ is a pure state, then

$$\|\Xi_{\Delta,Q}\|_2^2 \le d\|\Delta\|_1^2 \|Q\|_2^2 \le \min\{4d\epsilon, 4(d-1)\|\Delta\|_2^2\} \|Q\|_2^2, \tag{S90}$$

$$\|\Xi_{\Delta,Q}\|_{2}^{2} \leq \sqrt{d} \|\Delta\|_{1} \|\Delta\|_{2} \|\Xi_{Q}\|_{4}^{2} \leq \min \left\{ 2\sqrt{2d}\epsilon, 2\sqrt{d-1} \|\Delta\|_{2}^{2} \right\} \|\Xi_{Q}\|_{4}^{2}. \tag{S91}$$

If σ is a pure state and $Q = \sigma - 1/d$, then

$$\|\Xi_{\Delta,Q}\|_2^2 = \|\Xi_{\Delta,\sigma}\|_2^2 \le d\|\Delta\|_2^2 \le 2d\epsilon,\tag{S92}$$

$$\|\Xi_{\Delta,Q}\|_{2}^{2} = \|\Xi_{\Delta,\sigma}\|_{2}^{2} \le 2^{-M_{2}(\sigma)/2} d\|\Delta\|_{1} \|\Delta\|_{2} \le 2^{1-M_{2}(\sigma)/2} d\min\{\sqrt{2}\epsilon, \|\Delta\|_{2}^{2}\}.$$
 (S93)

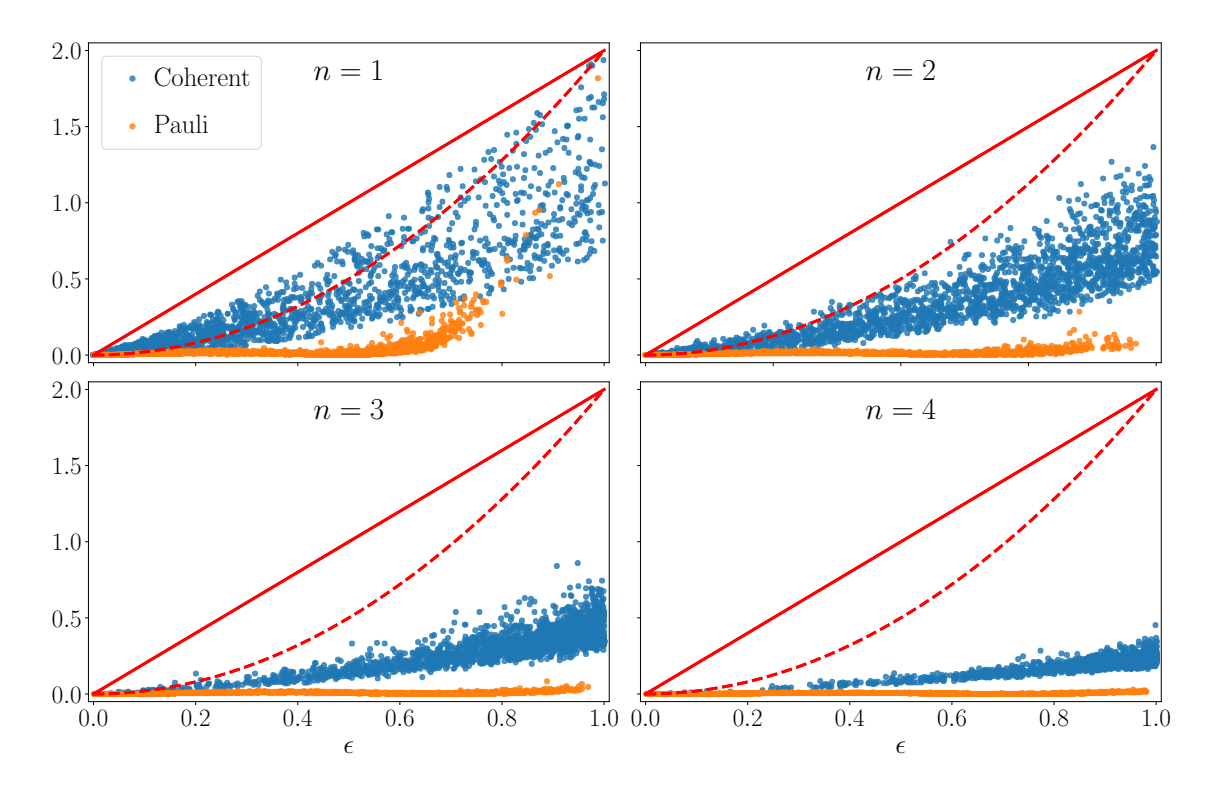


FIG. S2. Scatter plots on the relation between $\|\Xi_{\Delta,O}\|_2^2/d$ and the infidelity ϵ , where $\Delta=\rho-\sigma$ and $O=\sigma-1/d$. Here each σ is an n-qubit Haar-random pure state with $n=1,2,3,4,\,\rho=\mathscr{N}(\sigma)$, and \mathscr{N} is either a random coherent channel or a random Pauli channel as in Fig. S1. For each plot, 2000 Haar-random pure states together with 2000 random coherent channels and 2000 random Pauli channels are generated. The red solid line denotes the upper bound 2ϵ for $\|\Xi_{\Delta,O}\|_2^2$ as shown in Eq. (S92), while the red dashed line denotes the upper bound $2\epsilon^2$ for $\|\Xi_{\Delta,O}\|_2^2$ when \mathscr{N} is a Pauli channel as shown in Lemma S10.

Next, suppose σ is a pure state and ρ is tied to σ by a Pauli channel. Our goal is to derive a nontrivial upper bound for $\|\Xi_{\Delta,\sigma}\|_2^2$ in terms of the infidelity ϵ between ρ and σ . To this end, we need to introduce some auxiliary notation and results. Given two Pauli operators P_i, P_j in $\overline{\mathcal{P}}_n$, define

$$\eta_{i} = 1 - [\text{Tr}(\sigma P_{i})]^{2}, \quad K_{\sigma}(P_{i}) := \sum_{k \mid \{P_{k}, P_{i}\} = 0} [\text{Tr}(\sigma P_{k})]^{4}, \quad K_{\sigma}(P_{i}, P_{j}) := \sum_{k \mid \{P_{k}, P_{i}\} = \{P_{k}, P_{j}\} = 0} [\text{Tr}(\sigma P_{k})]^{4}.$$
(S94)

By definition $K_{\sigma}(P_j, P_i) = K_{\sigma}(P_i, P_j)$ and $K_{\sigma}(P_i, P_i) = K_{\sigma}(P_i)$; if i = 0, then $K_{\sigma}(P_i, P_j) = K_{\sigma}(P_i) = \eta_i = 0$.

Lemma S9. Suppose σ is a pure state on \mathcal{H} and $P_i, P_j \in \overline{\mathcal{P}}_n$ with $i, j \geq 1$. Then

$$K_{\sigma}(P_i) \le \frac{d\eta_i^2}{2}, \quad K_{\sigma}(P_i, P_j) \le \frac{d\eta_i \eta_j}{2},$$
 (S95)

where the first inequality is saturated when σ is a stabilizer state, and the second inequality is saturated when σ is a stabilizer state and $P_i = P_j$.

Lemma S10. Suppose σ is a pure state on \mathcal{H} , \mathscr{P} is the Pauli channel characterized by the vector $\mathbf{p} = (p_1, p_2, \dots, p_{d^2-1}), \ \rho = \mathscr{P}(\sigma), \ \Delta = \rho - \sigma, \ and \ \epsilon$ is the infidelity between ρ and σ . Then

$$\epsilon = \sum_{i=1}^{d^2 - 1} p_i \eta_i, \quad \|\Xi_{\Delta, \sigma}\|_2^2 = 4 \sum_{i, j=1}^{d^2 - 1} p_i p_j K_{\sigma}(P_i, P_j) \le 2d\epsilon^2, \tag{S96}$$

where the inequality is saturated when σ is a stabilizer state and \mathscr{P} is a single-error Pauli channel.

Next, we determine the expectation value of $\|\Xi_{\Delta,\sigma}\|_2^2$ when $\sigma = |\phi\rangle\langle\phi|$ is a Haar-random pure state on \mathcal{H} .

Proposition S10. Suppose $\sigma = |\phi\rangle\langle\phi|$ is a Haar-random pure state on \mathcal{H} , \mathscr{P} is the Pauli channel characterized by the vector $\mathbf{p} = (p_1, p_2, \dots, p_{d^2-1})$, $\rho = \mathscr{P}(\sigma)$, $\Delta = \rho - \sigma$, and ϵ is the infidelity between ρ and σ . Then

$$\mathbb{E}_{|\phi\rangle \sim \text{Haar}} \|\Xi_{\Delta,\sigma}\|_{2}^{2} = \frac{3d^{2}}{(d+1)(d+3)} (\|\mathbf{p}\|_{1}^{2} + \|\mathbf{p}\|_{2}^{2}) = \frac{3d}{d+3} \mathbb{E}_{|\phi\rangle \sim \text{Haar}} \|\Delta\|_{2}^{2}, \tag{S97}$$

$$\frac{3d\bar{\epsilon}^2}{d+2} \le \mathbb{E}_{|\phi\rangle \sim \text{Haar}} \|\Xi_{\Delta,\sigma}\|_2^2 \le \frac{6(d+1)}{d+3} \bar{\epsilon}^2.$$
 (S98)

Figure S2 illustrates the relation between $\|\Xi_{\Delta,O}\|_2^2/d$ and the infidelity ϵ , where $\Delta = \rho - \sigma$, $O = \sigma - 1/d$, σ is an n-qubit Haar-random pure state, $\rho = \mathcal{N}(\sigma)$, and \mathcal{N} is either a coherent channel or a Pauli channel. Note that $\|\Xi_{\Delta,O}\|_2^2/d \leq 2\epsilon$ according to Eq. (S92) in Lemma S8. When \mathcal{N} is a Pauli channel, we have a tighter upper bound $\|\Xi_{\Delta,O}\|_2^2/d \leq 2\epsilon^2$ thanks to Lemma S10 (see also Proposition S10). When \mathcal{N} is a coherent channel, the upper bound $2\epsilon^2$ is also applicable with a high probability, except when n is very small.

2. Technical proofs

Proof of Lemma S8. The first inequality and equality in Eq. (S89) follow from Ref. [29]. The second inequality in Eq. (S89) can be proved as follows:

$$\|\Xi_{\Delta,Q}\|_{2}^{2} = \sum_{P \in \overline{\mathcal{P}}_{n}} [\text{Tr}(\Delta P)]^{2} [\text{Tr}(QP)]^{2} \le \|\Delta\|_{1}^{2} \sum_{P \in \overline{\mathcal{P}}_{n}} [\text{Tr}(QP)]^{2} = d\|\Delta\|_{1}^{2} \|Q\|_{2}^{2}, \tag{S99}$$

$$\|\Xi_{\Delta,Q}\|_{2}^{2} \leq \sqrt{\sum_{P \in \overline{\mathcal{P}}_{n}} [\operatorname{Tr}(\Delta P)]^{4}} \sqrt{\sum_{P \in \overline{\mathcal{P}}_{n}} [\operatorname{Tr}(QP)]^{4}} \leq \sqrt{d} \|\Delta\|_{1} \|\Delta\|_{2} \|\Xi_{Q}\|_{4}^{2}. \tag{S100}$$

Here the first inequality in Eq. (S99) and the second inequality in Eq. (S100) hold because $|\operatorname{Tr}(\Delta P)| \leq ||\Delta||_1$ for all $P \in \overline{\mathcal{P}}_n$. The first inequality in Eq. (S100) follows from the Cauchy-Schwarz inequality. The last inequality in Eq. (S89) follows from the fact that $||\Delta||_1^2 \leq 4\epsilon$ by Proposition S7.

If σ is a pure state, then Eqs. (S90) and (S91) follow from Eq. (S89) and Proposition S8.

Finally, suppose σ is a pure state and $Q = \sigma - 1/d$. Then

$$|\operatorname{Tr}(QP)| \le |\operatorname{Tr}(\sigma P)| \le 1, \quad |\operatorname{Tr}(\Delta P)\operatorname{Tr}(QP)| = |\operatorname{Tr}(\Delta P)\operatorname{Tr}(\sigma P)| \le 1 \quad \forall P \in \overline{\mathcal{P}}_n.$$
 (S101)

Therefore,

$$\|\Xi_{\Delta,Q}\|_2^2 = \|\Xi_{\Delta,\sigma}\|_2^2 = \sum_{P \in \overline{\mathcal{P}}_n} [\operatorname{Tr}(\Delta P)]^2 [\operatorname{Tr}(\sigma P)]^2 \le \sum_{P \in \overline{\mathcal{P}}_n} [\operatorname{Tr}(\Delta P)]^2 = d\|\Delta\|_2^2 \le 2d\epsilon, \tag{S102}$$

which confirms Eq. (S92) and the equality in Eq. (S93). Here the last inequality follows from Proposition S8. The two inequalities in Eq. (S93) follow from Eq. (S91) and the fact that $\|\Xi_{\sigma}\|_{4}^{4} = 2^{-M_{2}(\sigma)}d$ according to the definition of 2-SRE. This observation completes the proof of Lemma S8.

Proof of Lemma S9. By assumption σ is the projector onto a pure state $|\phi\rangle$ in \mathcal{H} that can be expressed as follows:

$$|\phi\rangle = \alpha_i |\psi_i^+\rangle + \sqrt{1 - \alpha_i^2} |\psi_i^-\rangle,$$
 (S103)

where $0 \le \alpha_i \le 1$ and $|\psi_i^+\rangle$ ($|\psi_i^-\rangle$) is an eigenstate of P_i with eigenvalue +1 (-1), so

$$\eta_i = 1 - [\text{Tr}(\sigma P_i)]^2 = 4\alpha_i^2 (1 - \alpha_i^2).$$
 (S104)

If $P_k \in \overline{\mathcal{P}}_n$ anticommutes with P_i , that is, $\{P_k, P_i\} = 0$, then

$$\operatorname{Tr}(\sigma P_k) = 2\alpha_i \sqrt{1 - \alpha_i^2} \operatorname{Tr}(M_i P_k) = \sqrt{\eta_i} \operatorname{Tr}(M_i P_k), \tag{S105}$$

where

$$M_i = \frac{|\psi_i^+\rangle\langle\psi_i^-| + |\psi_i^-\rangle\langle\psi_i^+|}{2}.$$
 (S106)

Now, the first inequality in Eq. (S95) can be derived as follows:

$$K_{\sigma}(P_{i}) = \sum_{k \mid \{P_{k}, P_{i}\} = 0} \left[\text{Tr}(\sigma P_{k}) \right]^{4} = \eta_{i}^{2} \sum_{k \mid \{P_{k}, P_{i}\} = 0} \left[\text{Tr}(M_{i} P_{k}) \right]^{4} \le \eta_{i}^{2} \sum_{k=0}^{d^{2} - 1} \left[\text{Tr}(M_{i} P_{k}) \right]^{4}$$

$$\le \eta_{i}^{2} \sum_{k=0}^{d^{2} - 1} \left[\text{Tr}(M_{i} P_{k}) \right]^{2} = d\eta_{i}^{2} \operatorname{Tr}(M_{i}^{2}) = \frac{d\eta_{i}^{2}}{2}, \tag{S107}$$

where the second inequality follows from the fact that $|\operatorname{Tr}(M_i P_k)| \leq ||M_i||_1 ||P_k|| = 1$. As a corollary, we have

$$K_{\sigma}(P_i, P_j) \le \min[K_{\sigma}(P_i), K_{\sigma}(P_j)] \le \sqrt{K_{\sigma}(P_i)K_{\sigma}(P_j)} \le \frac{d\eta_i\eta_j}{2},$$
 (S108)

which confirms the second inequality in Eq. (S95).

Next, suppose σ is a stabilizer state. Then $\text{Tr}(\sigma P)$ for $P \in \overline{\mathcal{P}}_n$ can take on three possible values, namely, 0, 1, and -1. Let

$$\mathcal{G}_{\sigma} = \left\{ P \in \overline{\mathcal{P}}_n \,|\, [\text{Tr}(\sigma P)]^2 = 1 \right\}; \tag{S109}$$

then \mathcal{G} contains d Pauli operators. If in addition P_i or $-P_i$ is a stabilizer of σ , then $[\operatorname{Tr}(\sigma P_i)]^2 = 1$ and $\eta_i = 0$. Meanwhile, all Pauli operators in \mathcal{G}_{σ} commute with P_i . In other words, any Pauli operator P_k that anticommutes with P_i cannot be a stabilizer of σ and satisfies $\operatorname{Tr}(P_k\sigma) = 0$. So $K_{\sigma}(P_i) = 0 = d\eta_i^2/2$. If instead neither P_i nor $-P_i$ is a stabilizer of σ , then $[\operatorname{Tr}(\sigma P_i)]^2 = 0$ and $\eta_i = 1$. Meanwhile, exactly one half of the Pauli operators in \mathcal{G}_{σ} anticommutes with P_i . So $K_{\sigma}(P_i) = d/2 = d\eta_i^2/2$. In both cases, the first inequality in Eq. (S95) is saturated. If in addition i = j, then $\eta_i = \eta_j$ and $K_{\sigma}(P_i, P_j) = K_{\sigma}(P_i)$, so the second inequality in Eq. (S95) is also saturated. This observation completes the proof of Lemma S9.

Proof of Lemma S10. By assumption σ is a pure state and $\rho = \mathscr{P}(\sigma) = (1 - \|\mathbf{p}\|_1)\sigma + \sum_{i=1}^{d^2-1} p_i P_i \sigma P_i$, so we have

$$\epsilon = 1 - \text{Tr}(\rho\sigma) = \sum_{i=1}^{d^2 - 1} p_i [1 - \text{Tr}(P_i \sigma P_i \sigma)] = \sum_{i=1}^{d^2 - 1} p_i \{1 - [\text{Tr}(\sigma P_i)]^2\} = \sum_{i=1}^{d^2 - 1} p_i \eta_i,$$
 (S110)

which confirms the first equality in Eq. (S96). In addition,

$$\Delta = \sum_{i=1}^{d^2 - 1} p_i (P_i \sigma P_i - \sigma), \quad \text{Tr}(\Delta P_k) = \sum_{i=1}^{d^2 - 1} p_i \, \text{Tr}(P_i \sigma P_i P_k - \sigma P_k) = -2 \, \text{Tr}(\sigma P_k) \sum_{i \ge 1 \mid \{P_i, P_k\} = 0} p_i \quad \forall \, k \ge 1.$$
(S111)

Therefore,

$$\|\Xi_{\Delta,\sigma}\|_{2}^{2} = \sum_{k=1}^{d^{2}-1} [\operatorname{Tr}(\Delta P_{k})]^{2} [\operatorname{Tr}(\sigma P_{k})]^{2} = 4 \sum_{k=1}^{d^{2}-1} [\operatorname{Tr}(\sigma P_{k})]^{4} \sum_{i,j\geq 1} \sum_{\substack{|\{P_{i},P_{k}\}=\{P_{j},P_{k}\}=0\\k \mid \{P_{k},P_{i}\}=\{P_{k},P_{j}\}=0}} p_{i} p_{j}$$

$$= 4 \sum_{i,j=1}^{d^{2}-1} p_{i} p_{j} \sum_{\substack{k \mid \{P_{k},P_{i}\}=\{P_{k},P_{j}\}=0\\k \mid \{P_{k},P_{i}\}=\{P_{k},P_{j}\}=0}} [\operatorname{Tr}(\sigma P_{k})]^{4} = 4 \sum_{i,j=1}^{d^{2}-1} p_{i} p_{j} K_{\sigma}(P_{i},P_{j}) \leq 2d \left(\sum_{i=1}^{d^{2}-1} p_{i} \eta_{i}\right)^{2} = 2d\epsilon^{2},$$
 (S112)

which confirms the second equality and the inequality in Eq. (S96). Here the inequality follows from Lemma S9.

Next, suppose σ is a stabilizer state and \mathscr{P} is a single-error Pauli channel. Then

$$\epsilon = p_i \eta_i, \quad \|\Xi_{\Delta,\sigma}\|_2^2 = 4p_i^2 K_{\sigma}(P_i) = 2dp_i^2 \eta_i^2, \tag{S113}$$

for some $i \in \{1, 2, ..., d^2 - 1\}$, where the last equality follows from Lemma S9. So the inequality in Eq. (S96) is saturated, which completes the proof of Lemma S10.

Proof of Proposition S10. According to Schur-Weyl duality, we have

$$\mathbb{E}_{|\phi\rangle \sim \text{Haar}}(\sigma^{\otimes 4}) = \frac{\sum_{\pi \in S_4} W_{\pi}}{d(d+1)(d+2)(d+3)},\tag{S114}$$

where W_{π} is the permutation operator on $\mathcal{H}^{\otimes 4}$ associated with the permutation $\pi \in S_4$. Based on this observation, for any Pauli operator $P \in \overline{\mathcal{P}}_n$ that is not proportional to the identity operator, we can deduce that

$$\mathbb{E}_{|\phi\rangle \sim \text{Haar}}[\text{Tr}(\sigma P)]^4 = \text{Tr}\left[P^{\otimes 4}\mathbb{E}_{|\phi\rangle \sim \text{Haar}}(\sigma^{\otimes 4})\right] = \frac{\sum_{\pi \in S_4} \text{Tr}(W_{\pi}P^{\otimes 4})}{d(d+1)(d+2)(d+3)} = \frac{3[\text{Tr}(P^2)]^2 + 6\,\text{Tr}(P^4)}{d(d+1)(d+2)(d+3)}$$
$$= \frac{3d^2 + 6d}{d(d+1)(d+2)(d+3)} = \frac{3}{(d+1)(d+3)}.$$
 (S115)

Furthermore,

$$\mathbb{E}_{|\phi\rangle \sim \text{Haar}} \|\Xi_{\Delta,\sigma}\|_{2}^{2} = \mathbb{E}_{|\phi\rangle \sim \text{Haar}} \sum_{k=1}^{d^{2}-1} [\text{Tr}(\Delta P_{k})]^{2} [\text{Tr}(\sigma P_{k})]^{2}$$

$$= 4\mathbb{E}_{|\phi\rangle \sim \text{Haar}} \sum_{k=1}^{d^{2}-1} [\text{Tr}(\sigma P_{k})]^{4} \sum_{i,j\geq 1 \mid \{P_{i},P_{k}\}=\{P_{j},P_{k}\}=0} p_{i}p_{j}$$

$$= 4\sum_{i,j=1}^{d^{2}-1} p_{i}p_{j} \sum_{k \mid \{P_{k},P_{i}\}=\{P_{k},P_{j}\}=0} \mathbb{E}_{|\phi\rangle \sim \text{Haar}} [\text{Tr}(\sigma P_{k})]^{4} = \frac{12}{(d+1)(d+3)} \sum_{i,j=1}^{d^{2}-1} p_{i}p_{j}C_{i,j}, \tag{S116}$$

where $C_{i,j}$ denotes the number of Pauli operators in $\overline{\mathcal{P}}_n$ that anti-commute with both P_i and P_j . It is straightforward to verify that

$$C_{i,j} = \frac{d^2(1+\delta_{ij})}{4} \quad \forall i, j \ge 1.$$
 (S117)

Therefore,

$$\mathbb{E}_{|\phi\rangle\sim \text{Haar}} \|\Xi_{\Delta,\sigma}\|_{2}^{2} = \frac{3d^{2}}{(d+1)(d+3)} \sum_{i,j=1}^{d^{2}-1} p_{i} p_{j} (1+\delta_{ij}) = \frac{3d^{2}(\|\mathbf{p}\|_{1}^{2} + \|\mathbf{p}\|_{2}^{2})}{(d+1)(d+3)} = \frac{3d}{d+3} \mathbb{E}_{|\phi\rangle\sim \text{Haar}} \|\Delta\|_{2}^{2}, \quad (S118)$$

which confirms Eq. (S97). Here the last equality follows from Eq. (S66) in Proposition S9. Finally, Eq. (S98) follows from Eqs. (S97) and (S67), which completes the proof of Proposition S10.

Appendix S8: Variances in CRM shadow estimation based on Clifford measurements

In this section, we first derive an alternative formula for the variance $\mathbb{V}_*(O, \Delta)$ in CRM shadow estimation based on the Clifford group (see Lemma S11 below) and then prove Theorems 3 and 5 in the main text. In the course of study, we also clarify the variances $\mathbb{V}(O, \rho)$, $\mathbb{V}_*(O, \rho)$, and $\mathbb{V}_*(O, \Delta)$ in CRM shadow estimation in the presence of depolarizing noise.

1. Alternative formula for the variance $V_*(O, \Delta)$

Lemma S11. Suppose O is a traceless observable on \mathcal{H} . Then the variance $\mathbb{V}_*(O,\Delta)$ in $CRM(Cl_n,\sigma,R)$ reads

$$V_{*}(O, \Delta) = \frac{2(d+1)}{d^{2}(d+2)} \sum_{\substack{i,j \geq 1 \mid i \neq j, \\ [P_{i}, P_{j}] = 0}} \text{Tr}(OP_{i}) \, \text{Tr}(OP_{j}) \, \text{Tr}(\Delta P_{i}) \, \text{Tr}(\Delta P_{j})$$

$$+ \frac{(d+1)}{d^{2}} \sum_{i=1}^{d^{2}-1} \left[\text{Tr}(OP_{i}) \right]^{2} \left[\text{Tr}(\Delta P_{i}) \right]^{2} - \left[\text{Tr}(\Delta O) \right]^{2}. \tag{S119}$$

Before proving Lemma S11, we first introduce an auxiliary result. Given two Pauli operators P_i , P_j in \mathcal{P}_n , define $\mathcal{D}(P_i)$ as the set of Clifford unitaries in Cl_n that can diagonalize P_i with respect to the computational basis; define $\mathcal{D}(P_i, P_j)$ as the set of Clifford unitaries that can diagonalize P_i and P_j simultaneously. Note that $\mathcal{D}(P_i, P_j)$ is empty whenever P_i and P_j do dot commute.

Lemma S12. Suppose P_i and P_j are two distinct Pauli operators (with $i \neq j$) in \overline{P}_n that commute with each other. Then

$$\mathbb{E}_{U \sim \operatorname{Cl}_n} \left[\delta_{U \in \mathscr{D}(P)} \right] = \frac{1}{d+1}, \quad \mathbb{E}_{U \sim \operatorname{Cl}_n} \left[\delta_{U \in \mathscr{D}(P_1, P_2)} \right] = \frac{2}{(d+1)(d+2)}. \tag{S120}$$

Lemma S12 follows from the fact that the Clifford group acts transitively on nontrivial Pauli operators and also on commuting pairs of distinct nontrivial Pauli operators [45]; in other words, the Clifford group is both Pauli-mixing and Pauli 2-mixing [44].

Proof of Lemma S11. Since the Clifford group Cl_n is a unitary 3-design and O is traceless, the reconstruction map $\mathcal{M}^{-1}(\cdot)$ has a simple form: $\mathcal{M}^{-1}(O) = (d+1)O$ [23]. In conjunction with Eq. (5) we can deduce that

$$V_*(O, \Delta) = (d+1)^2 \operatorname{Tr} \left[\Omega(\operatorname{Cl}_n)(O \otimes \Delta)^{\otimes 2} \right] - \left[\operatorname{Tr}(\Delta O) \right]^2, \tag{S121}$$

where $\Omega(Cl_n)$ is defined according to Eq. (3):

$$\Omega(\mathrm{Cl}_n) = \sum_{\mathbf{s}, \mathbf{t}} \mathbb{E}_{U \sim \mathrm{Cl}_n} U^{\dagger \otimes 4} \left[(|\mathbf{s}\rangle \langle \mathbf{s}|)^{\otimes 2} \otimes (|\mathbf{t}\rangle \langle \mathbf{t}|)^{\otimes 2} \right] U^{\otimes 4}.$$
 (S122)

Next, decompose O in terms of Pauli operators: $O = \sum_{i=0}^{d^2-1} \text{Tr}(OP_i)P_i/d$. Then $\text{Tr}[\Omega(\text{Cl}_n)(O \otimes \Delta)^{\otimes 2}]$ featured in Eq. (S121) can be expressed as follows:

$$\operatorname{Tr}\left[\Omega(\operatorname{Cl}_n)(O\otimes\Delta)^{\otimes 2}\right] = \sum_{\mathbf{s},\mathbf{t}} \mathbb{E}_{U\sim\operatorname{Cl}_n}\left(\langle \mathbf{s}|UOU^{\dagger}|\mathbf{s}\rangle\langle \mathbf{s}|U\Delta U^{\dagger}|\mathbf{s}\rangle\langle \mathbf{t}|UOU^{\dagger}|\mathbf{t}\rangle\langle \mathbf{t}|U\Delta U^{\dagger}|\mathbf{t}\rangle\right)$$

$$= \frac{1}{d^2} \sum_{\mathbf{s}, \mathbf{t}} \sum_{i,j=1}^{d^2 - 1} \operatorname{Tr}(OP_i) \operatorname{Tr}(OP_j) \mathbb{E}_{U \sim \operatorname{Cl}_n} \left(\langle \mathbf{s} | UP_i U^{\dagger} | \mathbf{s} \rangle \langle \mathbf{s} | U\Delta U^{\dagger} | \mathbf{s} \rangle \langle \mathbf{t} | UP_j U^{\dagger} | \mathbf{t} \rangle \langle \mathbf{t} | U\Delta U^{\dagger} | \mathbf{t} \rangle \right). \tag{S123}$$

If $U \notin \mathcal{D}(P_i)$, then $\langle \mathbf{s} | U P_i U^{\dagger} | \mathbf{s} \rangle = 0$ for all \mathbf{s} . Otherwise, $U P_i U^{\dagger}$ is diagonal in the computational basis, and

$$\sum_{\mathbf{s}} \langle \mathbf{s} | U P_i U^{\dagger} | \mathbf{s} \rangle \langle \mathbf{s} | U \Delta U^{\dagger} | \mathbf{s} \rangle = \text{Tr} \left(U P_i U^{\dagger} U \Delta U^{\dagger} \right) = \text{Tr}(\Delta P_i). \tag{S124}$$

Based on this observation, Eq. (S123) can be simplified as follows:

$$\operatorname{Tr}\left[\Omega(\mathcal{U})(O\otimes\Delta)^{\otimes 2}\right] = \frac{1}{d^{2}} \sum_{i,j=1}^{d^{2}-1} \operatorname{Tr}(OP_{i}) \operatorname{Tr}(OP_{j}) \mathbb{E}_{U\sim\operatorname{Cl}_{n}}\left[\delta_{U\in\mathscr{D}(P_{i},P_{j})}\right] \operatorname{Tr}(\Delta P_{i}) \operatorname{Tr}(\Delta P_{j})$$

$$= \frac{1}{d^{2}} \sum_{\substack{i,j\geq 1 \mid i\neq j,\\ [P_{i},P_{j}]=0}} \operatorname{Tr}(OP_{i}) \operatorname{Tr}(OP_{j}) \operatorname{Tr}(\Delta P_{i}) \operatorname{Tr}(\Delta P_{j}) \mathbb{E}_{U\sim\operatorname{Cl}_{n}}\left[\delta_{U\in\mathscr{D}(P_{i},P_{j})}\right]$$

$$+ \frac{1}{d^{2}} \sum_{i=1}^{d^{2}-1} \left[\operatorname{Tr}(OP_{i})\right]^{2} \left[\operatorname{Tr}(\Delta P_{i})\right]^{2} \mathbb{E}_{U\sim\operatorname{Cl}_{n}}\left[\delta_{U\in\mathscr{D}(P_{i})}\right]$$

$$= \frac{2}{d^{2}(d+1)(d+2)} \sum_{\substack{i,j\geq 1 \mid i\neq j,\\ [P_{i},P_{j}]=0}} \operatorname{Tr}(OP_{i}) \operatorname{Tr}(OP_{j}) \operatorname{Tr}(\Delta P_{i}) \operatorname{Tr}(\Delta P_{j})$$

$$+ \frac{1}{d^{2}(d+1)} \sum_{i=1}^{d^{2}-1} \left[\operatorname{Tr}(OP_{i})\right]^{2} \left[\operatorname{Tr}(\Delta P_{i})\right]^{2}, \tag{S125}$$

where the last equality follows from Lemma S12. Together with Eq. (S121), this equation implies Eq. (S119) and completes the proof of Lemma S11. \Box

2. Proof of Theorem 3

Proof of Theorem 3. First, we will show that the formula for $\mathbb{V}_*(O,\Delta)$ in Eq. (12) in Theorem 3 is equivalent to the formula in Eq. (S119) in Lemma S12. To this end, we need to expand $\|\Xi_{\Delta,O}\|_2^2$ and $\tilde{\Xi}_{\Delta,O} \cdot \Xi_{\Delta,O}$. According to the definitions in Eq. (10), for $P \in \overline{\mathcal{P}}_n$ we have

$$\Xi_{\Delta,O}(P) = \operatorname{Tr}(OP)\operatorname{Tr}(\Delta P),$$

$$\tilde{\Xi}_{\Delta,O}(P) = \operatorname{Tr}(\Delta POP) = \frac{1}{d}\sum_{j=1}^{d^2-1}\operatorname{Tr}(OP_j)\operatorname{Tr}(\Delta PP_jP) = \frac{1}{d}\sum_{j=1}^{d^2-1}f(P,P_j)\operatorname{Tr}(OP_j)\operatorname{Tr}(\Delta P_j),$$
(S126)

where

$$f(P, P_j) = \begin{cases} 1 & \text{if } [P, P_j] = 0, \\ -1 & \text{if } \{P, P_j\} = 0. \end{cases}$$
 (S127)

Note that $f(P, P_j) = f(P_j, P)$ by definition. Therefore,

$$\|\Xi_{\Delta,O}\|_{2}^{2} = \sum_{i=1}^{d^{2}-1} [\text{Tr}(OP_{i})]^{2} [\text{Tr}(\Delta P_{i})]^{2},$$

$$\tilde{\Xi}_{\Delta,O} \cdot \Xi_{\Delta,O} = \frac{1}{d} \sum_{i,j=1}^{d^{2}-1} f(P_{i}, P_{j}) \operatorname{Tr}(OP_{i}) \operatorname{Tr}(OP_{j}) \operatorname{Tr}(\Delta P_{i}) \operatorname{Tr}(\Delta P_{j})$$

$$= \frac{1}{d} \sum_{i} [\text{Tr}(OP_{i})]^{2} [\text{Tr}(\Delta P_{i})]^{2} + \frac{1}{d} \sum_{\substack{i,j \geq 1 \mid i \neq j, \\ [P_{i}, P_{j}] = 0}} \operatorname{Tr}(OP_{i}) \operatorname{Tr}(OP_{j}) \operatorname{Tr}(\Delta P_{i}) \operatorname{Tr}(\Delta P_{j})$$

$$- \frac{1}{d} \sum_{\substack{i,j \geq 1 \mid \{P_{i}, P_{i}\} = 0}} \operatorname{Tr}(OP_{i}) \operatorname{Tr}(\Delta P_{j}) \operatorname{Tr}(\Delta P_{i}) \operatorname{Tr}(\Delta P_{j}).$$
(S128)

In addition, we have

$$[\operatorname{Tr}(\Delta O)]^{2} = \frac{1}{d^{2}} \sum_{i,j=1}^{d^{2}-1} \operatorname{Tr}(\Delta P_{i}) \operatorname{Tr}(\Delta P_{j}) \operatorname{Tr}(O P_{i}) \operatorname{Tr}(O P_{j})$$

$$= \frac{1}{d^{2}} \sum_{i} [\operatorname{Tr}(O P_{i})]^{2} [\operatorname{Tr}(\Delta P_{i})]^{2} + \frac{1}{d^{2}} \sum_{\substack{i,j \geq 1 \mid i \neq j, \\ [P_{i}, P_{j}] = 0}} \operatorname{Tr}(O P_{i}) \operatorname{Tr}(O P_{j}) \operatorname{Tr}(\Delta P_{i}) \operatorname{Tr}(\Delta P_{j})$$

$$+ \frac{1}{d^{2}} \sum_{\substack{i,j \geq 1 \mid \{P_{i}, P_{j}\} = 0}} \operatorname{Tr}(O P_{i}) \operatorname{Tr}(O P_{j}) \operatorname{Tr}(\Delta P_{i}) \operatorname{Tr}(\Delta P_{j}). \tag{S129}$$

In conjunction with Lemmas S11 and S12 we can deduce that

$$\mathbb{V}_{*}(O,\Delta) = \frac{2(d+1)}{d^{2}(d+2)} \sum_{\substack{i,j \geq 1 \mid i \neq j, \\ [P_{i},P_{j}] = 0}} \operatorname{Tr}(OP_{i}) \operatorname{Tr}(OP_{j}) \operatorname{Tr}(\Delta P_{i}) \operatorname{Tr}(\Delta P_{j})
+ \frac{d+1}{d^{2}} \sum_{i=1}^{d^{2}-1} [\operatorname{Tr}(OP_{i})]^{2} [\operatorname{Tr}(\Delta P_{i})]^{2} - [\operatorname{Tr}(\Delta O)]^{2}
= \frac{d+1}{d(d+2)} (\|\Xi_{\Delta,O}\|_{2}^{2} + \tilde{\Xi}_{\Delta,O} \cdot \Xi_{\Delta,O}) - \frac{[\operatorname{Tr}(\Delta O)]^{2}}{d+2} \leq \frac{2}{d} \|\Xi_{\Delta,O}\|_{2}^{2} \leq 2\|\Delta\|_{1}^{2} \|O\|_{2}^{2} \leq 8\epsilon \|O\|_{2}^{2}, \quad (S130)$$

which confirms Eq. (12). Here the three inequalities follow from Eq. (S89) in Lemma S8.

If σ is a pure state and $O = \sigma - 1/d$, then Eq. (13) follows from Eq. (S130) above [or Eq. (12)] and Eq. (S93) in Lemma S8. This observation completes the proof of Theorem 3.

3. Variances in HPFE in the presence of depolarizing noise

In this section we clarify the variances $\mathbb{V}(O,\rho)$, $\mathbb{V}_*(O,\rho)$, and $\mathbb{V}_*(O,\Delta)$ in HPFE in the presence of depolarizing noise and the impacts of the 2-SRE and the number R of circuit reusing on these variances and circuit sample cost. The discussions in this section also pave the way for proving Theorem 5 in the main text.

Lemma S13. Suppose σ is a pure state on \mathcal{H} , $\rho = (1-p)\sigma + p\mathbb{1}/d$, $\Delta = \rho - \sigma$, $\epsilon = 1 - \text{Tr}(\rho\sigma)$, and $O = \sigma - \mathbb{1}/d$. Then the variances $\mathbb{V}(O, \rho)$, $\mathbb{V}_*(O, \rho)$, and $\mathbb{V}_*(O, \Delta)$ in $CRM(Cl_n, \sigma, R)$ read

$$\mathbb{V}(O,\rho) = \left(\frac{d-1}{d}\right)^2 \left[-p^2 + \frac{4dp}{(d-1)(d+2)} + \frac{d^2 - 3d - 2}{(d-1)(d+2)} \right] + \frac{d^2 - 1}{d^2} \le \frac{2d(d+1)}{(d+2)^2},\tag{S131}$$

$$V_*(O,\rho) = \frac{(1-p)^2 \left[2^{1-M_2(\sigma)}(d+1) - 4\right]}{d+2},\tag{S132}$$

$$V_*(O,\Delta) = \frac{p^2 \left[2^{1-M_2(\sigma)}(d+1) - 4\right]}{d+2} \le 2^{1-M_2(\sigma)} \epsilon^2.$$
 (S133)

Here Eqs. (S131) and (S132) are known before [29]. According to Lemma 2, the variances in THR and CRM shadow estimation of the observable O are respectively given by

$$\mathbb{V}_{R}^{(\mathrm{T})}(\hat{O}) = \mathbb{V}_{*}(O,\rho) + \frac{\mathbb{V}(O,\rho) - \mathbb{V}_{*}(O,\rho)}{R}, \quad \mathbb{V}_{R}^{(\mathrm{C})}(\hat{O}) = \mathbb{V}_{*}(O,\Delta) + \frac{\mathbb{V}(O,\rho) - \mathbb{V}_{*}(O,\rho)}{R}. \tag{S134}$$

In HPFE, usually ρ is close to the target state σ , that is, $p \ll 1$, in which case Lemma S13 implies that

$$\mathbb{V}(O,\rho) \approx \mathbb{V}(O,\sigma) \approx 2, \quad \mathbb{V}_*(O,\rho) \approx \mathbb{V}_*(O,\sigma) \approx 2^{1-M_2(\sigma)}, \quad \mathbb{V}_*(O,\Delta) \approx 2^{1-M_2(\sigma)}\epsilon^2, \tag{S135}$$

which in turn implies that

$$\mathbb{V}_{R}^{(T)}(\hat{O}) \approx 2\left(2^{-M_{2}(\sigma)} + \frac{1 - 2^{-M_{2}(\sigma)}}{R}\right), \quad \mathbb{V}_{R}^{(C)}(\hat{O}) \approx 2\left(2^{-M_{2}(\sigma)}\epsilon^{2} + \frac{1 - 2^{-M_{2}(\sigma)}}{R}\right). \tag{S136}$$

In conjunction with Lemma 1 we can derive the circuit sample costs required in THR and CRM shadow estimation:

$$N_U^{(T)} = \mathcal{O}\left(\frac{2^{-M_2(\sigma)}}{r^2 \epsilon^2} + \frac{1 - 2^{-M_2(\sigma)}}{Rr^2 \epsilon^2}\right), \quad N_U^{(C)} = \mathcal{O}\left(\frac{2^{-M_2(\sigma)}}{r^2} + \frac{1 - 2^{-M_2(\sigma)}}{Rr^2 \epsilon^2}\right). \tag{S137}$$

In the large-R limit $(R \gg 2^{M_2(\sigma)}/\epsilon^2)$, the above formulas simplify to

$$N_U^{(T)} = \mathcal{O}\left(\frac{2^{-M_2(\sigma)}}{r^2 \epsilon^2}\right), \quad N_U^{(C)} = \mathcal{O}\left(\frac{2^{-M_2(\sigma)}}{r^2}\right).$$
 (S138)

Both $N_U^{(\mathrm{T})}$ and $N_U^{(\mathrm{C})}$ decrease monotonically with the 2-SRE $M_2(\sigma)$. On the other hand, $N_U^{(\mathrm{T})}$ scales as $1/\epsilon^2$, while $N_U^{(\mathrm{C})}$ is independent of ϵ . In THR, when $R \geq 5 \times 2^{M_2(\sigma)}$, further increasing R has negligible influence on $N_U^{(\mathrm{T})}$. In CRM, by contrast, R needs to scale with $1/\epsilon^2$ to guarantee that $N_U^{(\mathrm{C})}$ is independent of ϵ as shown in Eq. (S138). If R is too small, then the second term in the expression of $N_U^{(\mathrm{C})}$ in Eq. (S137) will dominate, and $N_U^{(\mathrm{C})}$ will scale with $1/\epsilon^2$, just like $N_U^{(\mathrm{T})}$. Moreover, when $R < 1/\epsilon^2$, $N_U^{(\mathrm{C})}$ may increase (rather than decrease) with $M_2(\sigma)$, so the impact of the 2-SRE on the circuit sample cost of CRM shadow estimation is quite subtle.

When depolarizing noise is replaced by general Pauli noise, it is difficult to derive precise and informative formulas for the variances as shown above. Nevertheless, the above conclusions still hold approximately, which is confirmed by extensive numerical calculations presented in Sec. S101.

Proof of Lemma S13. Equations (S131) and (S132) follow from Propositions 3 and 4 in Ref. [29], so it remains to prove (S133). By assumption $\Delta = \rho - \sigma = p(1/d - \sigma)$ and $O = \sigma - 1/d$, where σ is a pure state. Therefore,

$$\operatorname{Tr}(\Delta\sigma) = \operatorname{Tr}(\Delta O) = -p \operatorname{Tr}\left[\left(\sigma - \frac{1}{d}\right)^{2}\right] = -p\left(1 - \frac{1}{d}\right),$$

$$\epsilon = 1 - \operatorname{Tr}(\rho\sigma) = -\operatorname{Tr}(\Delta\sigma) = p\left(1 - \frac{1}{d}\right).$$
(S139)

Now, from the definitions of cross characteristic functions in Eq. (10) we can deduce that

$$\|\Xi_{\Delta,O}\|_{2}^{2} = \sum_{i=1}^{d^{2}-1} [\operatorname{Tr}(\Delta P_{i})]^{2} [\operatorname{Tr}(OP_{i})]^{2} = p^{2} \sum_{i=1}^{d^{2}-1} [\operatorname{Tr}(\sigma P_{i})]^{4} = p^{2} [2^{-M_{2}(\sigma)}d - 1],$$

$$\tilde{\Xi}_{\Delta,O} \cdot \Xi_{\Delta,O} = \sum_{i=1}^{d^{2}-1} \operatorname{Tr}(\Delta P_{i}OP_{i}) \operatorname{Tr}(OP_{i}) \operatorname{Tr}(\Delta P_{i}) = p^{2} \sum_{i=1}^{d^{2}-1} [\operatorname{Tr}(\sigma P_{i}\sigma P_{i}) - \frac{1}{d}] [\operatorname{Tr}(\sigma P_{i})]^{2}$$

$$= p^{2} \sum_{i=1}^{d^{2}-1} [\operatorname{Tr}(\sigma P_{i})]^{4} - \frac{p^{2}}{d} \sum_{i=1}^{d^{2}-1} [\operatorname{Tr}(\sigma P_{i})]^{2} = p^{2} [2^{-M_{2}(\sigma)}d - 2 + \frac{1}{d}].$$
(S140)

In conjunction with Eqs. (11) and (12) we can prove Eq. (S133) as follows:

$$\mathbb{V}_{*}(O,\Delta) = \frac{d+1}{d(d+2)} \left(\|\Xi_{\Delta,O}\|_{2}^{2} + \tilde{\Xi}_{\Delta,O} \cdot \Xi_{\Delta,O} \right) - \frac{[\text{Tr}(\Delta O)]^{2}}{d+2} \\
= \frac{d+1}{d(d+2)} p^{2} \left[2^{1-M_{2}(\sigma)} d - 3 + \frac{1}{d} \right] - \frac{p^{2}(d-1)^{2}}{d^{2}(d+2)} = \frac{p^{2} \left[2^{1-M_{2}(\sigma)} (d+1) - 4 \right]}{d+2} \\
\leq \frac{2^{1-M_{2}(\sigma)} p^{2} (d-1)}{d+2} = \frac{2^{1-M_{2}(\sigma)} d^{2}}{(d-1)(d+2)} \epsilon^{2} \leq 2^{1-M_{2}(\sigma)} \epsilon^{2}, \tag{S141}$$

where the first inequality holds because $M_2(\sigma) \ge 0$, and the second inequality holds because $d \ge 2$, which means $d^2 \le (d-1)(d+2)$. This observation completes the proof of Lemma S13.

4. Proof of Theorem 5

Proof of Theorem 5. By assumption σ is a pure state and $\rho = \mathscr{P}(\sigma)$, where \mathscr{P} is a Pauli channel. In conjunction with Theorem 3 and Lemma S10 we can deduce that

$$V_*(O, \Delta) \le \frac{2}{d} \|\Xi_{\Delta, O}\|_2^2 \le 4\epsilon^2.$$
 (S142)

So Eq. (15) in Theorem 5 is a simple corollary of Lemma 3.

Next, suppose \mathscr{P} is a depolarizing channel. Then $\mathbb{V}_*(O,\Delta) \leq 2^{1-M_2(\sigma)}\epsilon^2$ according to Lemma S13. So Eq. (16) is also a simple corollary of Lemma 3, which completes the proof of Theorem 5.

Appendix S9: Variances in CRM shadow estimation based on Pauli measurements

To complement the results on 4-design and Clifford measurements, here we derive general analytical formulas for the variances $\mathbb{V}(O,\rho)$, $\mathbb{V}_*(O,\rho)$, and $\mathbb{V}_*(O,\Delta)$ in CRM shadow estimation based on Pauli measurements. Although this topic has been studied before [31], such general analytical formulas were not known before. Now, the underlying unitary ensemble \mathcal{U} corresponds to the uniform distribution on the n-qubit local Clifford group $\mathrm{Cl}_1^{\otimes n}$.

Let P_i and P_j be two Pauli operators in $\overline{\mathcal{P}}_n$. The two Pauli operators are locally commutative, denoted by $P_i \diamond P_j$, if their Pauli factors on each qubit are commutative. The weight (also known as the locality) of P_i , denoted by $w(P_i)$, is the number of nontrivial (single-qubit) Pauli factors in P_i , that is, the number of qubits on which P_i acts nontrivially. As generalization, we denote by $w(P_i \cap P_j)$ the number of common nontrivial Pauli factors in P_i and P_j and denote by $w(P_i \cup P_j)$ the number of qubits on which P_i or P_j acts nontrivially. By definition it is easy to verify that $w(P_i \cup P_j) = w(P_i) + w(P_j) - w(P_i \cap P_j)$. In addition, define $\mathscr{D}_{LC}(P_i)$ as the set of unitaries in $\operatorname{Cl}_1^{\otimes n}$ that can diagonalize P_i with respect to the computational basis; define $\mathscr{D}_{LC}(P_i, P_j)$ as the set of unitaries in $\operatorname{Cl}_1^{\otimes n}$ that can diagonalize P_i and P_j simultaneously. Note that $\mathscr{D}_{LC}(P_i, P_j)$ is not empty only when $P_i \diamond P_j$.

Theorem S1. Suppose $\mathcal{U} = \mathrm{Cl}_1^{\otimes n}$, O is a traceless observable on \mathcal{H} , and $\rho \in \mathcal{D}(\mathcal{H})$ is the system state. Then the variances $\mathbb{V}(O,\rho)$, $\mathbb{V}_*(O,\rho)$, and $\mathbb{V}_*(O,\Delta)$ in $\mathrm{CRM}(\mathcal{U},\sigma,R)$ read

$$\mathbb{V}(O,\rho) = \sum_{i,j>1}^{d^2-1} \frac{3^{w(P_i \cap P_j)}}{d^2} \operatorname{Tr}(OP_i) \operatorname{Tr}(OP_j) \operatorname{Tr}(\rho P_i P_j) - \left[\operatorname{Tr}(O\rho)\right]^2, \tag{S143}$$

$$\mathbb{V}_*(O,\rho) = \sum_{i,j>1}^{d^2-1} \frac{3^{w(P_i \cap P_j)}}{d^2} \operatorname{Tr}(OP_i) \operatorname{Tr}(OP_j) \operatorname{Tr}(\rho P_i) \operatorname{Tr}(\rho P_j) - [\operatorname{Tr}(O\rho)]^2, \tag{S144}$$

$$\mathbb{V}_*(O,\Delta) = \sum_{i,j>1}^{d^2-1} \frac{3^{w(P_i \cap P_j)}}{d^2} \operatorname{Tr}(OP_i) \operatorname{Tr}(OP_j) \operatorname{Tr}(\Delta P_i) \operatorname{Tr}(\Delta P_j) - [\operatorname{Tr}(O\Delta)]^2.$$
 (S145)

Before proving Theorem S1, we first introduce an auxiliary lemma, which is straightforward to verify (cf. Lemma S12).

Lemma S14. Suppose P_i and P_j are two Pauli operators in $\overline{\mathcal{P}}_n$ and $P_i \diamond P_j$. Then

$$\mathbb{E}_{U \sim \text{Cl}_1^{\otimes n}} \left[\delta_{U \in \mathscr{D}_{\text{LC}}(P_i)} \right] = \frac{1}{3^{w(P_i)}}, \quad \mathbb{E}_{U \sim \text{Cl}_1^{\otimes n}} \left[\delta_{U \in \mathscr{D}_{\text{LC}}(P_i, P_j)} \right] = \frac{1}{3^{w(P_i \cup P_j)}}. \tag{S146}$$

Proof of Theorem S1. Let $\mathcal{M}^{-1}(\cdot)$ be the reconstruction map associated with Pauli measurements. By assumption O is traceless, so $\mathcal{M}^{-1}(O)$ can be expressed as follows:

$$\mathcal{M}^{-1}(O) = \sum_{i=1}^{d^2 - 1} \frac{3^{w(P_i)}}{d} \operatorname{Tr}(OP_i) P_i.$$
 (S147)

In conjunction with the definition of $\mathbb{V}(O,\rho)$ [23] we can derive that

$$\mathbb{V}(O,\rho) = \mathbb{E}_{U \sim \text{Cl}_{1}^{\otimes n}} \left(\sum_{\mathbf{s}} P_{\rho}(\mathbf{s} \mid U) \left\{ \left[\mathcal{M}^{-1}(O) \right] (U,\mathbf{s}) \right\}^{2} \right) - \left[\text{Tr}(O\rho) \right]^{2}$$

$$= \sum_{i,j=1}^{d^{2}-1} \frac{3^{w(P_{i})+w(P_{j})}}{d^{2}} \operatorname{Tr}(OP_{i}) \operatorname{Tr}(OP_{j}) \sum_{\mathbf{s}} \mathbb{E}_{U \sim \text{Cl}_{1}^{\otimes n}} \left(\langle \mathbf{s} | U\rho U^{\dagger} | \mathbf{s} \rangle \langle \mathbf{s} | UP_{i}U^{\dagger} | \mathbf{s} \rangle \langle \mathbf{s} | UP_{j}U^{\dagger} | \mathbf{s} \rangle \right) - \left[\operatorname{Tr}(O\rho) \right]^{2}.$$
(S148)

If $U \notin \mathscr{D}_{LC}(P_i, P_j)$, then $\langle \mathbf{s}|UP_iU^{\dagger}|\mathbf{s}\rangle\langle \mathbf{s}|UP_jU^{\dagger}|\mathbf{s}\rangle = 0$ for all \mathbf{s} ; otherwise, UP_iU^{\dagger} and UP_jU^{\dagger} are diagonal in the computational basis, and we have

$$\sum_{\mathbf{s}} \langle \mathbf{s} | U \rho U^{\dagger} | \mathbf{s} \rangle \langle \mathbf{s} | U P_i U^{\dagger} | \mathbf{s} \rangle \langle \mathbf{s} | U P_j U^{\dagger} | \mathbf{s} \rangle = \text{Tr} \left(U \rho U^{\dagger} U P_i U^{\dagger} U P_j U^{\dagger} \right) = \text{Tr} (\rho P_i P_j). \tag{S149}$$

Based on this observation, $\mathbb{V}(O, \rho)$ can be expressed as follows:

$$\mathbb{V}(O,\rho) = \sum_{i,j>1}^{d^2-1} \frac{3^{w(P_i)+w(P_j)}}{d^2} \operatorname{Tr}(OP_i) \operatorname{Tr}(OP_j) \operatorname{Tr}(\rho P_i P_j) \mathbb{E}_{U \sim \operatorname{Cl}_1^{\otimes n}} \left[\delta_{U \in \mathscr{D}_{\operatorname{LC}}(P_i, P_j)} \right] - \left[\operatorname{Tr}(O\rho) \right]^2$$

$$= \sum_{i,j>1}^{d^2-1} \frac{3^{w(P_i \cap P_j)}}{d^2} \operatorname{Tr}(OP_i) \operatorname{Tr}(OP_j) \operatorname{Tr}(\rho P_i P_j) - \left[\operatorname{Tr}(O\rho) \right]^2, \tag{S150}$$

which confirms Eq. (S143). Here the last equality follows from Lemma S14.

Next, let τ be an arbitrary linear operator on \mathcal{H} . By virtue of Eqs. (5) and (S147) we can derive that

$$\mathbb{V}_*(O,\tau) = \sum_{\mathbf{s},\mathbf{t}} \mathbb{E}_{U \sim \mathrm{Cl}_1^{\otimes n}} \left[\langle \mathbf{s} | U \mathcal{M}^{-1}(O) U^\dagger | \mathbf{s} \rangle \langle \mathbf{s} | U \tau U^\dagger | \mathbf{s} \rangle \langle \mathbf{t} | U \mathcal{M}^{-1}(O) U^\dagger | \mathbf{t} \rangle \langle \mathbf{t} | U \tau U^\dagger | \mathbf{t} \rangle \right] - \left[\mathrm{Tr}(O\tau) \right]^2$$

$$= \sum_{i,j=1}^{d^2-1} \frac{3^{w(P_i)+w(P_j)}}{d^2} \operatorname{Tr}(OP_i) \operatorname{Tr}(OP_j) \sum_{\mathbf{s},\mathbf{t}} \mathbb{E}_{U \sim \operatorname{Cl}_1^{\otimes n}} \left[\langle \mathbf{s} | U P_i U^{\dagger} | \mathbf{s} \rangle \langle \mathbf{s} | U \tau U^{\dagger} | \mathbf{s} \rangle \langle \mathbf{t} | U P_j U^{\dagger} | \mathbf{t} \rangle \langle \mathbf{t} | U \tau U^{\dagger} | \mathbf{t} \rangle \right] - \left[\operatorname{Tr}(O\tau) \right]^2.$$
(S151)

If $U \notin \mathscr{D}_{LC}(P_i)$, then $\langle \mathbf{s} | U P_i U^{\dagger} | \mathbf{s} \rangle = 0$ for all \mathbf{s} ; otherwise, $U P_i U^{\dagger}$ is diagonal in the computational basis, and

$$\sum_{\mathbf{s}} \langle \mathbf{s} | U P_i U^{\dagger} | \mathbf{s} \rangle \langle \mathbf{s} | U \tau U^{\dagger} | \mathbf{s} \rangle = \text{Tr} \left(U P_i U^{\dagger} U \tau U^{\dagger} \right) = \text{Tr} (\tau P_i). \tag{S152}$$

Based on this observation, $V_*(O, \tau)$ can be expressed as follows:

$$\mathbb{V}_{*}(O,\tau) = \sum_{i,j=1}^{d^{2}-1} \frac{3^{w(P_{i})+w(P_{j})}}{d^{2}} \operatorname{Tr}(OP_{i}) \operatorname{Tr}(OP_{j}) \operatorname{Tr}(\tau P_{i}) \operatorname{Tr}(\tau P_{j}) \mathbb{E}_{U \sim \operatorname{Cl}_{1}^{\otimes n}} \left[\delta_{U \in \mathscr{D}_{LC}(P_{i},P_{j})} \right] - \left[\operatorname{Tr}(O\tau) \right]^{2}$$

$$= \sum_{i,j>1}^{d^{2}-1} \frac{3^{w(P_{i} \cap P_{j})}}{d^{2}} \operatorname{Tr}(OP_{i}) \operatorname{Tr}(OP_{j}) \operatorname{Tr}(\tau P_{i}) \operatorname{Tr}(\tau P_{j}) - \left[\operatorname{Tr}(O\tau) \right]^{2}, \tag{S153}$$

where the last equality follows from Lemma S14. This equation implies Eqs. (S144) and (S145) and completes the proof of Theorem S1. \Box

Appendix S10: Additional numerical results

In this section, we first provide additional numerical results on the performance of THR and CRM shadow estimation based on Clifford measurements and discuss the impacts nonstabilizerness and the number R of circuit reusing on the circuit sample cost. Then we compare the performance of Clifford measurements with 4-design and Pauli measurements.

Thanks to Lemmas 1 and 2, the circuit sample cost N_U is determined by the variance $\mathbb{V}_R(\hat{O})$, which in turn is determined by $\mathbb{V}(O,\rho)$, $\mathbb{V}_*(O,\rho)$, and $\mathbb{V}_*(O,\Delta)$. When the measurement ensemble forms a 3-design (including Clifford and 4-design measurements), $\mathbb{V}(O,\rho)$ is determined by Eq. (A1). For Clifford measurements, $\mathbb{V}_*(O,\Delta)$ is determined by Eq. (12), and $\mathbb{V}_*(O,\rho)$ is determined by Eq. (12) with Δ replaced by ρ ; in the presence of depolarizing noise, we can also use more explicit formulas in Lemma S13. For 4-design measurements, $\mathbb{V}_*(O,\rho)$ and $\mathbb{V}_*(O,\rho)$ are determined by Lemma S5. For Pauli measurements, $\mathbb{V}(O,\rho)$, $\mathbb{V}_*(O,\rho)$, and $\mathbb{V}_*(O,\Delta)$ are determined by Theorem S1 (see also Eq. (S158) below).

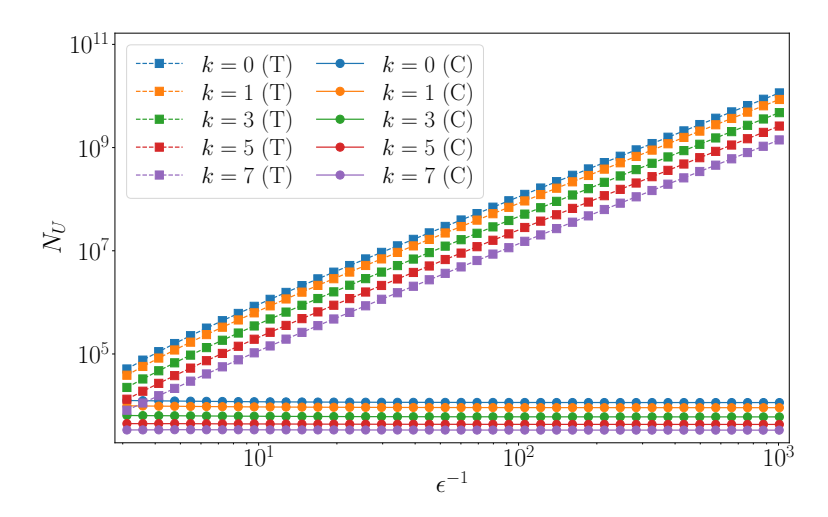


FIG. S3. The circuit sample costs N_U required for HPFE in THR (T) and CRM (C) shadow estimation based on Clifford measurements. Here, r=0.25, $\delta=0.01$, and $R=\lceil 10/\epsilon^2 \rceil$. The target and prior state has the form $\sigma=|S_{7,k}\rangle\langle S_{7,k}|$ with k=0,1,3,5,7, and different system states ρ are generated by applying depolarizing noise to the target state and have the form $\rho=(1-p)\sigma+p\mathbb{1}/d$ with $p=\epsilon/(1-d^{-1})$.

1. CRM shadow estimation based on Clifford measurements

a. HPFE in the presence of depolarizing noise

Here we consider HPFE in the presence of depolarizing noise. This case is particularly instructive because exact and informative formulas for the variances $\mathbb{V}(O,\rho)$, $\mathbb{V}_*(O,\rho)$, and $\mathbb{V}_*(O,\Delta)$ can be derived as shown in Lemma S13. Accordingly, we can derive a simple upper bound for the circuit sample cost as shown in Eq. (16) in Theorem 5 [see also Eq. (S137)]. In numerical simulation, we choose $|\phi\rangle = |S_{7,k}\rangle$ as the target and prior state, where k = 0, 1, 3, 5, 7. Figure S3 illustrates the circuit sample costs associated with THR and CRM shadow estimation as functions of the target infidelity ϵ , where each circuit is reused $R = \lceil 10/\epsilon^2 \rceil$ times. Notably, CRM only requires a constant circuit sample cost, while THR requires $\mathcal{O}(1/\epsilon^2)$ circuits. This result highlights the significant advantages of CRM over THR. Meanwhile, in both CRM and THR, the circuit sample costs decrease exponentially with the 2-SRE $M_2(\phi)$ of the target state $|\phi\rangle$. Similar results also hold when depolarizing noise is replaced by general Pauli noise, as illustrated in the right plot in Fig. 2 (see also Theorem 5), given that random Pauli noise has a similar effect to the depolarizing noise.

b. HPFE in the presence of a special type of coherent noise

To better understand the scaling behavior of the circuit sample cost in CRM shadow estimation based on Clifford measurements, here we consider HPFE in the presence of a special type of coherent noise, which corresponds to a collective rotation described as follows:

$$U = [U(\theta)]^{\otimes n}, \quad U(\theta) = \begin{pmatrix} e^{-i\theta} \cos(\theta/2) & -\sin(\theta/2) \\ \sin(\theta/2) & e^{i\theta} \cos(\theta/2) \end{pmatrix}.$$
 (S154)

In the numerical simulation, we choose $|\phi\rangle = |S_{7,k}\rangle$ with k=1,4,7 as the target and prior states. Figure S4 illustrates the circuit sample costs associated with THR and CRM shadow estimation based on Clifford measurements as functions of the infidelity ϵ , where each circuit is reused $R = \lceil 10/\epsilon^2 \rceil$ times. As expected, the circuit sample cost of THR shadow estimation scales as $1/\epsilon^2$. By contrast, the cost of CRM shadow estimation scales as $1/\epsilon$, which is compatible with the prediction of Theorem 4 given that $\|\Delta\|_2^2 = 2\epsilon$ for coherent noise by Proposition 3. Note that CRM shadow estimation is substantially better than THR shadow estimation, but fails to achieve the constant scaling behavior observed in Fig. 2. This result demonstrates that the $1/\epsilon$ scaling behavior is inevitable for certain coherent noise although a constant scaling behavior can usually be achieved in the presence of random coherent noise.

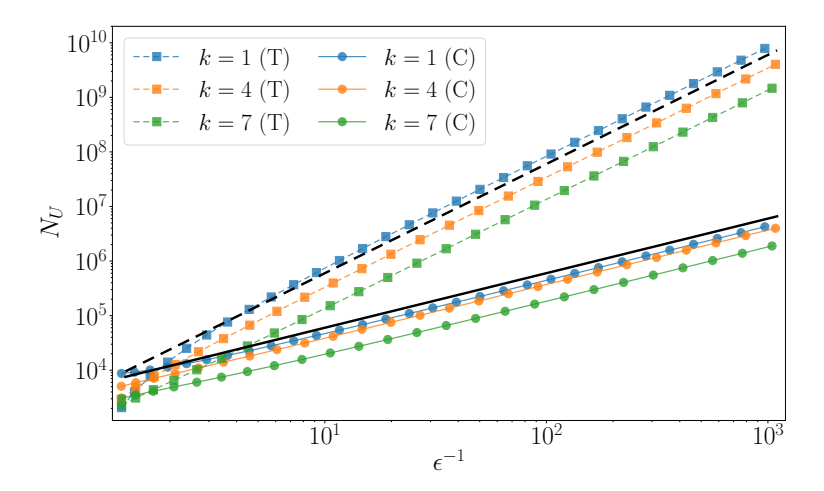


FIG. S4. The circuit sample costs N_U required for HPFE in THR (T) and CRM (C) shadow estimation based on Clifford measurements. Here, r=0.25, $\delta=0.01$, and $R=\lceil 10/\epsilon^2 \rceil$. The target and prior state has the form $\sigma=|S_{7,k}\rangle\langle S_{7,k}|$ with k=1,4,7. Different system states ρ are generated by applying random local rotations described in Eq. (S154) to the target state σ . The black solid and dashed lines represent $N_U=6000/\epsilon$ and $N_U=6000/\epsilon^2$, respectively.

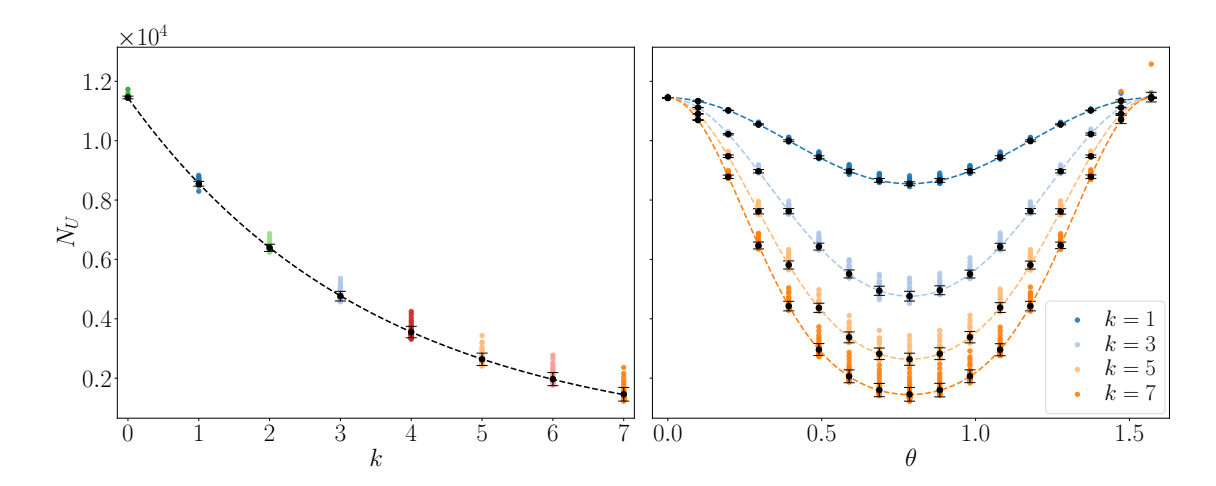


FIG. S5. The circuit sample cost N_U required for HPFE in CRM shadow estimation based on Clifford measurements. Here, r=0.25, $\delta=0.01$, and $R=\lceil 10/\epsilon^2 \rceil$. The target and prior state has the form $\sigma=|S_{7,k}(\theta)\rangle\langle S_{7,k}(\theta)|$, and different system states ρ are generated by applying random Pauli noise (described in Sec. S52), sampled 50 times for given values of k and θ , to the target state σ . The fitting curves follow the formula in Eq. (S157). In the left plot, we set $\theta=\pi/4$, and the fitting parameters read a=11538.21 and b=94.87; in the right plot, the fitting parameters depend on k and satisfy $a \in [11537, 11571]$ and $b \in [93, 128]$.

c. Impact of nonstabilizerness

According to Theorems 4 and 5, nonstabilizerness can significantly reduce the circuit sample cost required for HPFE in CRM shadow estimation based on the Clifford group, as illustrated in Figs. 2 and S3. To further clarify the impact of nonstabilizerness, here we consider HPFE in which the target and prior state has the form

$$|S_{n,k}(\theta)\rangle := |0\rangle^{\otimes(n-k)} \otimes \left[\frac{1}{\sqrt{2}} (|0\rangle + e^{i\theta} |1\rangle)\right]^{\otimes k},$$
 (S155)

whose 2-SRE reads

$$M_2(S_{n,k}(\theta)) = -k \log_2 \left[\frac{7 + \cos(4\theta)}{8} \right].$$
 (S156)

In addition, the system state is affected by general Pauli noise. Figure S5 illustrates the dependence of N_U on the parameters k and θ . When r=0.25, $\delta=0.01$, and $R=\lceil 10/\epsilon^2 \rceil$, a pretty good fitting formula for N_U can be expressed as follows:

$$N_U = a \times 2^{-M_2(S_{7,k}(\theta))} - b, \quad a \approx 11500, \quad b \approx 100 \ll a,$$
 (S157)

which is similar to Eq. (16) in Theorem 5. Notably, N_U decreases exponentially with $M_2(S_{7,k}(\theta))$, and the effect of Pauli noise resembles the counterpart of depolarizing noise. This result also echoes the fact that nonstabilizerness can enhance the performance of THR shadow estimation [29].

d. Dependence of N_U on the number R of circuit reusing

In this section, we turn to the dependence of the circuit sample costs on the number R of circuit reusing in THR and CRM shadow estimation based on the Clifford group. In the numerical simulation, the target and prior state has the form $|\phi\rangle = |S_{7,k}\rangle$ with k=0,1,3,7, and the system state ρ is generated by applying a random Pauli channel (as described in Sec. S52) to the target state. Figure S6 illustrates the scaling behaviors of N_U with respect to the infidelity ϵ for three different choices of R, and Fig. S7 illustrates the variations of N_U with R directly for different choices of k. Not surprisingly, increasing R tends to decrease N_U in both THR and CRM shadow estimation. In THR, when $R \geq 5 \times 2^{M_2(\phi)}$, however, further increasing R has negligible influence on $N_U^{(T)}$. In CRM, by contrast, $N_U^{(C)}$ decreases with R until $R \gtrsim 2^{M_2(\phi)}/\epsilon^2$, and R

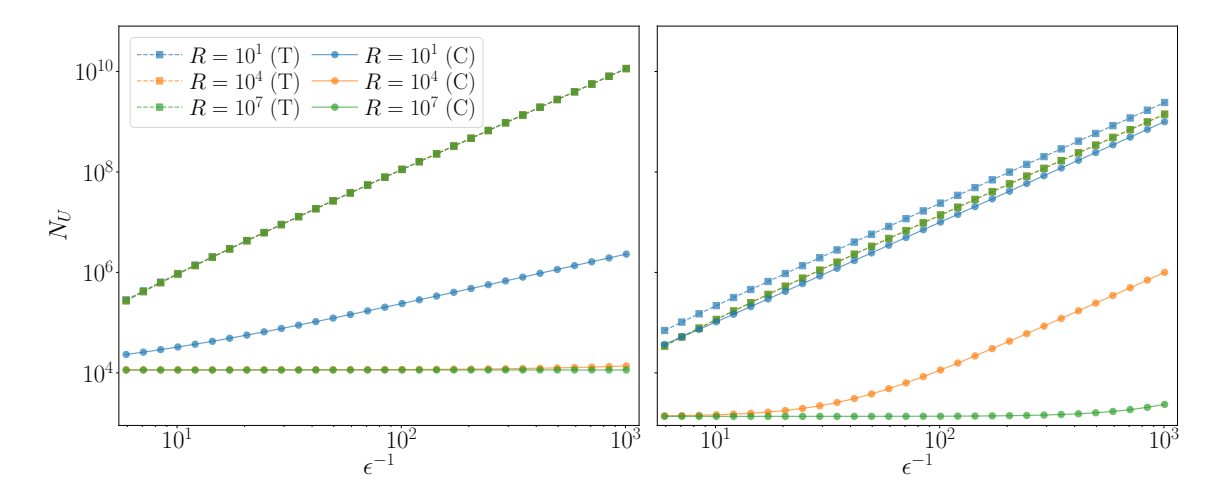


FIG. S6. The circuit sample costs N_U required for HPFE in THR (T) and CRM (C) shadow estimation based on Clifford measurements. Here, r=0.25 and $\delta=0.01$. The target and prior state has the form $\sigma=|S_{7,k}\rangle\langle S_{7,k}|$ with k=0 (left plot) and k=7 (right plot), and different system states ρ are generated by applying random Pauli channels (described in Sec. S5 2) to the target state σ . For THR, the dependence of N_U on R is invisible for all three choices of R in the left plot and for two choices of R ($R=10^4$ and $R=10^7$) in the right plot.

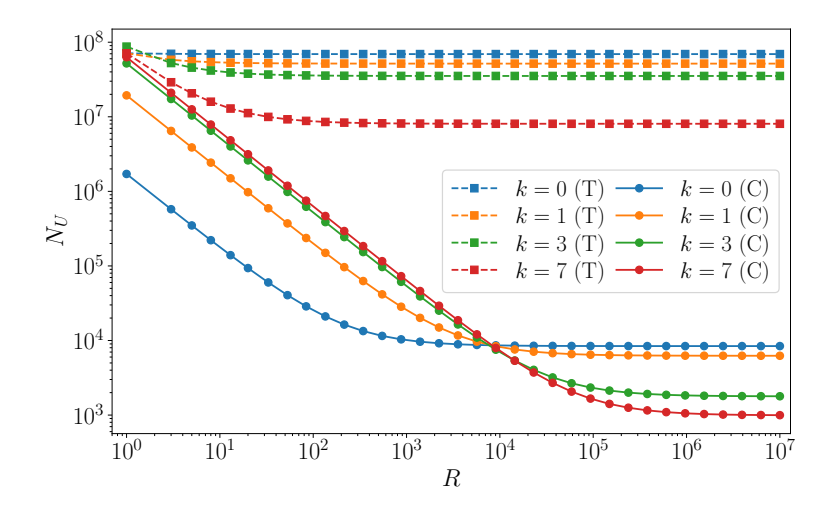


FIG. S7. The circuit sample costs N_U required for HPFE in THR (T) and CRM (C) shadow estimation based on Clifford measurements. Here, $r=0.25,\ \delta=0.01,\$ and $\epsilon=0.01.$ The target and prior state is $\sigma=|S_{7,k}\rangle\langle S_{7,k}|$ with k=0,1,3,7. For each value of k, the system state ρ is generated by applying a random Pauli channel (as described in Sec. S5 2) to the target state σ .

needs to scale with $1/\epsilon^2$ to guarantee that $N_U^{({\rm C})}$ is almost independent of ϵ . When R is sufficiently large, we have $N_U^{({\rm C})} \approx N_U^{({\rm T})} \epsilon^2$, so CRM can significantly reduce the circuit sample cost. In addition, both $N_U^{({\rm C})}$ and $N_U^{({\rm T})}$ decrease exponentially with $M_2(\phi)$. When R is small $(R \lesssim 1/\epsilon^2)$, however, $N_U^{({\rm C})}$ may increase (rather than decrease) with $M_2(\phi)$. These results resemble the counterparts on shadow estimation in the presence of depolarizing noise as discussed in Sec. S8 3.

2. Comparison of different measurement ensembles

In this section, we compare the efficiencies of three CRM shadow estimation protocols based on three measurement ensembles, namely, the Clifford measurements, Pauli measurements, and 4-design measurements.

First, we consider HPFE using CRM shadow estimation based on three measurement ensembles. Here the target state is the n-qubit GHZ state, and the system state is affected by phase-flip noise on the first qubit. Figure S8 illustrates the circuit sample costs associated with three measurement ensembles as functions of n. The sample cost N_U increases exponentially with n for Pauli measurements, is almost independent of n for Clifford measurements, and decreases exponentially with n for 4-design measurements. These results are consistent with the behaviors of $V_*(O, \Delta)$ as clarified in Theorems 1, 3, and S1.

Next, we consider the task of estimating Pauli observables. According to Lemma 2 and Theorem S1, for a Pauli operator O with weight (locality) w, we have [31]

$$V_R(\hat{O}) = (3^w - 1)[\text{Tr}(\Delta O)]^2 + \frac{3^w \{1 - [\text{Tr}(\rho O)]^2\}}{R} \le 3^w \{[\text{Tr}(\Delta O)]^2 + \frac{1}{R}\},\tag{S158}$$

which indicates that the variance tends to scale with 3^w . In CRM shadow estimation based on Clifford measurements, by contrast, the variance in estimating the Pauli operator O scales only with the system size:

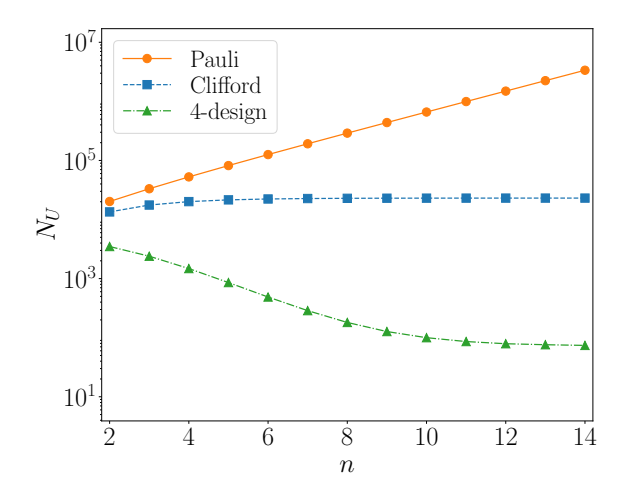
$$V_R(\hat{O}) = d[\text{Tr}(\Delta O)]^2 + \frac{(d+1)\{1 - [\text{Tr}(\rho O)]^2\}}{R},$$
(S159)

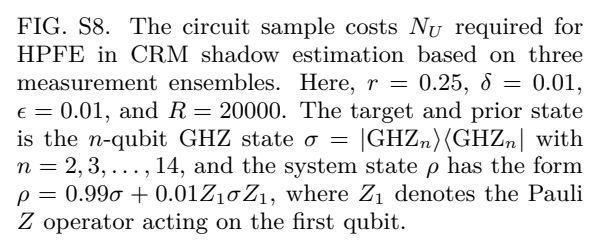
which follows from Eqs. (4), (11), and (12). Therefore, the relative efficiency of Pauli measurements versus Clifford measurements is determined by the competition between the operator weight and the system size. For CRM shadow estimation based on 4-design measurements, the variance scales with neither the weight nor the system size in the large-R limit according to Lemma 3 and Theorem 1.

In the example we consider, the prior state σ is the 14-qubit GHZ state, and the system state has the form $\rho = (\sigma + X_1 \sigma X_1)/2$, where X_1 denotes the Pauli X operator acting on the first qubit. In addition, the Pauli operators to be estimated have the form

$$O_i = \bigotimes_{j=1}^{2i} Z_j, \quad i = 1, 2, \dots, 7,$$
 (S160)

which have weights $w=2,4,\ldots,14$, respectively. Figure S9 shows the circuit sample costs required to estimate the expectation values of these Pauli operators in CRM shadow estimation based on three measurement ensembles. Not surprisingly, 4-design measurements require the smallest circuit sample costs and are thus the most efficient; Clifford measurements are better (worse) than Pauli measurements when $w \geq 9$ (w < 9).





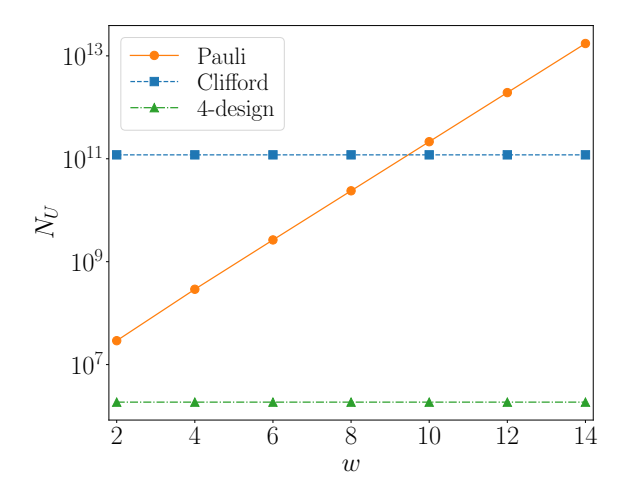


FIG. S9. The circuit sample costs required to estimate the Pauli operator O_i in Eq. (S160) using CRM shadow estimation based on three measurement ensembles, plotted as functions of the weight w. Here, $\varepsilon = 0.01$, $\delta = 0.01$, and R = 100. The prior state has the form $\sigma = |\text{GHZ}_{14}\rangle\langle\text{GHZ}_{14}|$, and the system state reads $\rho = (\sigma + X_1\sigma X_1)/2$, where X_1 denotes the Pauli X operator acting on the first qubit.

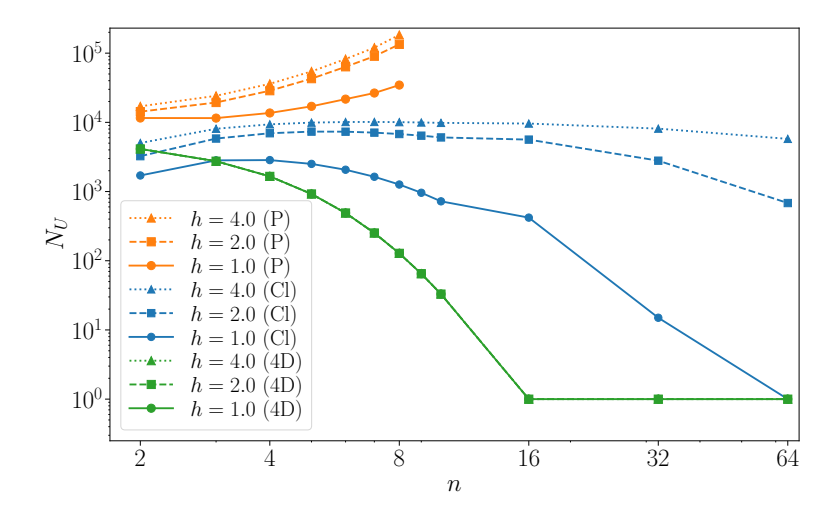


FIG. S10. The circuit sample costs N_U required for HPFE in CRM shadow estimation based on Pauli (P), Clifford (Cl), and 4-design (4D) measurements. Here r=0.25, $\delta=0.01$, $\epsilon=0.01$, and R=100000. For given values of n and h, the target and prior state is the ground state of the TFIM Hamiltonian in Eq. (S161) with J=1, and the system state ρ has the form $\rho=(1-p)\sigma+p\mathbb{1}/d$ with $p=\epsilon/(1-d^{-1})$. The results on 4-design measurements are almost independent of h.

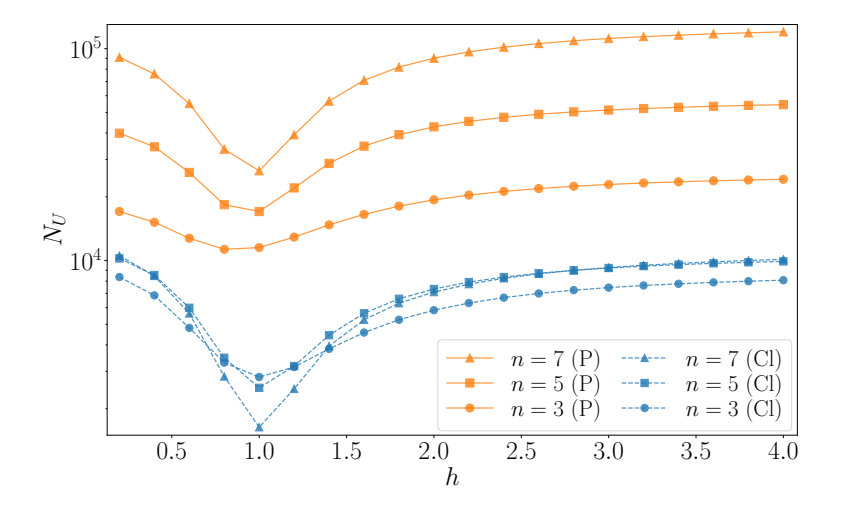


FIG. S11. The circuit sample costs N_U required for HPFE in CRM shadow estimation based on Pauli (P) and Clifford (Cl) measurements. Here r=0.25, $\delta=0.01$, $\epsilon=0.01$, and R=100000. For given values of n and h, the target and prior state is the ground state of the TFIM Hamiltonian in Eq. (S161) with J=1, and the system state ρ has the form $\rho=(1-p)\sigma+p\mathbb{1}/d$ with $p=\epsilon/(1-d^{-1})$.

$b. \quad \textit{HPFE of the ground state of the transverse-field Ising model}$

Here we consider HPFE of the ground state of the transverse-field Ising model (TFIM), which is a typical model widely used in condensed matter physics, quantum information, and quantum computation [37–42]. For a one-dimensional system with a periodic boundary condition, the Hamiltonian of the model reads

$$H = -J\sum_{\langle i,j\rangle} Z_i Z_j - h\sum_i X_i. \tag{S161}$$

Suppose J = 1; as h increases from 0, the system undergoes a phase transition at h = 1, changing from an ordered phase to a disordered phase and exhibits rich features at the critical point h = 1. In the numerical calculation, the target state is the ground state of the above Hamiltonian, which can be obtained by exact diagonalization, and the system state is affected by depolarizing noise.

Figures S10 and S11 illustrate the circuit sample costs associated with three measurement ensembles as functions of the system size n and the effective magnetic field h. The circuit sample cost required for HPFE

increases exponentially with n for CRM shadow estimation based on Pauli measurements, while it decreases exponentially with n for 4-design measurements, resembling the behaviors observed in HPFE of the GHZ state as shown in Fig. S8. For Clifford measurements, the circuit sample cost also decreases exponentially with n, especially when h is close to the critical point h=1. This behavior, in contrast with the constant scaling observed in Fig. S8, is tied to the increase in the 2-SRE of the ground state [39–42] (an open dataset on the 2-SRE is available at Ref. [42]), which is expected according to Eq. (16) (see also Lemma S13). Interestingly, for Pauli measurements, the circuit sample cost also exhibits a similar dependence on h.